NATIONAL SCIENCE FOUNDATION GRANT NO. ENG74-21131

FINAL REPORT

PART 3

Report SM77-2

EFFECT OF REINFORCING BAR SIZE ON SHEAR TRANSFER ACROSS A CRACK IN CONCRETE

by

Alan H. Mattock

Department of Civil Engineering
University of Washington
September, 1977

TECHNICAL REPORT STANDARD TITLE PAGE

1. Report No.	2. Government Accession No.	3. Recipient's Catalog No.
SM77-2		

4. Title and Subtitle	5. Report Date
EFFECT OF REINFORCING BAR SIZE ON SHEAR TRANSFER ACROSS A CRACK IN CONCRETE	September 1977
	6. Performing Organization Code

7. Author(s)	8. Performing Organization Report No.
Alan H. Mattock	SM77-2

9. Performing Organization Name and Address	10. Work Unit No.
University of Washington Department of Civil Engineering Seattle, Washington 98195	11. Contract or Grant No. ENG 74-21131
	13. Type of Report and Period Covered Final Report, Part 3 14 Oct. 1974 - 30 Sept. 1977
12. Sponsoring Agency Name and Address National Science Foundation Washington, D.C. 20550	14. Sponsoring Agency Code

15. Supplementary Notes

16. Abstract The total study is concerned with the shear transfer strength of reinforced concrete subject to both single direction and cyclically reversing loading, the latter simulating earthquake conditions. The primary topics studied were the influence of the existence in the shear plane of an interface between concretes cast at different times, and the influence of reinforcing bar diameter on shear transfer across a crack in monolithic concrete.

This Part 3 of the Final Report is concerned with the effect of size of reinforcing bar on shear transfer across a crack in concrete, under both monotonic and cyclically reversing shear. Monotonic and cyclically reversing shear transfer tests were made of initially cracked concrete push-off specimens, having reinforcement varying from #4 to #18 in size.

Some reduction in shear transfer strength occurred as the bar size was increased from #8 to #18, but the monotonic loading strength of all specimens was conservatively predicted by the shear-friction equation. The strength under reversed cyclic loading was about 0.8 of the strength under monotonic loading.

17. Key Words	18. Distribution Statement
connections, precast concrete, reinforced concrete, reinforcing bar, seismic loading, shear transfer.	approved for NTIS per telecon by Dr. Bobendrier NSF, ENG. 1-5-95

19. Security Classif. (of this report)	20. Security Classif. (of this page)	22. Price
None	None	PC A08-A01

PREFACE

This study was carried out in the Structural Research Laboratory of the University of Washington. It was made possible by the support of the National Science Foundation, through Grant No. ENGR74-21131.

Contributions were made to the execution of this project by graduate student research assistants, A. Bhalaik and D. Novstrup.

TABLE OF CONTENTS

LIST OF FIGURES

I - INTRODUCTION

1.1 Background

The purpose of this study has been to obtain further information on shear transfer in reinforced concrete subject to both single direction and cyclically reversing shear. In this connection, "shear transfer" is defined as the transfer of shear across a specific plane or crack in the concrete. Failure in shear transfer appears as slip along the plane or crack, under the action of a constant or decreasing shear force.

The principal topics included in the study were,-

(1) the influence on shear transfer behavior, of the existence in the shear plane of an interface between concretes cast at different times.

(2) the influence of reinforcing bar size on shear transfer across a crack in monolithic reinforced concrete.

The overall objectives of this study have been to improve understanding of the mechanics of shear transfer in reinforced concrete, and to develop design recommendations for shear transfer in reinforced concrete subject to static or cyclically reversing loading conditions.

1.2 Scope of the Entire Study

Tests have been made of "push-off" type specimens and such modified versions of the simple push-off type of specimen as will permit the desired loading condition to be imposed on the specimen.

The following variables have been included in the test program:-

1. The use of composite or monolithic specimens.
2. The compressive strengths of the concretes cast against one another.
3. The condition of the face of the precast concrete against which other concrete is cast, i.e. smooth or deliberately roughened, bond deliberately broken or not.

4. The existence of a crack in the shear plane.

5. The shear transfer reinforcement parameter ρf_y.

6. The size of the reinforcing bars used as shear transfer reinforcement.

7. The type of loading, i.e., single direction and cyclically reversing shear.

1.3 Sub-Division of the Final Report

Part 1 of the final report described[1] that part of the study concerned with shear transfer across interfaces between concretes cast at different times, when subject to monotonically increasing shear.

Part 2 of the final report described[2] that part of the study concerned with shear transfer across interfaces between concretes cast at different times, when subject to cyclically reversing shear.

Part 3 of the final report describes that part of the study concerned with the effect of size of reinforcing bar on shear transfer across a crack in concrete, under both monotonic and cyclically reversing shear.

1.4 Background to this Part of the Study

Data so far published on shear transfer behavior has been obtained in tests in which the shear transfer reinforcement was less than 3/4 inch diameter*. Within this range of sizes it was shown[3] that the shear transfer strength is only influenced by change in bar size to the extent that the shear transfer reinforcement percentage, ρ, is changed; i.e. if both bar size and spacing are changed so that ρ is not changed, then the shear transfer strength is unchanged.

Although the range of bar sizes included in previous tests covers the bar sizes used in many circumstances in precast concrete construction, an increasing number of design situations are arising where it is necessary to use larger bar

*This statement relates to tests in which the reinforcement is embedded in and bonded to the concrete.

sizes as shear transfer reinforcement. This is occurring in both precast concrete construction and cast-in-place concrete construction. An extreme case occurs in the design of nuclear reactor containment vessel walls.

It has been proposed by some engineers that the "shear friction" design concepts contained in ACI 318-71[4], which are based on data from tests of specimens reinforced with relatively small sized bars, should be applied to the membrane shear design of a containment vessel wall reinforced with #14 or #18 reinforcing bars. This would be a considerable extrapolation.

The transfer of shear across a crack involves a combination of resistance to shearing off of local "high spots," (or asperities,) on the crack faces, frictional resistance to sliding of one crack face over the other, and dowel action of the reinforcing bars. The relative contributions of each of these to shear transfer resistance depends upon the intensity of shear stress, the hardness and roughness of the crack faces, and the amount and possibly the size of the shear transfer reinforcement.

At the commencement of this study it was considered that the role of rebar dowel forces in the development of shear transfer strength, was analagous to the role of dowel forces in stud shear connector behavior in composite steel and concrete construction. Research[5] has shown that the useful strength of stud shear connectors of diameter greater than about 1 inch, is limited by splitting of the concrete as a result of dowel action, rather than by the tensile strength of the stud. It was considered possible that a similar limitation might be found in the case of large size reinforcing bars used as shear transfer reinforcement. It therefore appeared desirable to establish the maximum bar diameter for which current shear transfer design procedures are valid.

II - EXPERIMENTAL STUDY

2.1 Scope

This experimental study was concerned with the influence on shear transfer across a crack in monolithic concrete, of the size of reinforcing bar used as shear transfer reinforcement. In particular, it was desired to establish the maximum bar diameter for which current shear transfer design procedures are valid.

The variables included in the study were,-

1. The size of reinforcing bar
2. The loading history of the test specimens,-
   (a) monotonically increasing load,
   (b) cyclically reversing load.

2.2 The Test Specimen

A push-off specimen with two shear planes, each of 1000 in^2 area, was used for both the monotonic loading and cyclically reversing load tests. Details of a typical specimen reinforced with bars size 11 or less, are shown in Fig. 2.1. In the case of specimens reinforced with #14 or with #18 bars, straight bars with anchor plates on their ends were used instead of closed hoops. The specimen was supported on the bearing strips and was loaded concentrically, by a load distributed over most of the width of the specimen between the two shear planes. This produced a shear in each shear plane equal to half the applied load, together with a small moment.

One of the objectives of the tests was to establish the maximum bar diameter for which current shear transfer design procedures are valid. It was therefore decided to hold the reinforcement parameter as nearly constant as possible, and to make it as close as possible to the value of ρf_y corresponding to the maximum allowable shear transfer stress according to Sec. 11.15 - shear-

friction of ACI 318-71. For a concrete compressive strength f'_c, of 4000 psi, the maximum allowable shear transfer stress is 800 psi. The corresponding value of ρf_y is 571 psi, (using $\mu = 1.4$ for a crack in monolithic concrete.) It was considered that this approach to the design of the specimens would be conservative, since, if the potential strength of this quantity of reinforcement could be developed using a particular bar size, then it should also be possible to develope the full potential strength of any smaller quantity of the same size of reinforcing bar.

The numbers of bars crossing the shear plane in each specimen is shown in Table 2.1, together with the measured values of the reinforcement yield strength and the consequent actual values of ρf_y. The average value of ρf_y for the 8 specimens subject to monotonic loading was 540 psi, but individual values of ρf_y varied from 495 psi to 590 psi. This was because of the variation of the yield strength between different sizes of bars, (although all were nominally 60 grade bars,) and the fact that only a whole number of bars could be used in a specimen.

Six #10 bars were provided outside and parallel to the two shear planes, to act as compression reinforcement in the vicinity of the supporting bearings. These bars were machined to the same length, and a ½ inch deep hole was drilled and tapped in each end to fit a 3/8 inch diameter machine screw. The screw was used to attach each #10 bar directly to the bearing shoes at top and bottom of the specimen. This ensured that this compression reinforcement would be loaded directly by end bearing against the bearing shoe above the support bearing. #8 bar auxiliary reinforcement was also provided as shown.

Six 1 inch diameter prestressing bars, (f_y = 100 ksi,) were provided adjacent to the end faces of the specimen and passing through the top and bottom bearing

plates. These bars served both to clamp the bearing plates to the specimen, and also to make more uniform the compressive stresses under the bearing plate.

1 inch diameter, 12 inch long pigtail anchors were provided at the middle of each end face, to which swivel lifting plates were subsequently attached.

In the numbering of the specimens, the first letter indicates the type of loading to which the specimen was subjected, (i.e. M for monotonic and C for cyclically reversing,) the number is the size of bar used as shear transfer reinforcement in the specimen, and the final letter was to distinguish between duplicate specimens, if necessary.

2.3 Materials and Fabrication

The specimens were made from Type III Portland Cement, sand and 3/4 inch maximum size glacial outwash gravel. The concrete was obtained from a local ready-mixed concrete supplier. The nominal mix proportions were 1:2.98:4.26, with a 3 inch slump. However, as delivered, the slump varied considerably. It was therefore necessary to monitor the concrete strength from day to day and to test the specimen when the concrete strength was close to the target strength of 4000 psi. The actual concrete strength at the time of test for each specimen, is shown in Table 2.1.

The deformed bar reinforcement used, conformed to ASTM Specification A615. The rebars were nominally of grade 60. The measured values of yield strength are shown in Table 2.1. The closed hoops were each made from two U-shaped bars, welded together on the shorter sides of the hoop. In specimens M8A, C8A and M11A, it was necessary to provide an additional single bar at the middle of the specimen. In M8A and C8A it was possible to anchor this bar by providing a hook at each end. In the case of M11A it was necessary to weld a plate on each end of the bar in order to anchor it.

The #14 and #18 bar reinforcement was in the form of 54 inch long straight bars, each end of which was provided with an anchor plate, (3 x 6½ x 6½ inch for #14 bars, 4 x 8½ x 8½ inch for #18 bars.) The anchor plates were attached to the bars using a patent tapered thread. The bar and anchor plate assemblies were supplied by Fox-Howlett Industries. The tapered thread was of the same pattern as that used in the Fox-Howlett "No-slip Coupling" for large diameter rebars. The tensile tests of the #14 and #18 bars were made using similar assemblies, pulling against the anchor plates at each end. In these tensile tests, failure occurred approximately at the tensile strength of the bars, far in excess of the yield strength.

The specimens were cast lying on their side, (as in Sec. A-A of Fig. 2.1.). The inner bearing plates were incorporated in the form, so that the concrete should be cast against them and uniform contact be thus ensured. The forms were otherwise of plastic coated plywood, braced by a frame of steel angles. The vee-shaped grooves used to define the shear planes, were formed by stiff, steel members, to ensure dimensional accuracy.

The specimens were cured in the form under a polythene sheet, for three days. The companion cylinders were also cured for three days in their moulds, sealed by a polythene bag placed over their ends. The specimen and companion cylinders were then stripped and were immediately coated with a sealer to prevent the escape of moisture. By doing this, it was thought that the curing conditions for the concrete in the cylinders would more closely approximate those of the concrete in the large specimen; than if both had been left unsealed to dry in the ambient atmosphere of the laboratory. The majority of the specimens were tested at an age of about 5 days, but specimen M4A had to be held to age 15 days before the concrete strength reached 4000 psi.

After stripping and sealing the specimens, the prestressing bars were threaded through the holes formed in the specimens, and were each stressed to 40 kips tension. The outer bearing plates were then bolted in place.

2.4 Initial Cracking

Before testing, a crack was formed in each of the shear planes of each specimen. This was done by pressing vee-shaped steel bars into opposite vee-grooves on the front and back faces of the specimen, using the same Baldwin testing machine used for the shear tranfer tests. The opening of the crack was taken as the average reading of dial gages mounted across the crack at each end of the shear plane. Measurements were also made of the strain in the shear transfer reinforcement at the shear plane.

The objective in the cracking process, was to form a crack with a residual width of 0.01 in. after the load was removed from the vee-shaped steel bars. To achieve this, it was found to be necessary to load the specimen until an average crack width under load of about 0.025 in. was produced. This was considerably greater than had been necessary in the smaller scale specimens tested previously. It is believed the difference in behavior is due to bond slip occurring over a larger length of bar in the larger specimens than in the small specimens, leading to greater crack widths under load as a result of elastic strain in the bars. The load required to produce a crack width of 0.025 in. was found to decrease as the rebar size increased. This is thought to be due to the fact that, for a given load on the specimen, the bond stresses would be greater for the large size bars than for the smaller size bars, hence the load at which extensive bond slip would occur would decrease as the rebar diameter increased.

The maximum crack width under load and the residual crack width for each of the two cracks in each specimen, are shown in Table 2.2 Also shown in this

table are the maximum stress in the rebar under load, and the residual stress in the rebar after the cracking process was completed, at each of the two cracks in each specimen.

2.5 Testing Arrangements and Instrumentation

The specimens were tested using a 2.4 million pound capacity, Baldwin hydraulic testing machine. The specimen was supported on the two lower bearing strips, (see Fig. 2.1,) through roller bearings resting on the base plate of the testing machine, as may be seen in Fig. 2.2. The roller bearings were provided to ensure that lateral dilation of the specimen would not be restrained by the testing machine base.

The load was applied concentrically to the middle part of the specimen, through a double thickness 24 x 20 in. steel plate, attached to the end of a steel box section extension of the upper cross-head of the testing machine, as shown in Fig. 2.2. To ensure a uniformly distributed load on the specimen, a sheet of ½ in. thick fiber board was placed between the steel plate and the top face of the specimen, and a spherical seat was provided between the steel plate and the end of the cross-head extension. The steel box section cross-head extension was strain gaged, so that it could be used as a load cell to monitor the load during tests.

Both the slip (or relative motion parallel to the shear plane of the concrete on opposite sides of the crack,) and separation (or relative motion normal to the shear plane of the concrete on opposite sides of the crack,) were measured continuously, for both shear planes, during the shear transfer tests. The measurements were made using linear differential transformers as the sensing elements of slip and separation gages, which were attached to reference points embedded in the face of the specimen. The separation gages

were located at mid-height of the shear planes, and the slip gages were located 3 inches away. The embedded reference points were 1½ inches either side of the shear planes. The slip and separation gages were calibrated directly before test by imposing known displacements on them.

One eighth inch gage length, foil type, electrical resistance strain gages, were attached to one of the shear transfer reinforcing bars located near mid-height of the shear planes. One gage was located where the bar crossed each of the two shear planes, and an additional gage was attached to the bar 8 inches from shear plane No. 2. The gages were attached to the inside face of the bar on a horizontal diameter, so as to avoid registering flexural strains due to dowel action of the reinforcement. The gages were sealed and were covered with a strip of butyl rubber, so that they should not be subjected to forces from the adjacent concrete, either during the initial cracking procedure or during the shear transfer test.

The strain gages, the slip and separation gages, and the load cell were monitored continuously by a Sanborn strip chart recorder.

2.6 Testing Procedures

2.6.1 Monotonic Loading Tests - The specimen was first subjected to a monotonically increasing load up to an arbitrarily defined service load, equal to half the load corresponding to the calculated ultimate shear. The load was then reduced to zero. The specimen was then subjected to a monotonically increasing load until failure occurred. Failure was considered to have occurred when the applied load could not be increased further, and slip and separation both increased rapidly.

The ultimate shear was calculated using the shear-friction equation contained in Sec. 11.15 of ACI 318-71.

$$V_u = \phi A_{vf} f_y \mu \qquad (2.1)$$

In calculating the ultimate shear, the capacity reduction factor ϕ was taken as unity, since both the material strength properties and the dimensions of the specimens were accurately known. The coefficient of friction μ, was taken as 1.4, as prescribed for a crack in monolithic concrete. The actual value of f_y was used, although this was in excess of 60 ksi in all cases. In the case of M14A and C14A, the upper limit of 800 psi for the calculated ultimate shear stress specified in Sec. 11.15.3, was ignored.

2.6.2 Cyclically Reversing Shear Tests - The specimen was first subjected to a monotonically increasing load, up to 50 percent of the load corresponding to the ultimate shear calculated using Eq. (2.1). The load was then reduced to zero. The specimen was then lifted from its supporting bearings, by chains hanging from the testing machine cross-head and connected to the swivel lifting plates located at the middle of each end face of the specimen. While hanging from the cross-head, the specimen was inverted, as shown in Fig. 2.3. It was then lowered onto the roller bearings and the loading plate was brought into contact with the top of the specimen. The load was then once again increased monotonically to 50 percent of the load corresponding to the calculated ultimate shear, and subsequently reduced to zero. This second loading produced shear in the shear planes, of opposite sign to that produced by the first loading. The specimen was lifted and rotated back to its starting position. This completed one cycle of loading.

The process described above was repeated until 10 cycles of loading had been completed. The maximum positive and negative values of shear were then increased by 8 percent of the calculated shear transfer strength, i.e. to

$\pm$ 58 percent of V_u (calc.) for the next 5 load cycles. After each succeeding 5 cycles of load, the maximum positive and negative values of shear were increased by the same increment of 8 percent of the calculated shear transfer strength. This process was repeated until failure of the specimen occurred.

III - TEST RESULTS

3.1. Ultimate Strength and Loading History

The ultimate shear transfer strengths of the monotonically loaded specimens are given in Table 3.1. The loading history and the ultimate shear transfer strength, of each of the specimens subjected to cyclically reversing loading, are shown in Table 3.2.

The ultimate shear is defined as the maximum shear carried by one of the shear planes of the specimen during the test.* In a cyclic loading test this may be either the maximum shear to which the shear plane has been cycled, or the maximum shear reached when the maximum shear was being increased at the end of a group of cycles of loading to a constant maximum shear.

Specimen failure was characterized by both slip and separation increasing rapidly, with the load carried by the specimen either held constant or decreasing.

3.2 Specimen Behavior

3.2.1 Monotonic Loading Tests - No damage to or cracking of the concrete, was observed during both the initial loading and the reloading to service load. Slip and separation occurred at all levels of load, as may be seen in Figs. B1 through B10; however, the values at service load were very small. In Table 3.3 are shown values of the slip due to applying the service load, both on first loading and on reloading, together with the residual slip on removal of the service load after first loading. Also shown in Table 3.3 are the secant shear stiffnesses at service load, on both first-loading and on reloading.

A few fine diagonal tension cracks formed adjacent to the shear planes at loads about 25 percent above the service load. These cracks grew in length as the load was increased, but did not exceed 0.01 in. in width until very close to the ultimate shear. Typical crack patterns after failure are shown in Fig. 3.1.

---

*Because of the symmetry of the specimen, and of the loading and support systems, it was assumed that the shear in each shear plane was equal to half the load applied to the specimen.

At loads approaching ultimate, cracks formed in the top face of the center part of the specimens, around the perimeter of the loading head. This was apparently due to the high bearing stress under the loading head, which was approximately equal to f'_c at ultimate. These cracks propagated only a few inches into the concrete in most specimens, travelling diagonally outward. In some cases they linked with the cracks in the shear plane a few inches from the top of the specimen. In specimens M4A and C4A these cracks travelled almost vertically, parallel to the front and back faces of the specimen, and linked with splitting cracks in the plane of the shear transfer reinforcement. After the test of C4A, it was possible to pry off the concrete along the plane of this crack, over the whole depth of the specimen.

In some specimens, compression spalling of the surface of the concrete occurred close to the bearing shoes, at loads approaching failure. This distress was locallized, however, and is not thought to have affected the shear transfer behavior of the specimens.

The slip and the separation both increased at an increasing rate as failure was approached. The values of the slip and the separation at ultimate strength are listed in Table 3.1, together with the angle of inclination to the shear plane, of the direction of relative motion of the two faces of the crack at ultimate.

Failure occurred so abruptly in the case of M6A, M9A and M18A, that it was not possible to obtain slip and separation data after the maximum load was reached. Failure was still fairly abrupt in the other specimens, probably due to release of elastic strain energy from the testing machine, which was working near to its maximum capacity at ultimate load.

The variation of the stress in the shear transfer reinforcement with the applied shear and with the measured separation across the crack, is shown in

Fig. B11 through B18 and Fig. B19 through B26 respectively.

3.2.2 Cyclic Loading Tests - In the cyclic loading tests also, no damage to or cracking of the concrete, was observed during loading to service load. Fine diagonal tension cracks were first observed at maximum shears a little above service load. These cracks initiated close to the shear planes, and grew in length as the maximum shear per load cycle was increased. The width of the cracks did not exceed 0.01 in. until close to failure. The typical appearance of a specimen after failure can be seen in Fig. 3.2.

The general behavior of these large scale test specimens, and the form of the shear-slip and slip-separation curves, was similar to those observed in the previous cyclic loading tests [2] of smaller scale specimens.

Samples of the shear-slip and slip-separation curves for each specimen, are shown in Appendix C. These curves show examples of behavior at service load, at intermediate loads and approaching failure. Also shown in Appendix C are shear - steel stress curves, and separation - steel stress curves, for every fifth load cycle. These data relate to the cracked shear-plane in which failure eventually occurred. In these figures, positive shear and positive slip are shear and slip measured in the direction in which shear was first applied to the specimen. The separation plotted, is the change in separation due to application of shear to the specimen. To obtain the total separation, the initial crack width must be added to the separation shown in the figures of Appendix C.

As can be seen from the figures of Appendix C, the response of the specimens changed as the number of cycles of loading, and the level of loading increased. Specimen response to the first cycle of loading is characterized by a gradual reduction in shear stiffness as the applied shear is increased, in

both positive and negative directions; and by retention of most of the slip produced by the maximum shear, until the shear reduces to about half of its maximum value. Response to succeeding cycles of load is characterized by a low shear stiffness at low values of shear, and a gradual increase in shear stiffness with increase in shear in both the positive and negative directions.

The "Effective Stiffness" will be defined as the slope of a line joining the points of maximum positive and negative shear and slip, in the shear-slip hysteresis loop for a particular cycle of load. In Figs. 3.3 through 3.6 are shown the effective stiffness and the stiffness near zero shear for successively increasing cycles of load, for each of the specimens. It can be seen that both stiffnesses decrease as the number of cycles of load increase. The shear stiffness for low values of shear also decreases relative to the effective stiffness, for the same cycle of loading, as the number of load cycles increases.

The increase in slip with each loading cycle was initially very small, but increased as the value of the maximum applied shear increased. As the load which caused failure was approached, the tangent shear stiffness tended to decrease as the maximum shear was approached in each cycle. Failure occurred when the shear stiffness under increasing load reduced to zero, after which the slip increased rapidly, even though the shear was decreasing.

The slip-separation curves are approximately crescent shaped. Their exact shape, and their symmetry with respect to the separation axis, was presumably a function of the profile of the crack faces in each particular case. As the maximum shear per load cycle increased, both slip and separation at maximum shear increased. Approaching failure, the separation at zero shear also increased substantially with each cycle of loading. This increase in separation at zero shear, occurred in the same load cycles in which the tangent shear stiffness started to decrease approaching maximum shear.

IV - DISCUSSION OF TEST RESULTS

4.1 General Behavior

When shear acts along a crack which is crossed at right-angles by reinforcing bars, shear is transferred across the crack as a result of three types of action.

1. By friction between the faces of the crack; due to the tension force developed in the reinforcement, as a result of separation of the rough crack faces when slip occurs.

2. By direct bearing of asperities projecting from the faces of the crack.

3. By dowel action of the reinforcing bars crossing the crack; i.e. direct resistance of the bars to shearing action at the crack.

The relative importance of each of these contributions to shear transfer resistance varies with the intensity of the shear stress and the prior shear loading history.

4.1.1 Monotonic Loading Tests - For applied shears up to about half the ultimate shear, the slip along the crack in these tests was very small, (typically less than 0.005 in.,) and the shear-stiffness was consequently very high. This can be seen in Figs. B1 through B8 and also in Table 3.3. The separation across the crack was also very small at this stage of loading, being about the same as the slip. As a consequence of the small separation across the crack, the reinforcement was not strained very much due to the applied shear. This can be seen in Figs. B11 through B18, in which the measured shear transfer reinforcement stress is plotted against the applied shear. It can be seen that the increase in reinforcement stress up to "service load" was typically less than 5 ksi, while the average measured total reinforcement stress at service load in all the specimens was 11.6 ksi. It appears therefore, that in the service load range, only a small part of the shear transfer resis-

tance developed, is due to friction between the crack faces as a result of straining of the reinforcement caused by separation across the crack faces.

The small slips which occurred at service load lead to the conclusion that, at this stage of loading, little is contributed to shear transfer resistance by dowel action of the reinforcing bars crossing the crack. The average slip at service load was 0.0022 in.. Dowel action tests at Cornell University[6] showed that for a No. 11 reinforcing bar, the dowel action shear resistance was 3.8 kips for a slip of 0.0022 in. on first loading. In specimen M11A, 5 No. 11 bars cross the shear plane. It appears therefore that of a service load shear of 347 kips for M11A, dowel action could only have resisted about 19 kips, i.e. about 5 percent.

For the same specimen M11A, the clamping force across the crack corresponding to the average measured reinforcement stress at service load would be 90.5 kips. Using a coefficient of friction of 0.8, this clamping force would develop a shear resistance of 72 kips, i.e. about 21 percent of the service load shear. It appears therefore that at service load, 256 kips or 74 percent of the shear transfer resistance was being supplied by direct bearing of asperities projecting from the faces of the crack.

When the applied shear is increased beyond about 50 percent of the ultimate shear, both slip and separation increase more rapidly. This is probably a result of a combination of shearing off and over-riding of asperities on the crack faces. The more rapid increase in separation also results in a more rapid increase in reinforcement stress, so that at ultimate shear the recorded stresses were at or very close to the reinforcement yield point. (The average reinforcement stress measured at ultimate shear was 62.7 ksi.)

If it is assumed that, at ultimate shear, the reinforcement developed its yield strength, the average clamping force for all specimens would have been 540 kips. The corresponding shear resistance due to friction would have been 432 kips, or about 40 percent of the average of the measured ultimate shears. That is, about 60 percent of the ultimate shear was being resisted by a combination of dowel action and resistance to shearing off of asperities on the crack faces. The proportions of the ultimate shear carried by these two actions individually, cannot be deduced from the available data. Unfortunately, the Cornell University dowel action tests [6] only provide data for first loading up to a slip of 0.016, which occurred at a shear of 15 kips. At this slip, specimen M11A was carrying a shear of 840 kips. If it is assumed that the dowel resistance of the No. 11 bars was not affected by the axial tension stress in them, the resistance to shear by dowel action in M11A at a slip of 0.016 in. was 75 kips or 9 percent of the applied shear. It appears therefore that at ultimate shear, a major part of the shear transfer resistance is provided by the resistance to shearing off of asperities on the faces of the crack. Shear transfer failure after monotonic loading is probably initiated by the shearing off of asperities on the faces of the crack.

The direction of motion of one face of the crack relative to the opposite face is inclined at angle α to the crack, where $\alpha = \tan^{-1}$ (separation/slip). The average value of α at ultimate shear in these large scale tests was 44°. The average value of α at failure in previous smaller scale shear transfer tests[1][7] of cracked, monolithic specimens made of sand and gravel concrete was 32°. The larger value of α in the large scale tests, (A_{cr} = 1000 in.^{2}), as compared to the value found in the smaller scale tests, (A_{cr} = 50 in.^{2}), is probably due to the crack in the large specimen having a more irregular profile

than that in the smaller specimen. In both cases, the crack was produced by applying line loads simultaneously to front and back of the specimen. However, in the large specimen the line loads were 25 inches apart, while in the smaller specimen they were only 5 inches apart. It appears likely that the path of the crack would "wander" from the shear plane more in traversing the 25 inch thickness of the large specimens than in traversing the 5 inch thickness of the smaller specimens. This greater irregularity of the crack profile, i.e., greater roughness of the crack faces, may also have affected the ultimate shear strengths attained in these tests, as is discussed in Section 4.2.2.

The average slip at failure in the crack that failed, in these tests was 0.063 in. as compared with an average slip at failure of 0.022 in. the previous[1][7] comparable smaller scale shear transfer tests. It is believed that this difference in behavior is due to the greater length of reinforcing bar over which bond slip could occur in the large scale specimens as compared to the smaller scale specimens. (About 25 inches/shear plane as compared with 10 inches.) In order to develop the yield strain of the reinforcing bars, a larger total elongation of the bars would be necessary in the large scale specimens than in the smaller scale specimens, i.e. a larger separation across the crack would be necessary in the larger specimens than in the smaller specimens. Hence a larger slip would be needed in the large scale specimens than in the smaller scale specimens in order to develop the yield strength of the shear transfer reinforcement.

4.1.2 Cyclic Loading Tests - The general behavior of these large scale specimens was very similar to that previously observed[2] in cyclic loading tests of smaller scale specimens. The behavior of these large scale specimens

supports the following hypothesis concerning the mechanics of shear transfer behavior, which was proposed previously[2] on the basis of the smaller scale tests.

At low values of shear, on first loading, the shear stiffness is very high and very little separation occurs. As discussed in 4.1.1, this behavior indicates that at this stage most of the resistance to shear is due to the direct bearing of asperities on the faces of the crack. Slip would result from local crushing of asperities and would be very small. As increasing numbers of the asperities are crushed, the intensity of bearing pressure on the remaining asperities would increase more rapidly than the applied shear. The deformations would therefore increase more rapidly, and the shear stiffness would therefore decrease. This is the behavior observed in the first quarter of the first cycle of loading.

When the shear is reduced to zero, the only force tending to return the slip to zero is that due to the elastic deformation of the reinforcing bars and of the concrete against which they bear, as they develop dowel action. This restoring force is resisted by friction and any interlocking effect that may exist between the crack faces. The slip cannot return toward zero until the applied shear becomes less than the net restoring force. This would account for the observed behavior on unloading.

As the shear is increased in the reverse direction for the first time, the mechanisms by which shear resistance is developed will be the same as on first loading. The behavior on unloading will also be similar to the behavior on first unloading in the opposite direction.

In subsequent load cycles, in order for the asperities to be brought into bearing, a slip must occur almost equal to the maximum slip which has previously

occurred. Whilst this slip is occurring, shear resistance is developed only by dowel action of the reinforcement and by any small friction existing between the crack faces. The shear stiffness at low shears is consequently much lower than on first loading. When the asperities come into bearing, their resistance to deformation results in a sharp increase in resistance to shear and an increasing tangent shear stiffness until maximum shear is reached.

On removing the shear, the response and probable mechanism of behavior are the same as in the first cycle. When the shear is reversed in direction, the response and mechanism of behavior is the same as described above.

When the maximum shear is increased at the end of each group of cycles, additional damage is done to the surfaces of the crack by shearing off of additional asperities, and the slip increases. With each cycle of load, the crack faces are abraided and become smoother. This reduces the resistance to shear which can be developed at low shears, resulting in a reduction in shear stiffness at low values of applied shear.

As the maximum shear per cycle increased it was observed that both the slip and separation at maximum shear increased. This would lead to the development of larger dowel forces and tensile strains in the bars. It is therefore probable that, approaching failure, an increasing fraction of the shear is resisted by friction between the crack faces and by dowel action of the reinforcing bars.

In the load cycles preceding failure, the separation at zero shear increases markedly, the tangent shear stiffness approaching maximum shear starts to decrease, and both slip and separation at maximum shear increase significantly in each load cycle. This behavior is probably due in large part to the local crushing of the crack faces. Some of the mortar particles produced by this crushing becomes trapped between the faces of the crack, wedging it open,

and acting like "ball bearings" when the crack faces move relative to one another. Progressive yielding of the reinforcing bars, under the combination of direct tension and of bending and shear resulting from dowel action, will also contribute to deterioration in behavior at this stage. (The effect on the stress in the reinforcement, of increasing separation at zero shear, can be seen in Figs. C41 through C47.)

It can be seen in Figs. 3.3 through 3.6, that the effective stiffness and the stiffness near zero shear, both decrease substantially as the number of cycles of loading increase. The effective stiffness decreases with increasing cycles of load, even without any increase in the maximum shear per load cycle. This behavior contrasts with that observed previously[2] in the tests of smaller scale specimens. In that case, after about the first five cycles of loading, and for maximum shears less than about 75 percent of ultimate shear, the slip at maximum shear per cycle did not change significantly, (i.e. the effective stiffness did not change significantly.) This difference in behavior may be related to a progressive break-down in bond between the shear transfer reinforcement and the concrete in the large scale specimens, when subjected to a cyclic load of constant amplitude.

In Fig. 4.1, the effective stiffness, (expressed as a percentage P_{se} of the initial effective stiffness,) has been plotted against the number of load cycles, (expressed as a percentage P_c of the number of load cycles to cause failure.) It can be seen that, for the incrementally increasing loading history used in these tests, the effective stiffness of the large scale specimens is approximately related to the number of cycles of loading by,

$$P_{se} = 100 - 0.9P_c \qquad (4.1)$$

Also plotted in Fig. 4.1 are data from the smaller scale (A_{cr} = 50 in.^{2}), cracked monolithic specimen LC2, tested previously[2]. This specimen had a reinforcement index ρf_y, approximately the same as the average ρf_y for the large scale specimens. It can be seen that after the first five cycles of load, the effective stiffness remained at about 90 percent of the initial effective stiffness, until the number of cycles of load reached about 60 percent of the load cycles to cause failure, (and the shear reached about 75 percent of the ultimate shear.) Under subsequent cyclic loading, the effective stiffness decreased at an increasing rate as failure was approached. As already indicated above, it is thought that the difference in behavior may be due to the more favorable bond and anchorage conditions in the smaller scale specimens than in the large scale specimens.

The ratio of the stiffness near zero shear (S_o) to the effective stiffness (S_e) in the same load cycle, varied from about 0.4 for the first load cycle to about 0.3 for the load cycle before failure; but there is considerable scatter in the data. In Fig. 4.2, the stiffness near zero shear (expressed as a percentage of the initial effective stiffness), is plotted against the number of cycles of load (expressed as a percentage of the number of load cycles to cause failure.) Also plotted in Fig. 4.2 is a line which corresponds to the equation,

$$S_o/S_e = 0.40 - P_c/1000 \qquad (4.2)$$

This equation implies that the ratio S_o/S_e varies linearly with the number of load cycles, from a value of 0.4 for the initial cycle of loading, to a value of 0.3 just before failure occurs. It can be seen that although there is considerable scatter in the data, the line corresponding to equation (4.2) reflects the trend of the data reasonably well.

It should be noted that the slip and separation data obtained in the test of specimen C4A is somewhat erratic, and in some respects is not consistent with the data obtained in the tests of C8A, C10A and C14A. It is believed that the data obtained from specimen C4A is not so reliable as that obtained in the other three cyclic loading tests.

In Tables 4.1 through 4.3 are given the maximum shear, the energy dissipated per load cycle, (i.e. the area within the shear-slip hysteresis loop, A_h), the energy absorbed as the load is increased in each cycle, (i.e. the area A_1 shown in Fig. 4.6b), the damping factor, the effective stiffness and the stiffness near zero shear, for approximately every fifth cycle of loading of specimens C8A, C10A and C14A. The damping factor has been calculated both according to Jacobsen[10] and according to Hawkins et al.[11].

Jacobsen proposed that the damping factor be calculated using,

$$\beta_1 = \frac{1}{2\pi} \frac{\text{Area within hysteresis loop.}}{\text{Area under "skeleton curve".}} \tag{4.3}$$

Jacobsen proposes that for hysteresis curves of the type obtained in these tests, the skeleton curve should be as indicated in Fig. 4.4. No attempt was made to draw skeleton curves for the shear-slip hysteresis loops obtained in these tests. Instead, it was assumed that the skeleton curve divides the hysteresis loop into two equal areas, and hence equation (4.3) can also be stated as,--

$$\beta_1 = \frac{1}{2\pi} \cdot \frac{A_h}{(A_1 - A_h/2)} \tag{4.3A}$$

where A_h and A_1 are as indicated in Fig. 4.6. The damping factor calculated in this way has a maximum possible value of 0.318.

Hawkins et al.[11] proposed that the damping factor be calculated using,--

$$\beta_2 = \frac{1}{2\pi} \cdot \frac{\text{Energy dissipated in one load cycle.}}{\text{Energy absorbed in increasing the load in one load cycle}}$$

$$= \frac{1}{2\pi} \cdot \frac{A_h}{A_1} \qquad (4.4)$$

where A_h and A_1 are also as indicated in Fig. 4.6. The damping factor calculated in this way has a maximum possible value of 0.159.

The concept of an equivalent viscous damping factor is being strained severely when it is used to characterize hysteretic behavior of the type found in these shear transfer tests. The significance of individual numerical values obtained is questionable, but it is thought that the trends in variation of the values are of interest. In Figs. 4.3 and 4.5, the damping factors β_1 and β_2 are plotted against number of load cycles (expressed as a percentage of the number of load cycles to cause failure.) The results of the three tests are very consistent. The damping factor decreases after the first cycle of loading, as the hysteresis loop becomes pinched in shape. Then, until about 80 percent of the cycles to cause failure, the damping factor is essentially constant, indicating reasonably stable conditions regarding damage to the crack faces. As further cycles of loading are applied, the damping factor increases at an increasing rate. This rapid increase in the damping factor coincides with a significant increase in separation across the crack at zero shear, and is probably related to the occurrence of severe damage to the crack faces as failure is approached. It can be seen from Tables 4.1 through 4.3, that during this same time the energy dissipated per cycle increases by about 300 percent in the last 5 load cycles before failure.

In Figs. 4.7 through 4.10 comparisons are made of the shear-slip relations for companion specimens subjected to monotonic loading and to cyclic loading. The data shown in each case is that relating to the cracked shear plane in which failure eventually occurred. For the cyclic loading tests, the slips shown are equal to half the change in slip as the shear changes from the maximum positive value to the maximum negative value in a particular load cycle. It can be seen that in the case of the specimens reinforced with #8, #10, or #14 bars, the slip at a given level of load was always greater in the specimen subjected to cyclic loading than in the companion specimen subject to monotonic loading. As indicated above, there are some doubts as to the reliability of the data obtained from the test of specimen C4A and it is believed that the comparison shown in Fig. 4.7 should be discounted. The less stiff behavior of the other specimens subjected to cyclic loading, as compared to that of companion specimens subject to monotonic loading, is probably due to the progressive abrasion of the crack faces as they are rubbed backward and forward against one another.

4.2 Ultimate Strength

4.2.1 Monotonic Loading Tests - In Table 4.4 a comparison is made for each specimen, between the measured ultimate shear strength and the ultimate shear transfer strength calculated, (1) using the shear-friction equations,

$$V_u\ (calc)_1 = \phi A_{vf} \mu \tag{4.5}$$

$$= \phi A_{cr} \rho f_y \mu \quad \text{but} \quad \nmid \phi 0.2 f'_c A_{cr} \text{ nor } 800\, \phi A_{cr} \tag{4.5A}$$

and, (2) using the modified shear friction equation,

$$V_u\ (calc)_2 = \phi [0.8 A_{vf} f_y + 400\, A_{cr}] \tag{4.6}$$

$$= \phi A_{cr} [0.8\, \rho f_y + 400] \quad \text{but} \quad \nmid \phi 0.3 f'_c A_{cr} \tag{4.6A}$$

Since dimensions and material strengths were known accurately, ϕ was taken as 1.0 in the above equations.

It is seen that both equations yield conservative estimates of the ultimate strengths of these specimens. It therefore appears that either of these equations could be used for design purposes in situations involving the use of large diameter bars, providing that adequate anchorage is provided for the bars on each side of the shear plane.

If a straight, large diameter bar crossed a single crack and was anchored by bond only on each side of the crack, then there could be some question as to whether the yield strength of that bar could be developed as a result of separation occurring across the crack, due to shear acting along the crack. This, because bond slip would probably occur over a considerable length of bar on each side of the crack, requiring a large separation across the crack in order to strain the reinforcement to its yield point. In Fig. 4.11 a comparison is made of the values of the ratio (Reinforcement Stress)/(Separation), measured in these large scale push-off tests, with a comparable ratio obtained from anchorage bond pull-out tests[8,9] of large diameter reinforcing bars. In the case of the pull-out tests, the value plotted is equal to the ratio (two times displacement at loaded end of embedded bar)/(stress in bar). This is appropriate, since in the push-off tests the bars are being pulled from the concrete on both sides of the crack. The agreement is good for the #10 bar and reasonably good for the #14 and #18 bars, despite the fact that in the push-off specimens anchor plates were provided at each end of each #14 and #18 bar. If a lower bound value of 1000 ksi/in. is assumed for the large diameter bars, a separation of 0.06 in. would be required to develop a yield strength of 60 ksi. Separations of this magnitude were obtained in some of the push-off specimens tested. It therefore appears that under monotonic loading, it should be possible to develop the yield strength of straight large diameter bars crossing a crack, and relying on bond for anchorage.

If moment acts across the crack as well as shear acting along it, there would be no concern regarding development of the yield strength of bars crossing the crack, since the separation across the crack would not then depend only on the shearing action and the roughness of the crack faces.

It is not possible to show the effect of reinforcing bar diameter on the shear transfer strength directly, by plotting the measured shear transfer strength, since the value of the reinforcement parameter ρf_y varied between the specimens, as previously discussed. The modified shear friction equation (4.2) has previously been shown to reflect the effect on ultimate shear transfer strength, of change in ρf_y. In Fig. 4.12, therefore, a plot has been made of $V_u(\text{test})/V_u(\text{calc.})_2$ versus reinforcing bar diameter, where $V(\text{calc.})_2$ is the shear transfer strength calculated using the modified shear friction equation (4.6). This plot shows the change in ultimate shear transfer strength if the reinforcing bar size is changed, while holding the reinforcement parameter ρf_y constant. It can be seen that, for bar diameters greater than 1 inch, the ultimate shear transfer strength tends to decrease as the bar diameter increases. The ultimate strength using #18 bars is 15 percent less than when #8 bars are used. This trend may be due to the development of larger dowel forces per bar in the larger reinforcing bars, because of their greater flexural stiffness. These larger dowel forces could lead to local crushing and splitting of the concrete adjacent to the reinforcing bars, leading to the reduction in shear transfer strengths seen in Fig. 4.12. However, despite the reduction in strength with increase bar diameter, all the specimens had ultimate strengths in excess of the calculated strength. It is therefore, not considered necessary to reduce the calculated ultimate shear transfer strength when large diameter reinforcing bars are used.

Specimen M4A yielded a much lower ultimate strength than the other specimens. On examination after failure, a crack was found to have occurred in the plain of the reinforcing bars, parallel to the front and back faces of the specimen. This crack extended downward from the edge of the loading head on the top of the center section of the specimen. It is believed that this crack may have occurred due to a combination of four effects, -- (1) high splitting tensile stresses due to anchorage bond stresses, caused by close spacing of the reinforcing bars, (less than 2 in. centers); (2) splitting tensile stresses caused by bearing of the bars on the concrete as dowel action developes; (3) displacement of concrete in the plane of the bars by the large number of bars present; and (4) the development of spalling tensile stresses on the top face of the specimen, at the edge of the loading head. Similar cracks were found in the companion cyclically loaded specimen C4A. Despite its relatively low strength, this specimen was still stronger than the calculated ultimate strength.

The relatively high values of ultimate strength obtained in these large size push-off specimens, are thought to have been due to the greater roughness of the crack faces in these large specimens, as compared with the smaller scale specimens tested previously. The reason for this greater roughness was discussed in Section 4.1.1. The greater roughness of the crack faces would enable a larger shear to be resisted by direct interlock of asperities on the crack faces.

4.2.2 Cyclic Loading Tests - The ultimate strengths of the cyclically loaded specimens were in all cases less than the ultimate strengths of their companion monotonically loaded specimens. In Table 4.5 a comparison is made of the ultimate strengths of cyclically and monotonically loaded companion specimens. Except in the case of the specimens reinforced with #4 bars, the

strength under cyclic loading was about 80 percent of the strength under monotonic loading. This is in agreement with the results of previous cyclic loading tests[2] of smaller scale push-off specimens. The higher ratio for specimen C4A is probably due to the ultimate strength of the companion monotonically loaded specimen being low, rather than the strength of C4A being unusually high. This is apparent in Fig. 4.12. It therefore appears that the recommendation for design previously made[2], i.e., to assume that the strength under cyclic loading is 80 percent of the strength under monotonic loading, is also valid when large diameter reinforcing bars are used. It is probable that the reduction in shear transfer strength under cyclic loading is mainly due to a progressive abrasion of the crack faces, leading to a reduced contribution to shear transfer resistance from direct interlocking of asperities on the crack faces. It is also probable that under cyclic loading, the shear resistance due to dowel action would reduce due to fatigue break down of the concrete against which the reinforcing bars are bearing.

The shear transfer strengths developed in these tests are considerably in excess of those obtained in tests at Cornell University[6], although the general form of the shear-slip curves was similar in both cases. The difference in behavior is probably due to the positive anchorage provided for the shear transfer reinforcement in these tests, and also due to the provision of reinforcement adjacent to the shear plane, which prevents a premature failure due to excessive cracking of the concrete adjacent to the shear plane. In a design situation, it is necessary to consider both the transfer of shear across the crack and the ability of the adjacent concrete to carry the shear force, and to provide reinforcement to resist diagonal tension cracking if necessary.

V - PRINCIPAL CONCLUSIONS

Based on the test data reported, the following conclusions may be drawn concerning shear transfer across a crack in monolithic concrete, crossed at right-angles by reinforcing bars.

1. The shear transfer strength of cracked monolithic concrete, subjected to monotonic loading, may conservatively be calculated by either the shear-friction equation (4.5) or by the modified shear-friction equation (4.6), regardless of reinforcing bar size, providing that adequate anchorage is provided for the reinforcing bars.

2. For a given reinforcement index, the shear transfer strength of cracked monolithic concrete decreases about 15 percent as the reinforcing bar size increases from #8 to #18. (However, the strength is still greater than the strength calculated using either Eq. (4.5) or Eq. (4.6).)

3. The shear transfer strength of cracked monolithic concrete subjected to cyclically reversing shear may, for design purposes be taken as 80 percent of the calculated shear transfer strength for monotonic loading.

4. At service load, under monotonic loading, the transfer of shear across a crack is primarily due to direct bearing of asperities on the faces of the crack, secondarily due to friction between the crack faces, and to a very minor extent due to dowel action of the reinforcement.

5. At ultimate strength, under monotonic loading, the transfer of shear across a crack is primarily due to both direct bearing of asperities on the faces of the crack and to friction between the crack faces, and to a minor extent due to dowel action. (The proportionate contribution of friction to shear transfer resistance can be expected to increase as the reinforcement index ρf_y increases.)

6. Under cyclic loading, it is probable that at ultimate strength the contributions to shear transfer strength of direct bearing of asperities and of dowel action of the reinforcement, are both reduced relative to their contributions under monotonic loading.

7. At a given level of shear stress, the shear stiffness under cyclic loading is less than under monotonic loading.

8. Under cyclic loading, the effective shear stiffness decreases as the number of load cycles increases; and just before failure the effective stiffness will have decreased to about 10 percent of its initial value.

9. Under cyclic loading, the shear stiffness near zero shear is initially about 40 percent of the effective stiffness, and decreases to about 30 percent of the effective stiffness for the same load cycle, as failure is approached.

10. Under cyclic loading, the hysteretic damping is approximately constant after the first cycle of loading, up to about 80 percent of the cycles of loading causing failure; after which it increases rapidly.

11. In design situations involving shear transfer across a crack, attention must also be paid to the diagonal tension cracking resistance of the concrete adjacent to the primary crack, and appropriate reinforcement must be provided if necessary.

REFERENCES

1. Mattock, A.H., "Shear Transfer Under Monotonic Loading, Across an Interface Between Concretes Cast at Different Times," University of Washington, Structures and Mechanics Report SM76-3, September, 1976.

2. Mattock, A.H., "Shear Transfer Under Cyclically Reversing Loading, Across an Interface Between Concretes Cast at Different Times," University of Washington, Structures and Mechanics Report SM77-1, June, 1977.

3. Hofbeck, J.A., Ibrahim, I.O. and Mattock, A.H., "Shear Transfer in Reinforced Concrete," Journal of the American Concrete Institute, Vol. 66, No. 2, Feb. 1969, pp. 119 - 128.

4. "Building Code Requirements for Reinforced Concrete", (ACI 318-71), American Concrete Institute, 1971.

5. Viest, I.M., "Investigation of Stud Shear Connectors for Composite Concrete and Steel I-Beams," Journal of the American Concrete Institute, Vol. 52, No. 8, April 1956, pp. 875 - 891.

6. White, R.N., and Gergely, P., "Shear Transfer in Thick Walled Reinforced Concrete Structures Under Seismic Loading," Annual Report for NSF Grant AEN 73-03178 A01, Dept. of Structural Engineering Report No. 75 - 10, Cornell University, Dec. 1975.

7. Mattock, A.H., "Effect of Aggregate Type on Single Direction Shear Transfer Strength in Monolithic Concrete," University of Washington, Structures and Mechanics Report SM74-2, August, 1974.

8. Rostasy, F.S., and Hognestad, E., "Pilot Bond Tests of Large Reinforcing Bars," Journal of the American Concrete Institute, Vol. 32, No. 5, Nov. 1960, pp. 576 - 579.

9. Hassan, F.M., and Hawkins, N.M., "Effects of Post-Yield Loading Reversals on Bond Between Reinforcing Bars and Concrete," University of Washington, Structures and Mechanics Report SM73-2, March 1973.

10. Jacobsen, L.S., "Damping in Composite Structures," Vol. 2 of Proceedings, 2nd World Conference on Earthquake Engineering, Tokyo and Kyoto, Japan, 1960, pp. 1029 - 1044.

11. Hawkins, N.M., Mitchell, D., and Hanna, S.N., "Effects of Shear Reinforcement on the Reverse Cyclic Loading Behavior of Flat Plate Structures," Canadian Journal of Civil Engineering, Vol. 2, 1975.

TABLE 2.1 - PROPERTIES OF TEST SPECIMENS

Specimen No.	No. of bars Crossing Shear Plane	Reinft. Area, A_{vf} ($in.^2$)	Reinft. Yield Point, f_y (ksi)	ρf_y (psi)	Concrete Compn. Strength f'_c (psi)	Concrete Tensile Strength(3) f_t (psi)
M4A	42	8.40	65.25	548	4075(2)	374
M6A	20	8.80	62.12	547	4125(2)	420
M8A	11	8.69	61.23	532	4800(2)	390
M9A	8	8.00	67.63	541	4650(2)	390
M10A	6	7.62	67.50	514	3940(2)	420
M11A	5	7.80	63.40	495	4190(2)	370
M14A	4	9.00	65.60	590	4300(2)	485
M18A	2	8.00	68.75	550	4300(2)	410
C4A	40	8.00	68.90	551	3470(1) 3730(2)	--- 411
C8A	11	8.69	60.75	528	4305(1) 5235(2)	--- 487
C10A	6	7.62	65.56	499	3850(1) 4120(2)	--- 368
C14A	4	9.00	65.60	590	3485(1) 4630(2)	--- 470

(1) Concrete strength at beginning of test, measured on 6 x 12 in. cylinders.

(2) Concrete strength at end of test, measured on 6 x 12 in. cylinders.

(3) Concrete splitting tensile strength measured on 6 x 12 in. cylinders.

TABLE 2.2 - DATA FOR INITIAL CRACKING

Specimen No.	Crack No.	Maximum Crack Width (in.)	Residual Crack Width (in.)	Maximum Steel Stress (ksi)	Residual Steel Stress (ksi)
M4A	1	0.030	0.012	56.7	16.4
	2	0.022	0.013	38.8	9.8
M6A	1	0.025	0.010	50.3	12.0
	2	0.024	0.010	48.1	9.8
M8A	1	0.023	0.009	26.2	4.7
	2	0.025	0.009	32.5	5.3
M9A	1	0.025	0.010	33.1	8.8
	2	0.025	0.011	35.2	6.6
M10A	1	0.023	0.010	23.3	1.1
	2	0.024	0.010	36.0	3.2
M11A	1	0.025	0.010	43.4	1.7
	2	0.026	0.011	41.0	1.9
M14A	1	0.025	0.010	--(1)	--(1)
	2	0.025	0.011	34.3	7.8
M18A	1	0.025	0.011	22.2	4.8
	2	0.025	0.011	--(1)	--(1)
C4A	1	0.024	0.010	24.2	12.8
	2	0.024	0.010	30.0	--
C8A	1	0.025	0.010	30.7	15.0
	2	0.025	0.010	26.5	14.0
C10A	1	0.023	0.011	10.4	2.8
	2	0.023	0.010	23.8	3.0
C14A	1	0.027	0.010	29.5	6.4
	2	0.026	0.010	16.0	9.3

(1) Defective gage.

TABLE 3.1 - RESULTS OF MONOTONIC LOADING TESTS

Specimen No.	Shear Plane and Crack No.	Slip at Failure (in.)	Separation at Failure (in.)	Angle[3] α (degrees)	Ultimate[4] Shear Strength (kips)
M4A	1	0.053	0.037	35	865
	2[1]	0.114	0.085	41	
M6A	1	0.023	0.030	52	1150
	2[1]	0.061	0.054	42	
M8A	1	0.022	0.010	25	1148
	2[1]	0.047	0.046	46	
M9A	1[2]	0.042	0.060	55	1150
	2[2]	0.046	0.035	42	
M10A	1	0.021	0.017	46	1010
	2[1]	0.059	0.070	57	
M11A	1[1]	0.081	0.068	42	1091
	2	0.051	0.033	37	
M14A	1	0.019	0.019	46	1137
	2[1]	0.065	0.060	46	
M18A	1[1]	0.052	0.048	42	991
	2	0.041	0.044	53	

(1) Crack that failed first.

(2) Both cracks failed simultaneously.

(3) Inclination to the shear plane of the slip-separation curves at ultimate shear.

(4) Shear carried by one shear plane.

TABLE 3.2(a) - RESULTS OF CYCLIC LOADING TESTS

Specimen No.	Loading History		Slip at[1] Failure (in.)	Separation[1] at Failure (in.)	Ultimate[2] Shear Strength (kips)
	Load Cycles	Range of Load $\pm$% of V_u (calc.)			
C4A	1-10	50			
	11-15	58			
	16-20	66			
	21-25	74			
	26-30	82			
	31-35	90			
	36-40	98			
	41-42	106	0.081	0.060	816
C8A	1-10	50			
	11-15	58			
	16-20	66			
	21-25	74			
	26-30	82			
	31-35	90			
	36-40	98			
	41-45	106			
	46-50	114			
	51-55	122			
	56	123	0.106	0.091	910
C10A	1-10	50			
	11-15	58			
	16-20	66			
	21-25	74			
	26-30	82			
	31-35	90			
	36-40	98			
	41-45	106			
	46-49	114	0.098	0.083	796

TABLE 3.2(b) - RESULTS OF CYCLIC LOADING TESTS

Specimen No.	Loading History		Slip at[1] Failure (in.)	Separation[1] at Failure (in.)	Ultimate[3] Shear Strength (kips)
	Load Cycles	Range of Load $\pm$% of V_u (calc.)			
C14A	1-10	50			
	11-15	58			
	16-20	66			
	21-25	74			
	26-30	82			
	31-35	90			
	36-40	98			
	41-45	106			
	46-48	114	0.060	0.047	940

(1) The values of slip tabulated are equal to half the change in slip between the maximum positive and negative shears in the last complete load cycle before failure.

(2) The values of separation tabulated are the averages of the values measured at the maximum positive and negative shears in the last complete load cycle before failure.

(3) Shear carried by one shear plane.

TABLE 3.3 - SERVICE LOAD BEHAVIOR IN MONOTONIC LOADING TESTS

Specimen No.	Service load shear stress (psi)	On 1st loading		Residual slip after loading ($in.x10^{-3}$)	On reloading	
		Slip ($in.x10^{-3}$)	Shear stiffness (ksi/in.)		Slip ($in.x10^{-3}$)	Shear stiffness (ksi/in.)
M4A	384	2.63	146	1.80	1.38	278
M6A	383	2.25	170	1.25	1.00	383
M8A	373	2.81	133	1.25	1.63	229
M9A	379	2.00	190	1.50	1.00	379
M10A	360	1.31	270	1.00	0.75	480
M11A	347	1.85	187	1.60	1.00	347
M14A	413	2.25	184	0	1.75	236
M18A	385	2.63	146	1.90	1.25	308

TABLE 4.1 - DEFORMATION BEHAVIOR OF SPECIMEN C8A

Load Cycle	$V_{max.}$ (kips)	A_h (lb.in./in.^{2})	A_1 (lb.in./in.^{2})	Damping Factor		Effective Stiffness (ksi/in.)	Stiffness Near Zero Shear (ksi/in.)
				β_1 (1)	β_2 (2)		
1	370	1.08	1.54	0.173	0.112	109	45
5	370	0.57	1.12	0.109	0.081	92	37
10	370	0.53	1.14	0.097	0.074	87	34
15	429	0.81	1.63	0.104	0.079	87	31
20	488	0.95	2.18	0.088	0.069	80	28
25	547	1.89	3.66	0.111	0.082	65	25
30	606	2.40	4.64	0.111	0.082	56	18
35	665	3.17	6.28	0.107	0.080	53	21
40	724	4.09	8.38	0.103	0.078	47	18
45	783	6.01	11.44	0.114	0.084	42	14
50	843	11.40	19.30	0.133	0.094	30	7
54	901	26.51	35.37	0.191	0.119	20	5
55	901	46.27	55.91	0.225	0.132	15	4

(1) Calculated according to Jacobsen[10]

(2) Calculated according to Hawkins et al.[11]

14

TABLE 4.2 - DEFORMATION BEHAVIOR OF SPECIMEN C10A

Load Cycle	$V_{max.}$ (kips)	A_h (lb.in./in.^{2})	A_1 (lb.in./in.^{2})	Damping Factor		Effective Stiffness (ksi/in.)	Stiffness Near Zero Shear (ksi/in.)
				β_1 (1)	β_2 (2)		
1	350	0.93	1.28	0.180	0.115	126	56
5	350	0.53	0.97	0.121	0.088	109	50
10	350	0.59	1.06	0.122	0.088	102	44
15	405	0.71	1.30	0.119	0.087	110	43
20	461	0.99	1.89	0.112	0.083	98	40
25	517	1.44	2.56	0.124	0.089	91	27
30	573	1.99	3.92	0.108	0.081	70	21
35	629	3.13	6.13	0.109	0.081	54	15
40	685	4.14	8.16	0.108	0.081	47	14
45	741	9.69	16.00	0.138	0.096	29	8
48	796	38.85	48.63	0.212	0.127	15	4

(1) Calculated according to Jacobsen[10]

(2) Calculated according to Hawkins et al.[11]

TABLE 4.3 - DEFORMATION BEHAVIOR OF SPECIMEN C14A

Load Cycle	$V_{max.}$ (kips)	A_h (lb.in./in.^{2})	A_1 (lb.in./in.^{2})	Damping Factor		Effective Stiffness (ksi/in.)	Stiffness Near Zero Shear (ksi/in.)
				β_1 (1)	β_2 (2)		
1	413	0.94	1.38	0.166	0.109	167	71
5	413	0.63	1.18	0.116	0.085	145	63
10	413	0.69	1.44	0.100	0.076	110	42
15	479	0.87	2.04	0.085	0.067	100	30
20	545	1.42	3.03	0.097	0.074	91	26
25	611	1.93	3.91	0.104	0.078	78	17
30	677	2.95	5.86	0.107	0.080	67	20
35	743	4.40	8.41	0.113	0.083	57	14
40	810	5.70	11.12	0.110	0.082	49	13
45	876	14.94	26.41	0.125	0.090	28	8
46	940	33.57	45.59	0.185	0.117	23	8
47	940	58.56	71.54	0.221	0.130	16	6

(1) Calculated according to Jacobsen[10]

(2) Calculated according to Hawkins et al.[11]

TABLE 4.4 - COMPARISON OF CALCULATED AND MEASURED ULTIMATE SHEAR TRANSFER STRENGTH

Specimen No.	ρf_y (psi)	V_u (test) (kips)	V_u (calc)$_1$ (kips)	$\frac{V_u \text{ (test)}}{V_u \text{ (calc)}_1}$	V_u (calc)$_2$ (kips)	$\frac{V_u \text{ (test)}}{V_u \text{ (calc)}_2}$
M4A	548	865	767	1.13	838	1.03
M6A	547	1150	766	1.50	838	1.37
M8A	532	1148	745	1.54	826	1.39
M9A	541	1150	757	1.52	833	1.38
M10A	514	1010	720	1.40	811	1.25
M11A	495	1091	693	1.57	796	1.37
M14A	590	1137	826	1.38	872	1.30
M18A	550	991	770	1.29	840	1.18
C4A	551	816	771	1.06	841	0.97
C8A	528	910	739	1.23	822	1.11
C10A	499	796	699	1.14	799	1.00
C14A	590	940	826	1.14	872	1.08

$V_u \text{ (calc)}_1 = \mu \rho f_y A_{cr}$ (lb.), with $\mu = 1.4$

$V_u \text{ (calc)}_2 = (0.8 \rho f_y + 400) A_{cr}$ (lb.)

TABLE 4.5 - COMPARISON OF ULTIMATE STRENGTH FOR MONOTONIC AND CYCLIC LOADING

Cyclic Loading Specimen		Monotonic Loading Specimen		$\frac{V_u \text{ (cyclic)}}{V_u \text{ (monotonic)}}$
Specimen No.	Ultimate Shear (kips)	Specimen No.	Ultimate Shear (kips)	
C4A	816	M4A	865	0.94
C8A	910	M8A	1148	0.79
C10A	796	M10A	1010	0.79
C14A	940	M14A	1137	0.83

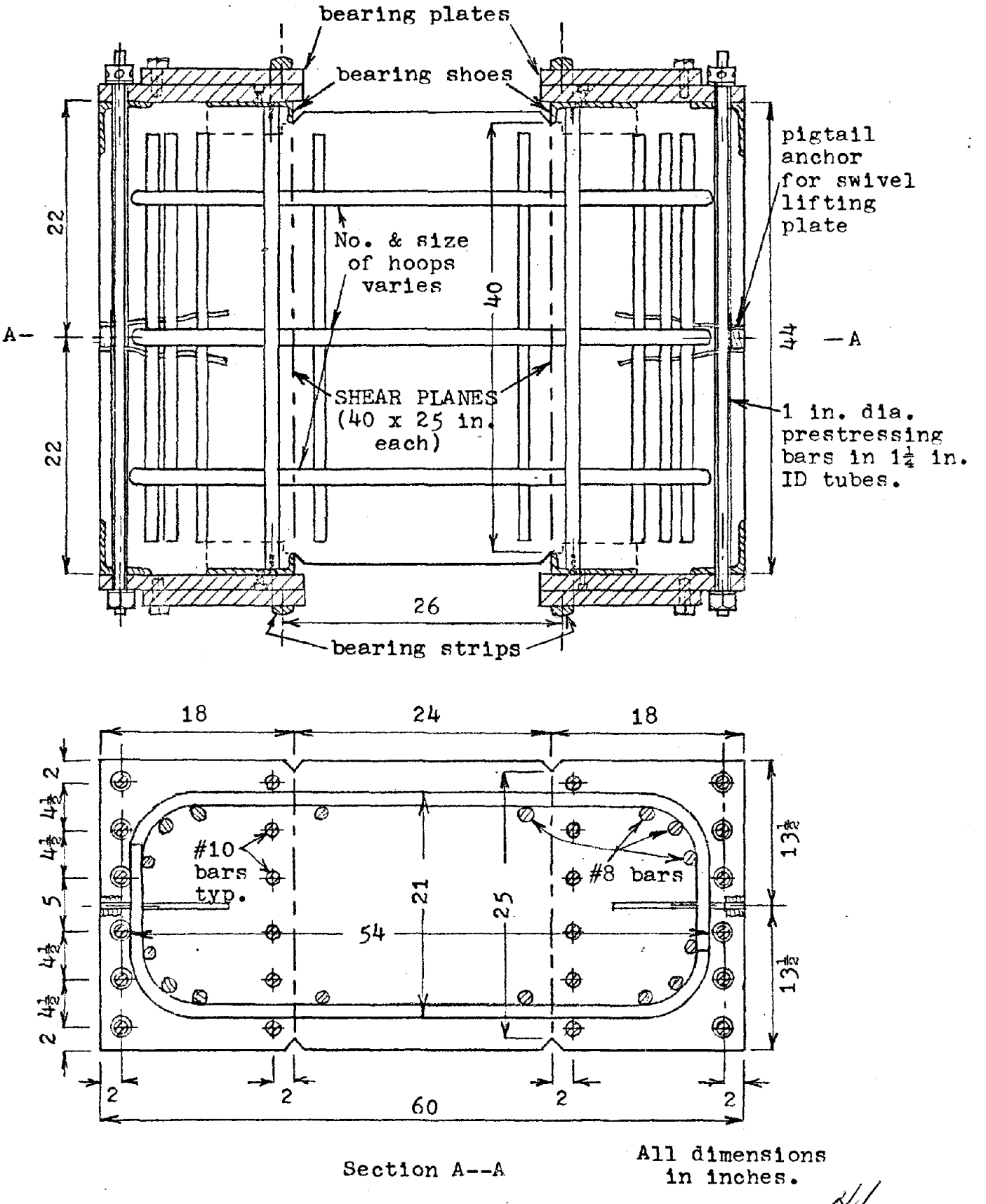

Section A--A

All dimensions in inches.

46

Fig. 2.1 - Specimen details

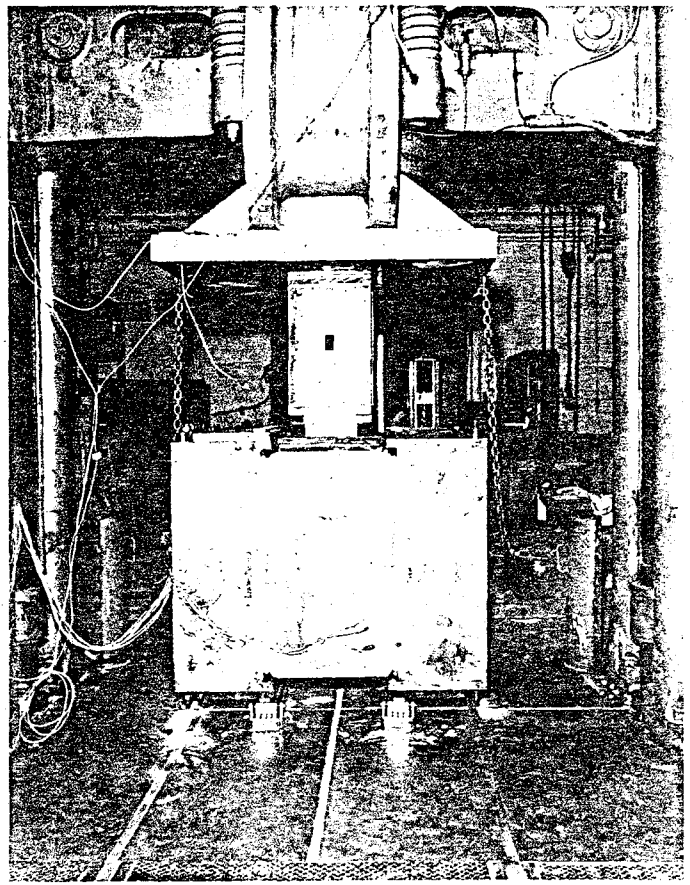

Fig. 2.2 - Arrangements for test

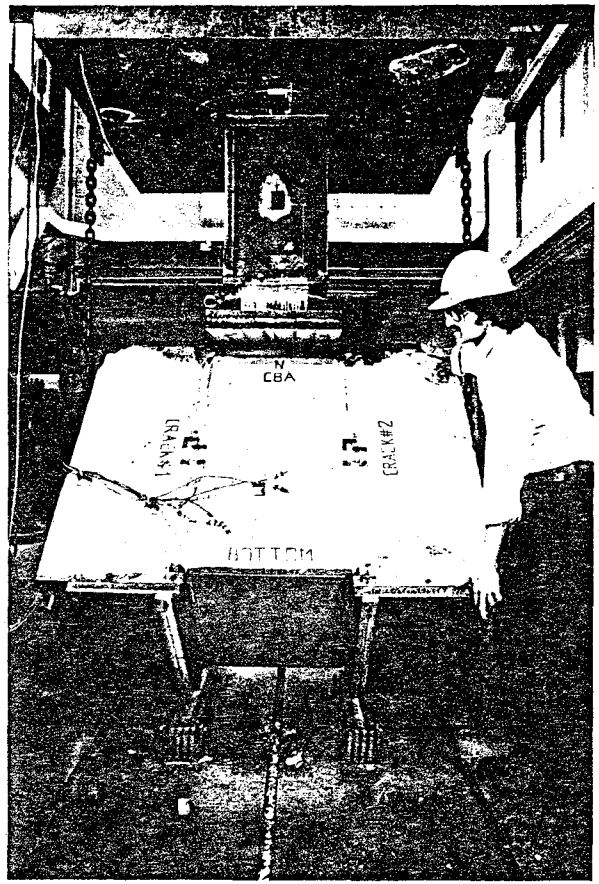

Fig. 2.3 - Inverting specimen in cyclic loading test

Fig. 3.1 - Typical appearance of a monotonic loading specimen after failure

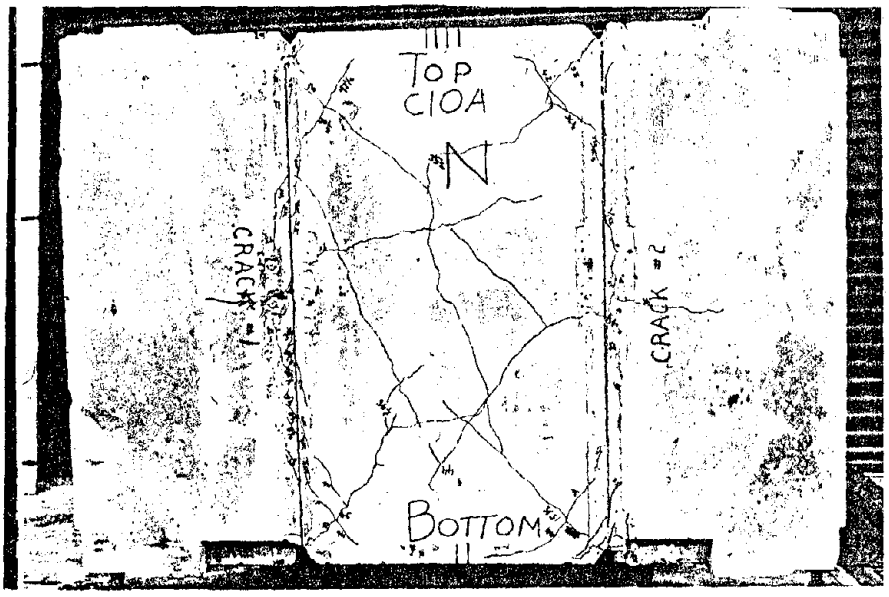

Fig. 3.2 - Typical appearance of a cyclic loading specimen after failure

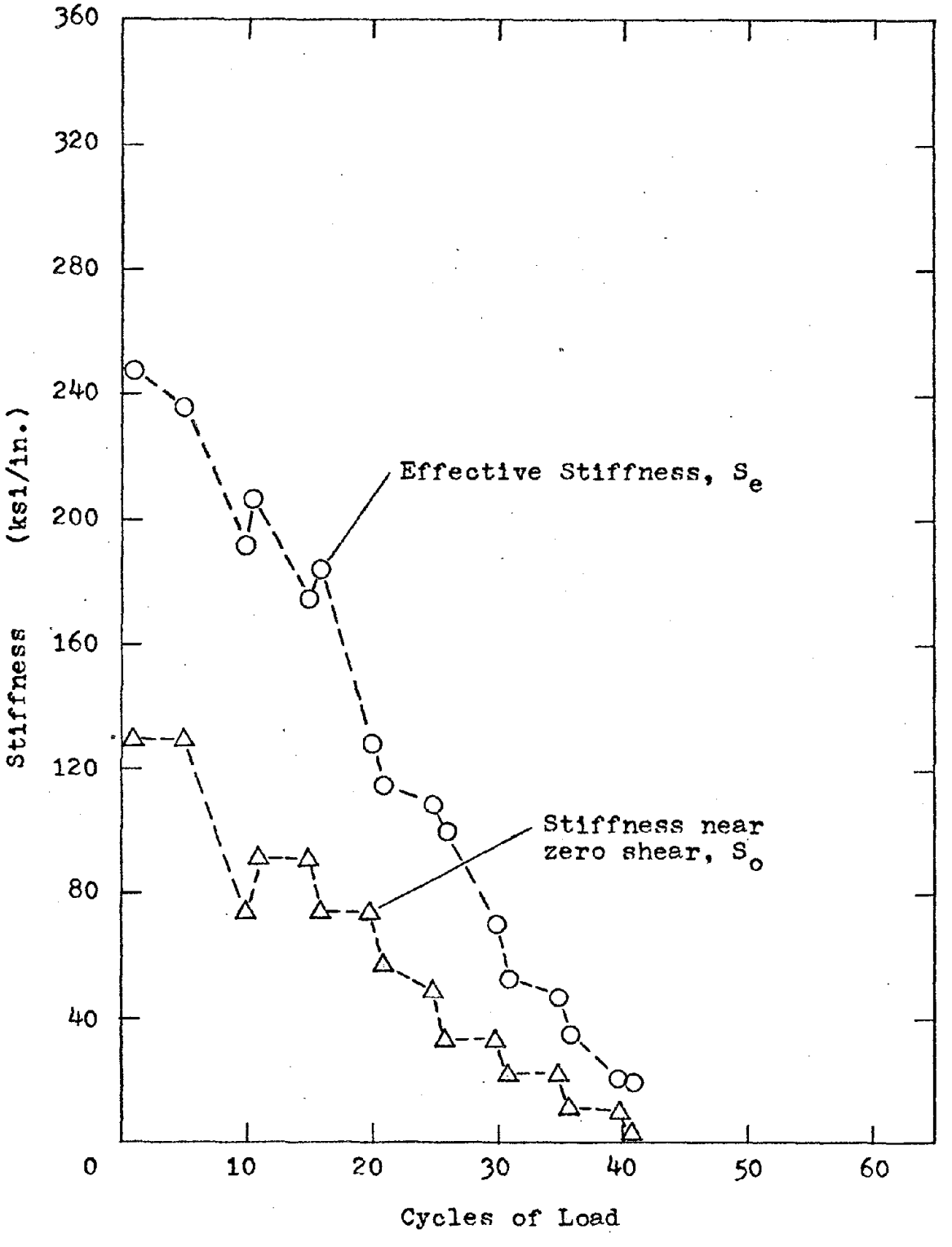

Fig. 3.3 - Variation of shear stiffness with number of cycles of loading, C4A.

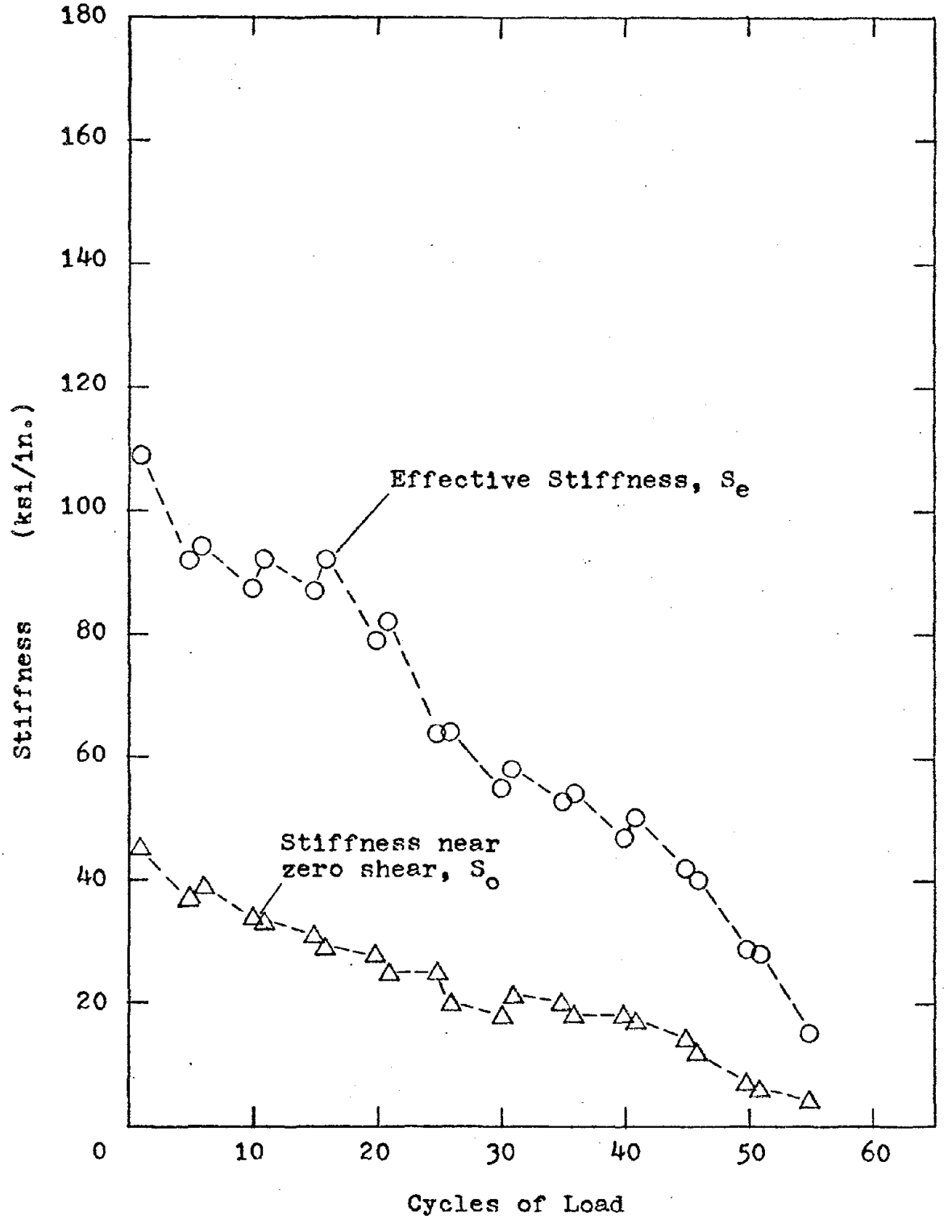

Fig. 3.4 - Variation of shear stiffness with number of cycles of loading, C8A.

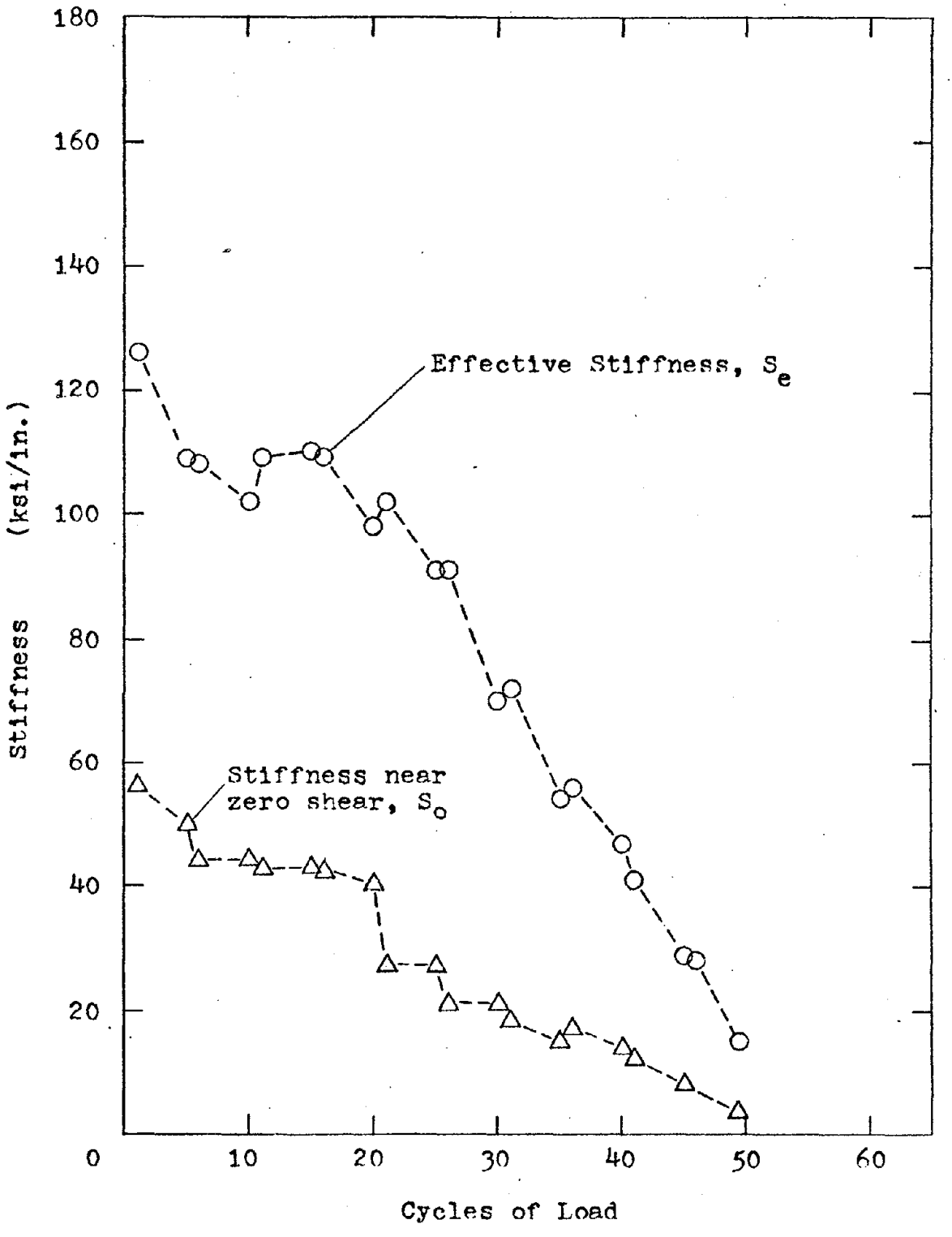

Fig. 3.5 - Variation of shear stiffness with number of cycles of loading, C10A.

51

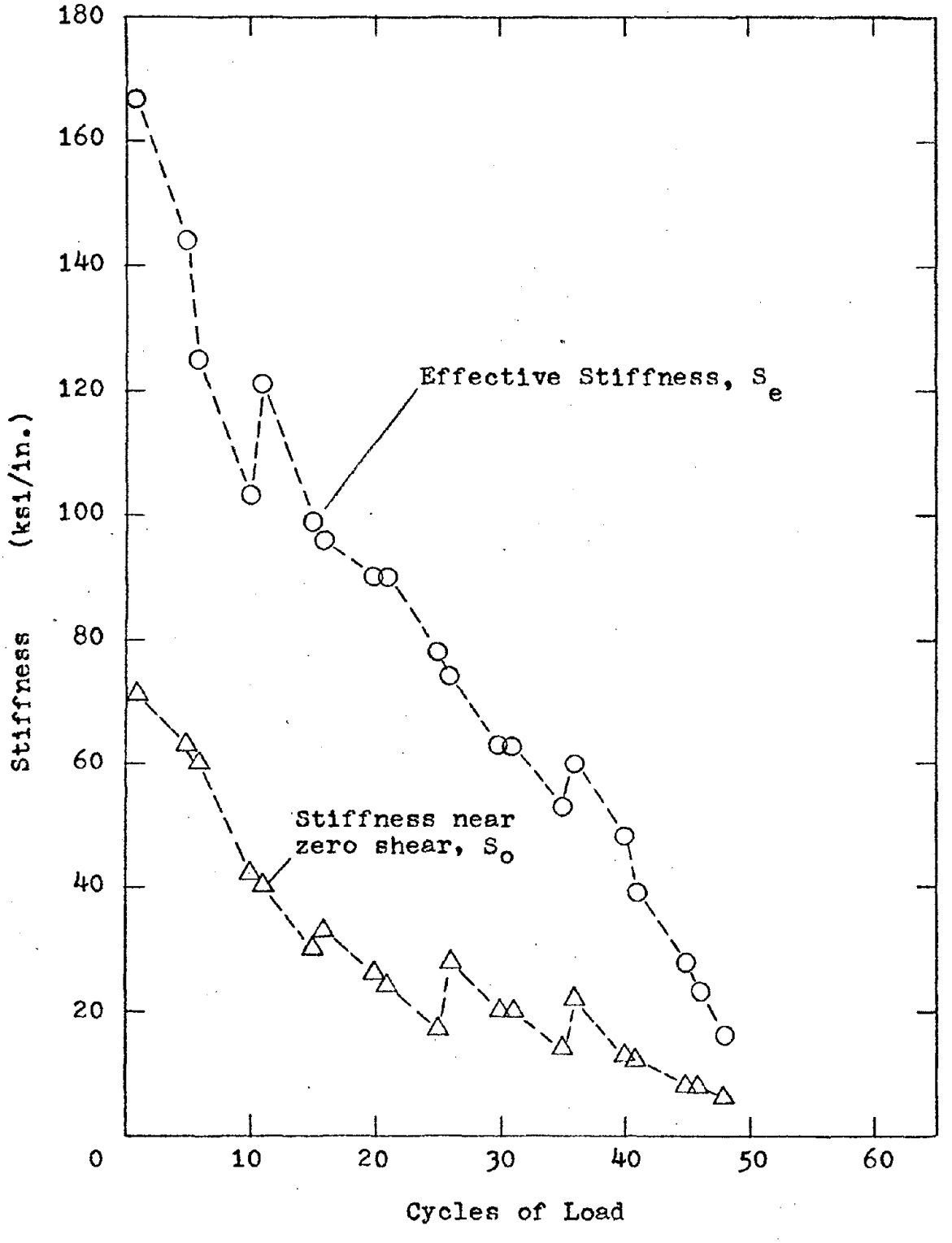

Fig. 3.6 - Variation of shear stiffness with number of cycles of loading, C14A.

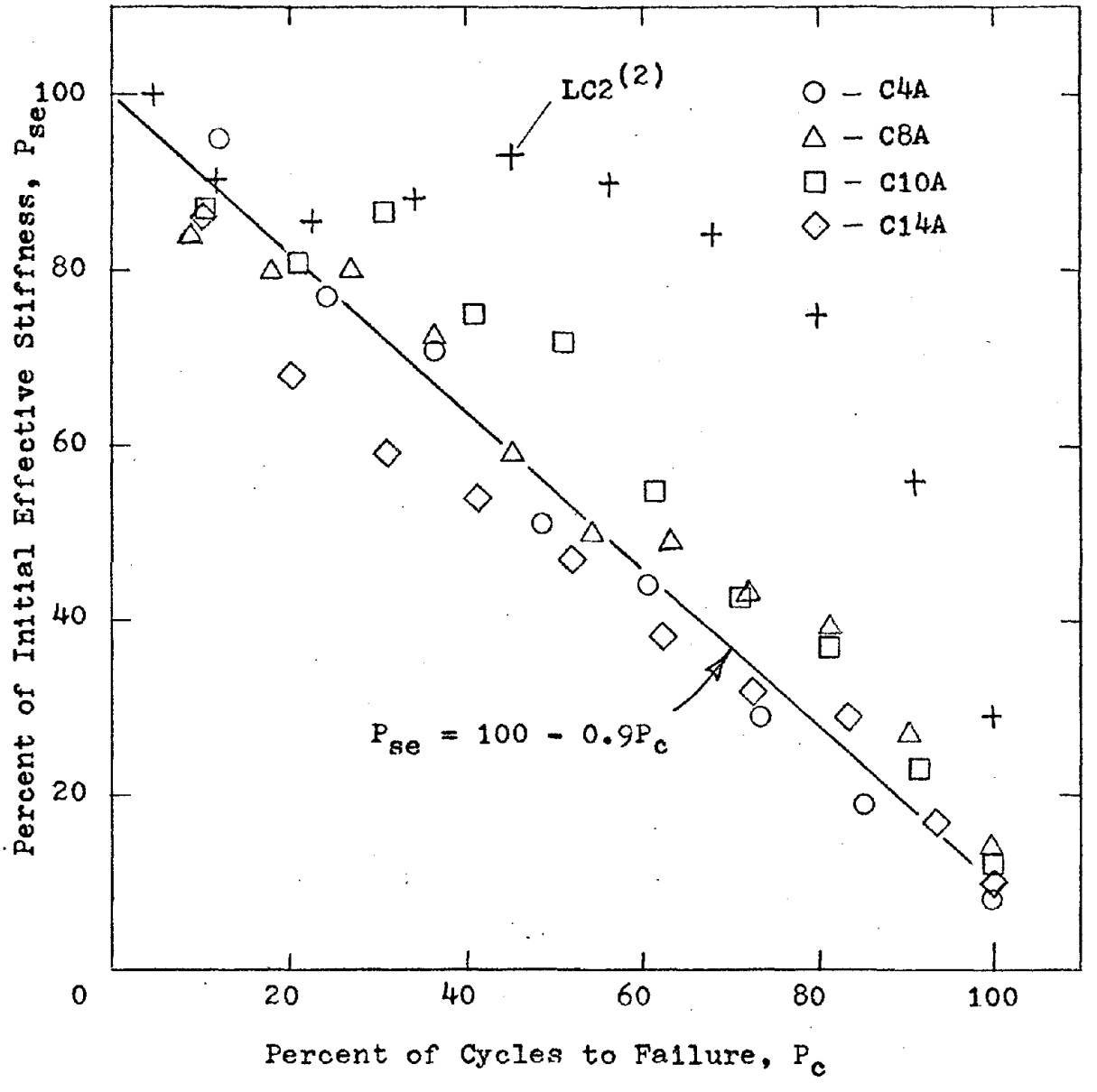

Fig. 4.1 - Variation of effective shear stiffness with percent of cycles of load causing failure.

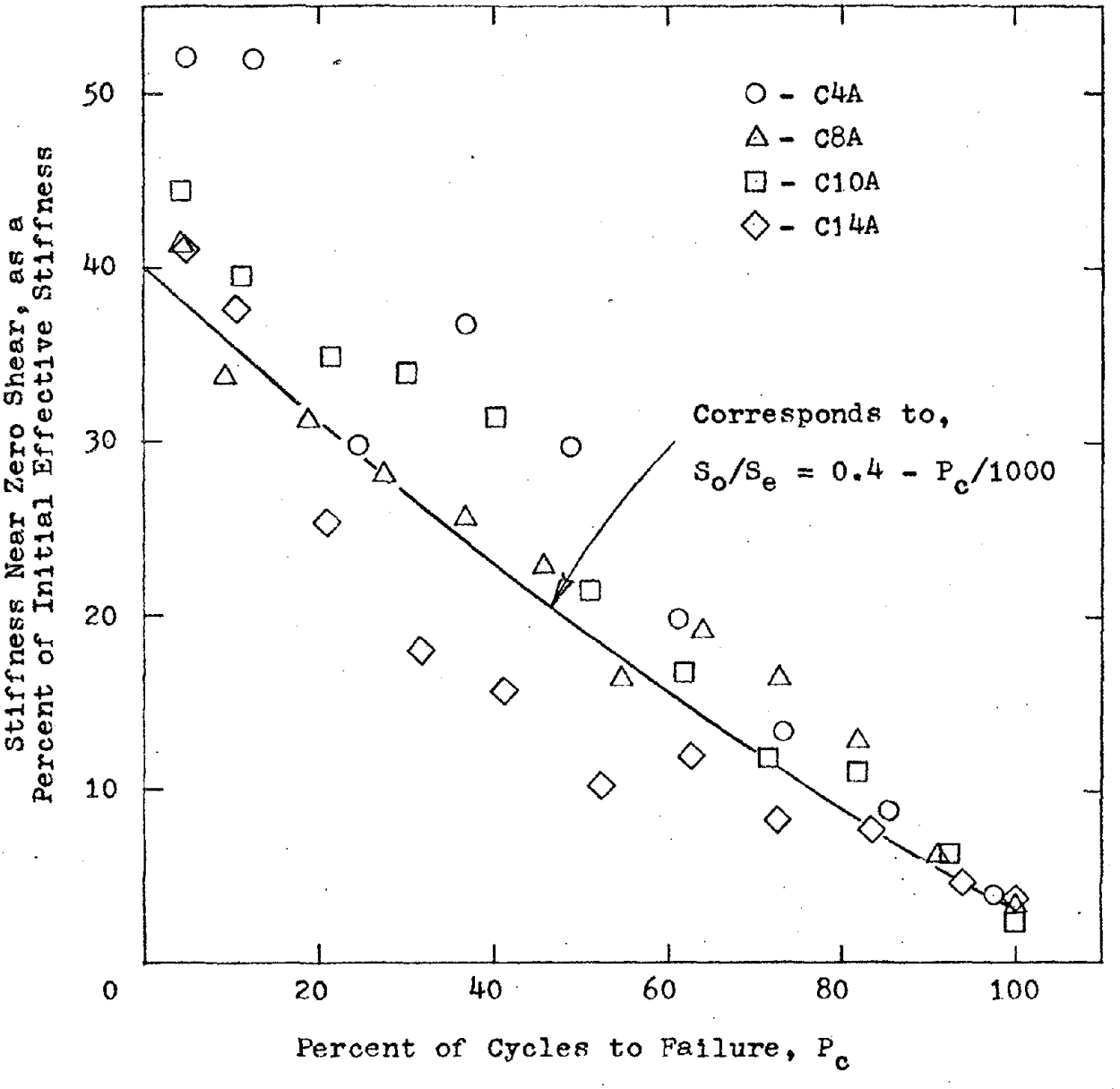

Fig. 4.2 - Variation of shear stiffness near zero shear, with percent of cycles of load causing failure.

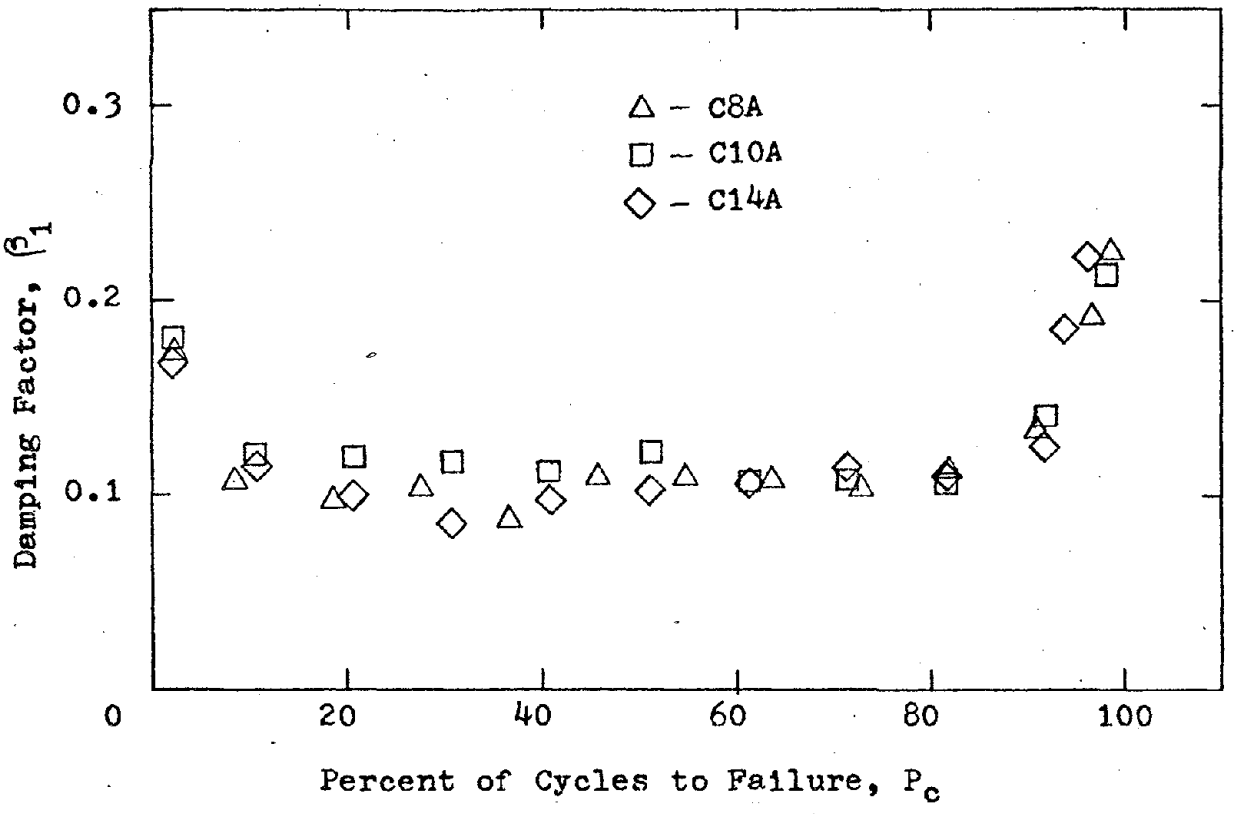

Fig. 4.3 - Variation of damping factor calculated according to Jacobsen[10]

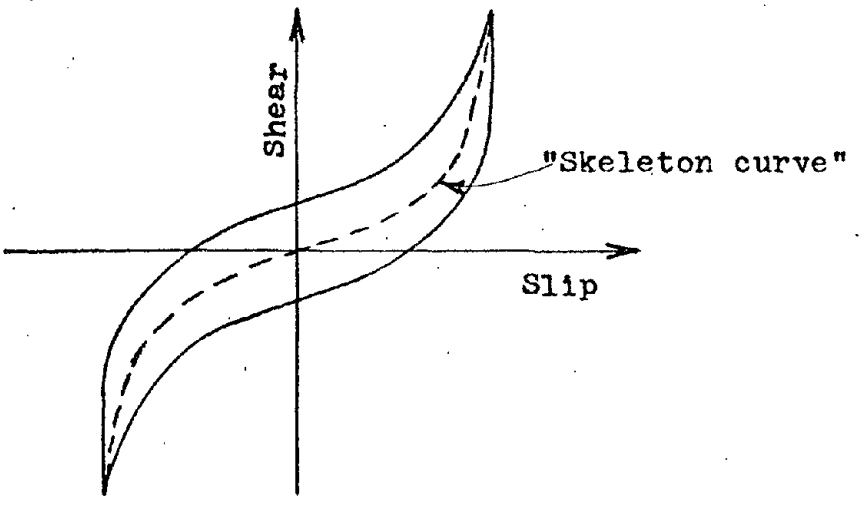

Fig. 4.4 - Calculation of damping factor according to Jacobsen[10]

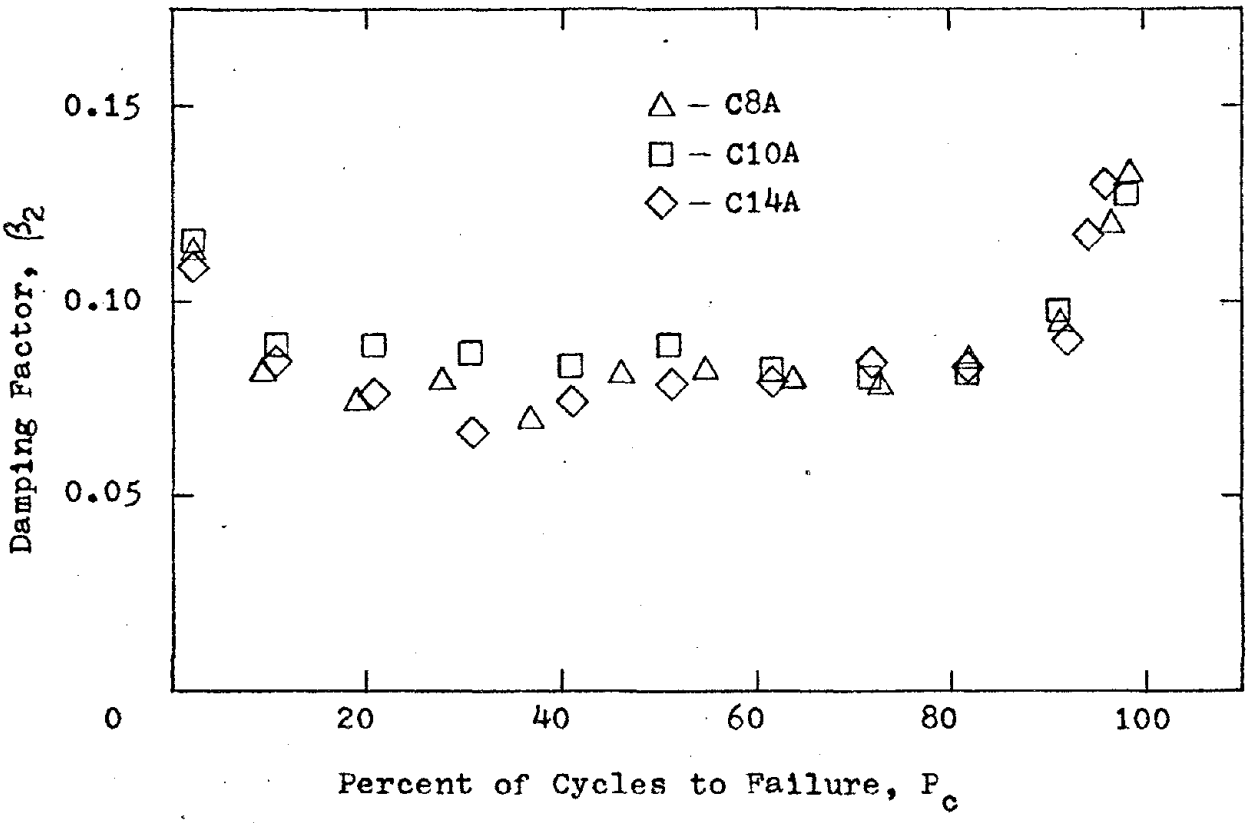

Fig. 4.5 - Variation of damping factor calculated according to Hawkins et al.[11]

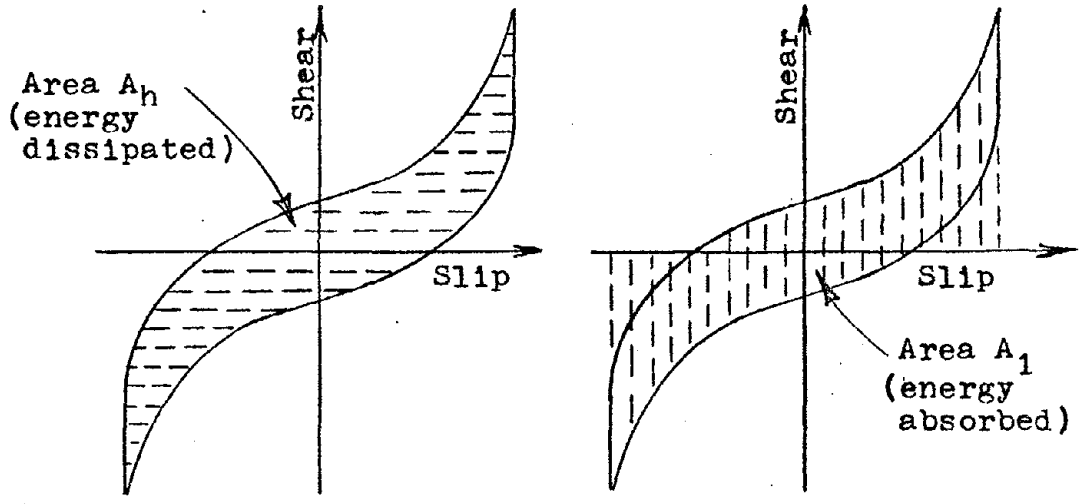

Fig. 4.6 - Calculation of damping factor according to Hawkins et al.[11]

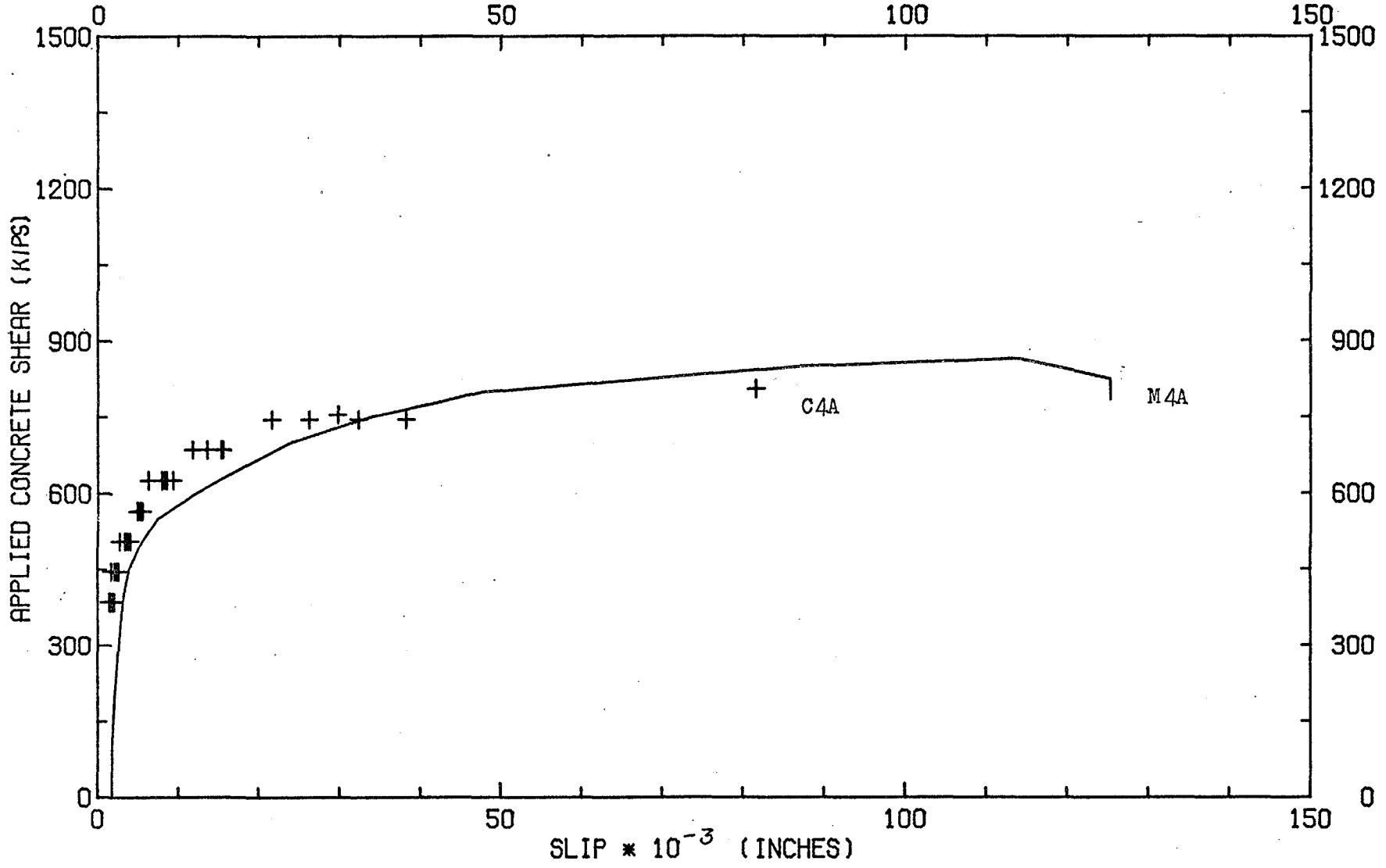

Fig. 4.7 - Comparison of shear - slip relations for M4A and C4A.

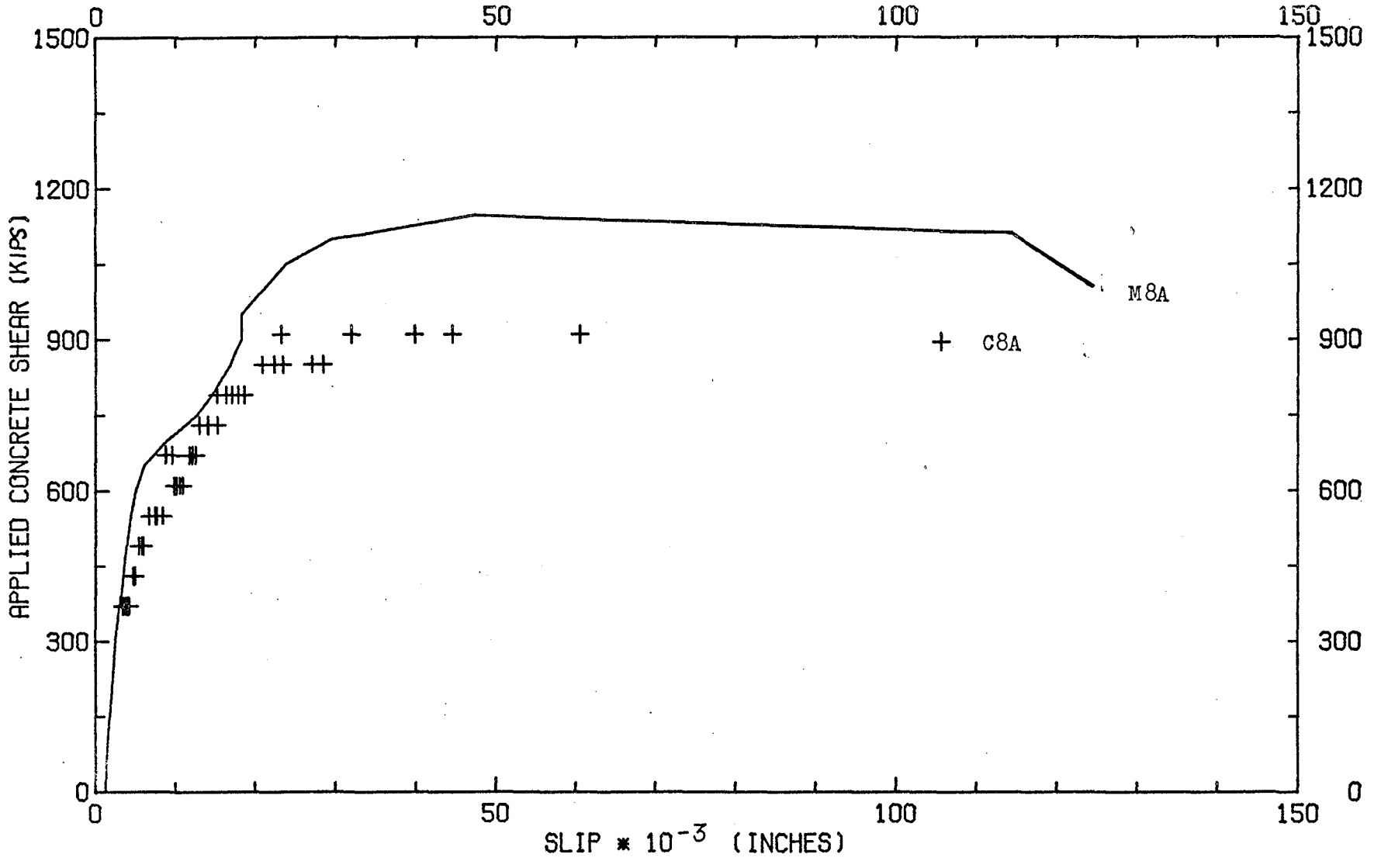

Fig. 4.8 - Comparison of shear - slip relations for M8A and C8A.

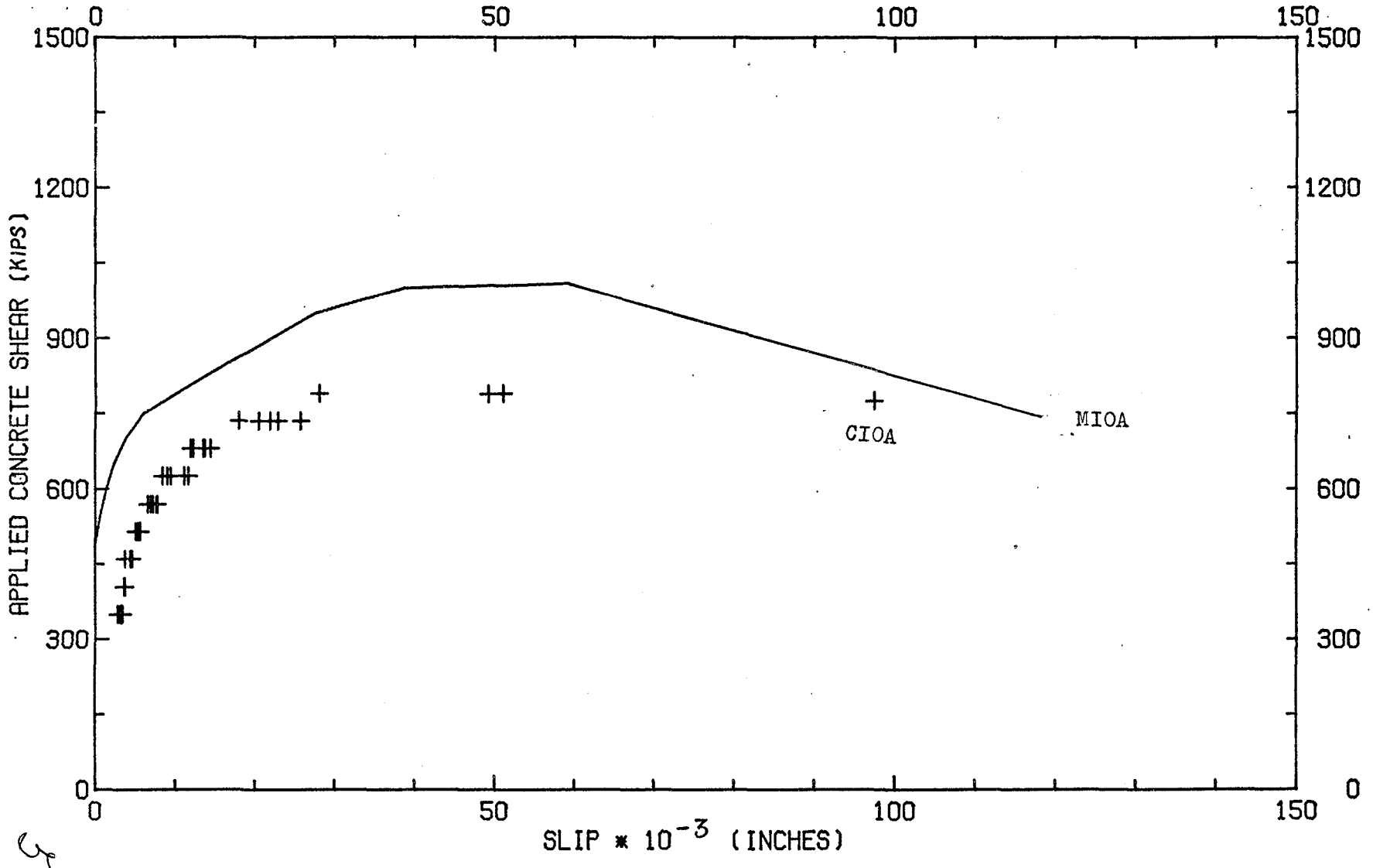

Fig. 4.9 - Comparison of shear - slip relations for M10A and C10A.

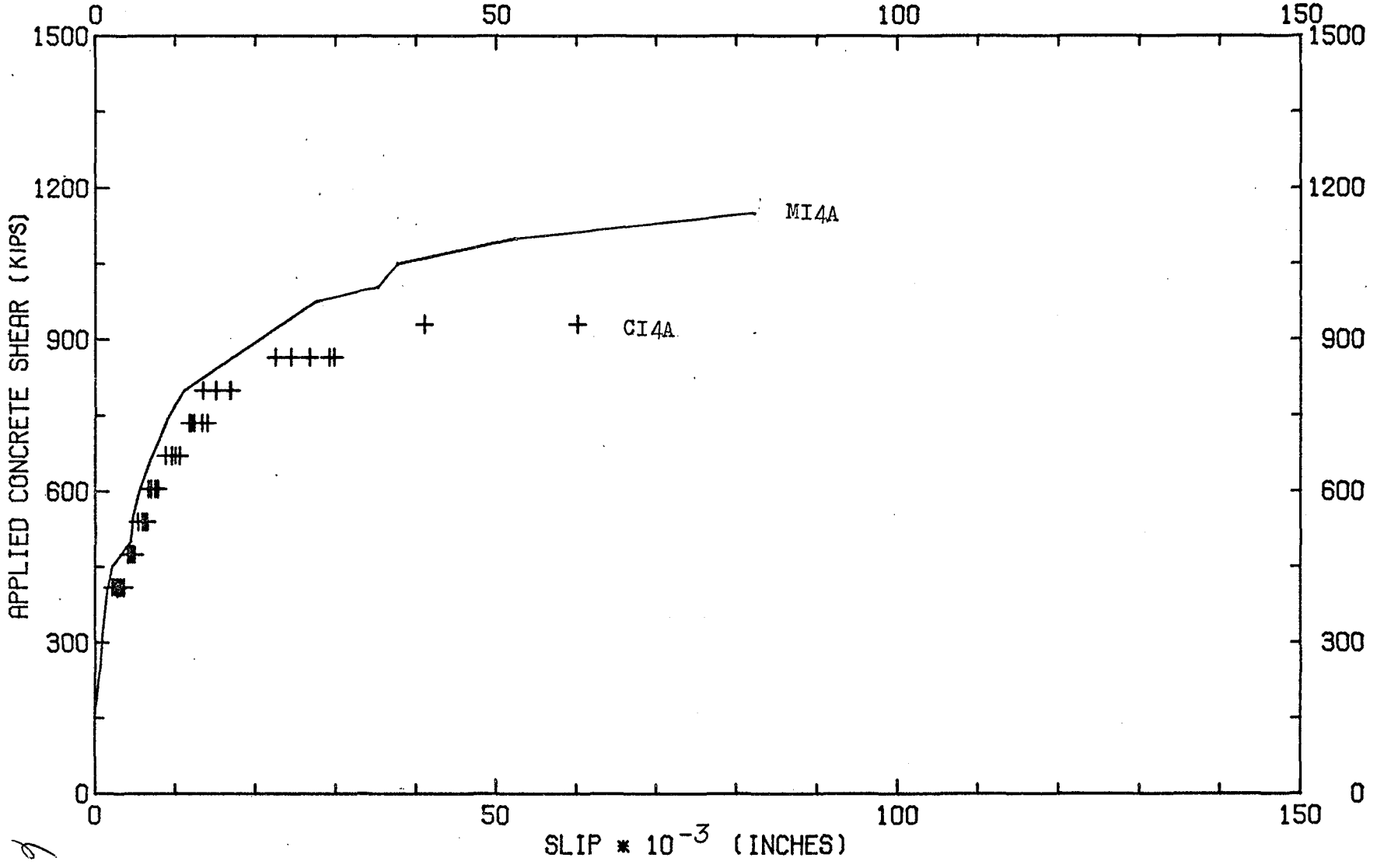

Fig. 4.10 - Comparison of shear - slip relations for M14A and C14A.

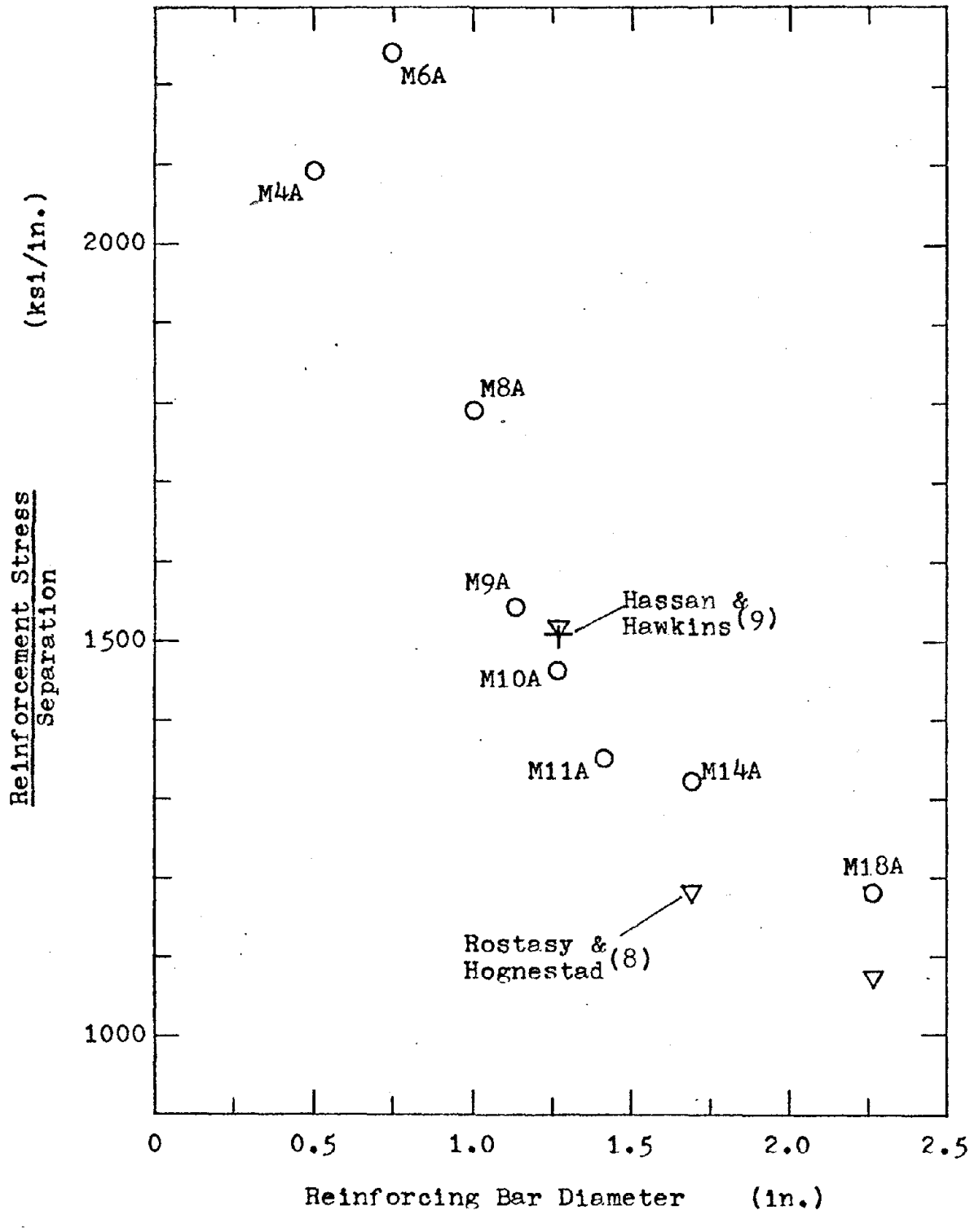

Fig. 4.11- Variation of (Reinforcement Stress)/(Separation) with bar diameter, in shear transfer push-off tests and bond pull-out tests.

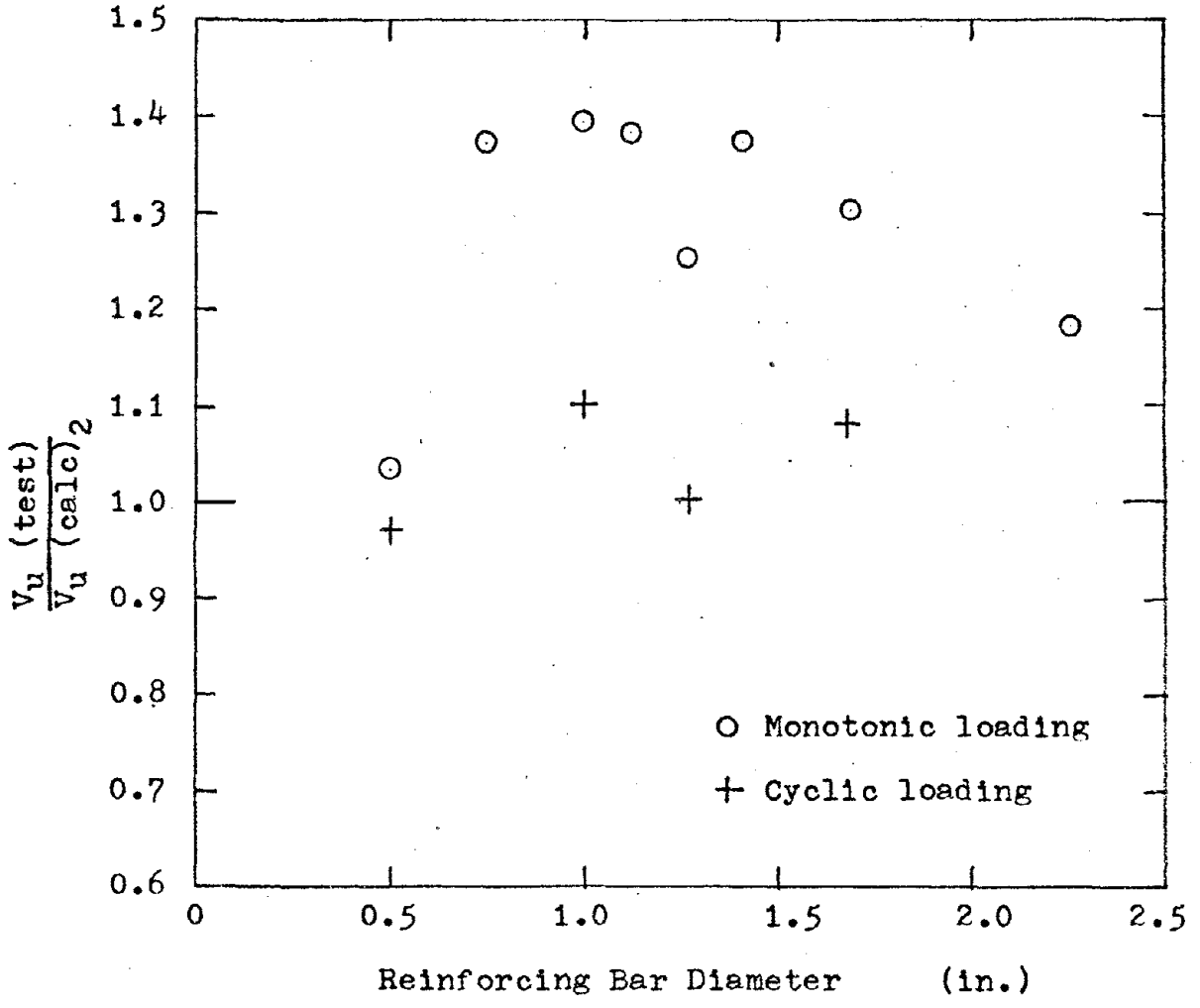

Fig. 4.12 - Variation of ultimate shear transfer strength with reinforcing bar diameter.

APPENDIX A

NOTATION

A_{cr} = Area of shear plane, sq. in.

A_{vf} = Area of reinforcement crossing the shear plane, sq. in.

f'_c = Compressive strength of concrete measured on 6 x 12 in. cylinders, psi.

f_y = Yield point stress of reinforcement, psi.

V_u = Ultimate shear force, kips.

v_u = Nominal ultimate shear stress, psi.

= $1000\ V_u/A_{cr}$, psi.

μ = Coefficient of friction used in shear-friction calculations.

ρ = A_{vf}/A_{cr}

ϕ = Capacity reduction factor, as per Sec. 9.2 of ACI 318-71.

APPENDIX B

DATA FROM MONOTONIC LOADING TESTS

Fig.	Title
B1	Applied concrete shear - slip curves, Specimen M4A
B2	Applied concrete shear - slip curves, Specimen M6A
B3	Applied concrete shear - slip curves, Specimen M8A
B4	Applied concrete shear - slip curves, Specimen M9A
B5	Applied concrete shear - slip curves, Specimen M10A
B6	Applied concrete shear - slip curves, Specimen M11A
B7	Applied concrete shear - slip curves, Specimen M14A
B8	Applied concrete shear - slip curves, Specimen M18A
B9	Slip - separation curves for crack that failed in Specimens M4A, M6A, M8A, M9A.
B10	Slip - separation curves for crack that failed in Specimens M10A, M11A, M14A, M18A.
B11	Applied concrete shear - steel stress curves, Specimen M4A
B12	Applied concrete shear - steel stress curves, Specimen M6A
B13	Applied concrete shear - steel stress curves, Specimen M8A
B14	Applied concrete shear - steel stress curves, Specimen M9A
B15	Applied concrete shear - steel stress curves, Specimen M10A
B16	Applied concrete shear - steel stress curves, Specimen M11A
B17	Applied concrete shear - steel stress curves, Specimen M14A
B18	Applied concrete shear - steel stress curves, Specimen M18A
B19	Steel stress - separation curves, Specimen M4A
B20	Steel stress - separation curves, Specimen M6A

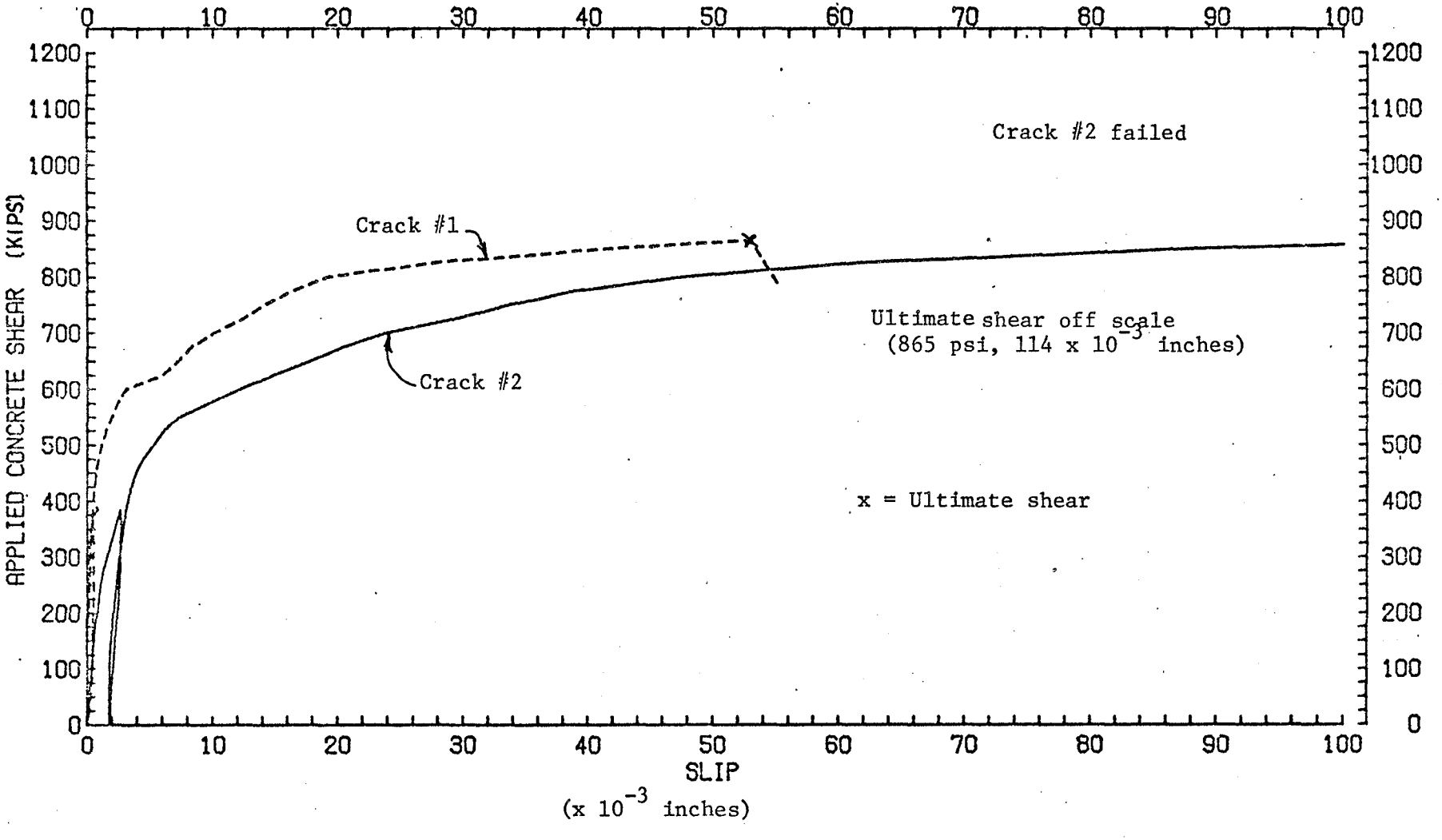

FIG. B1 Applied concrete shear-slip curves, Specimen M4A

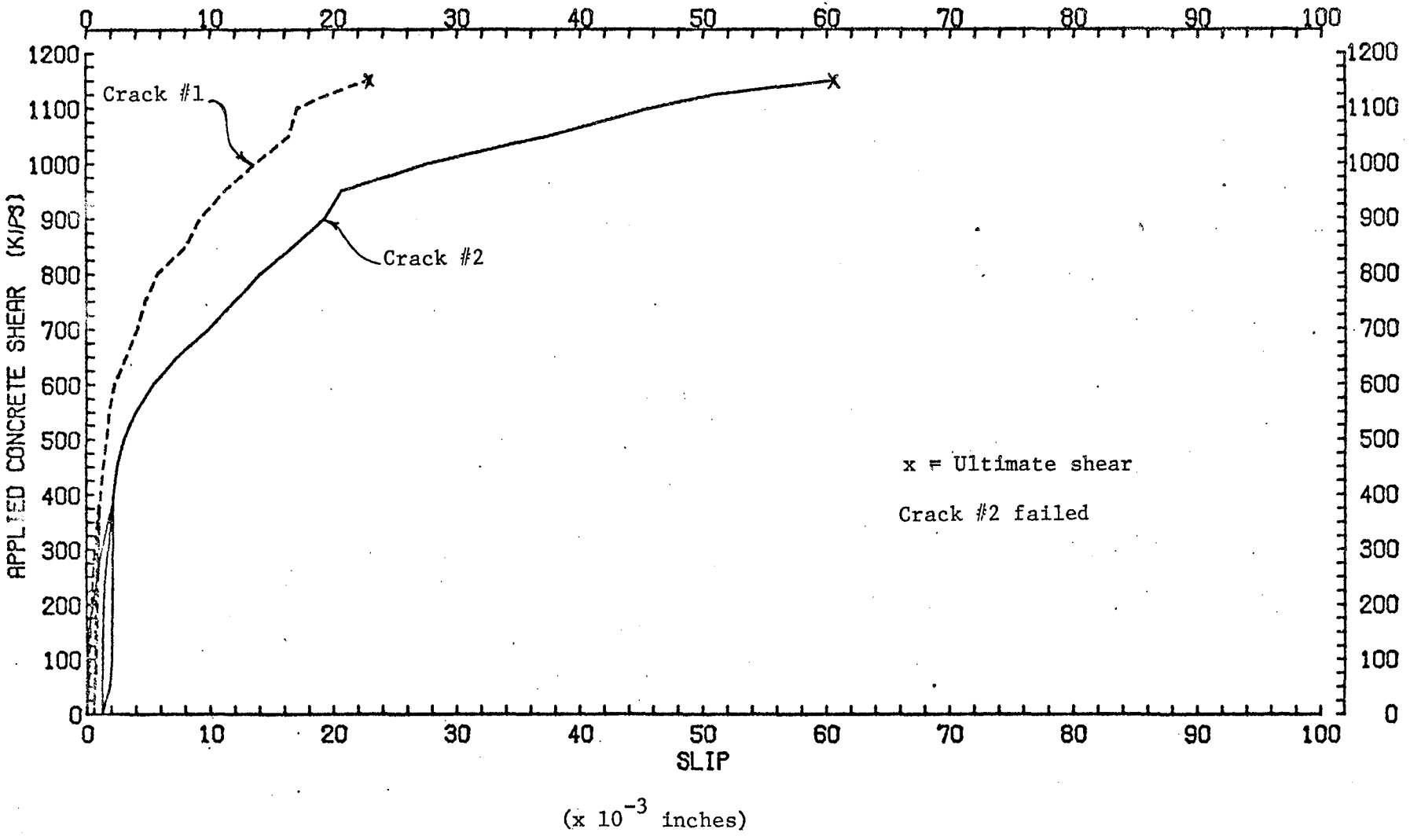

FIG. B2 Applied concrete shear-slip curves, Specimen M6A

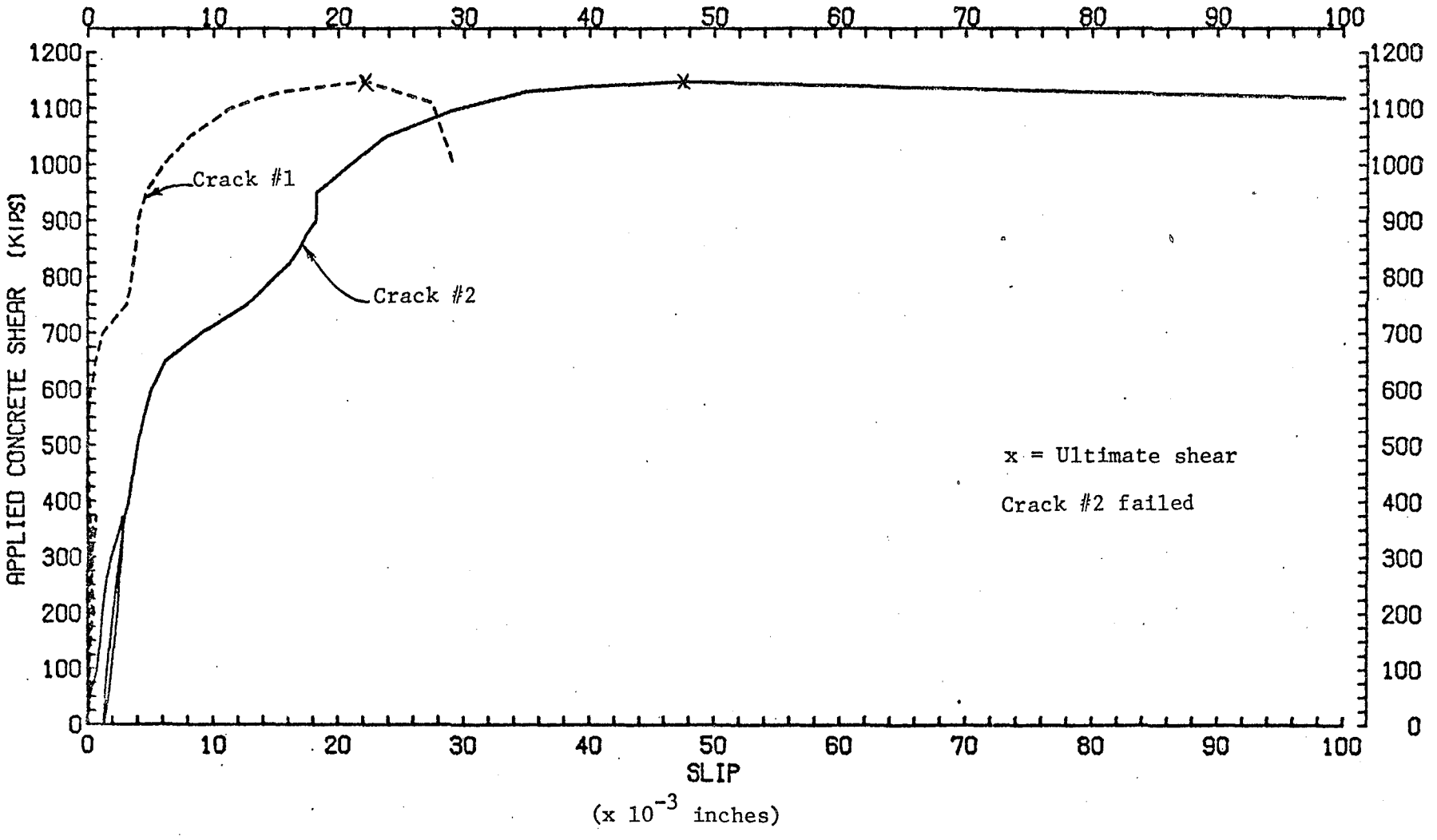

FIG B3 Applied concrete shear-slip curves, Specimen M8A

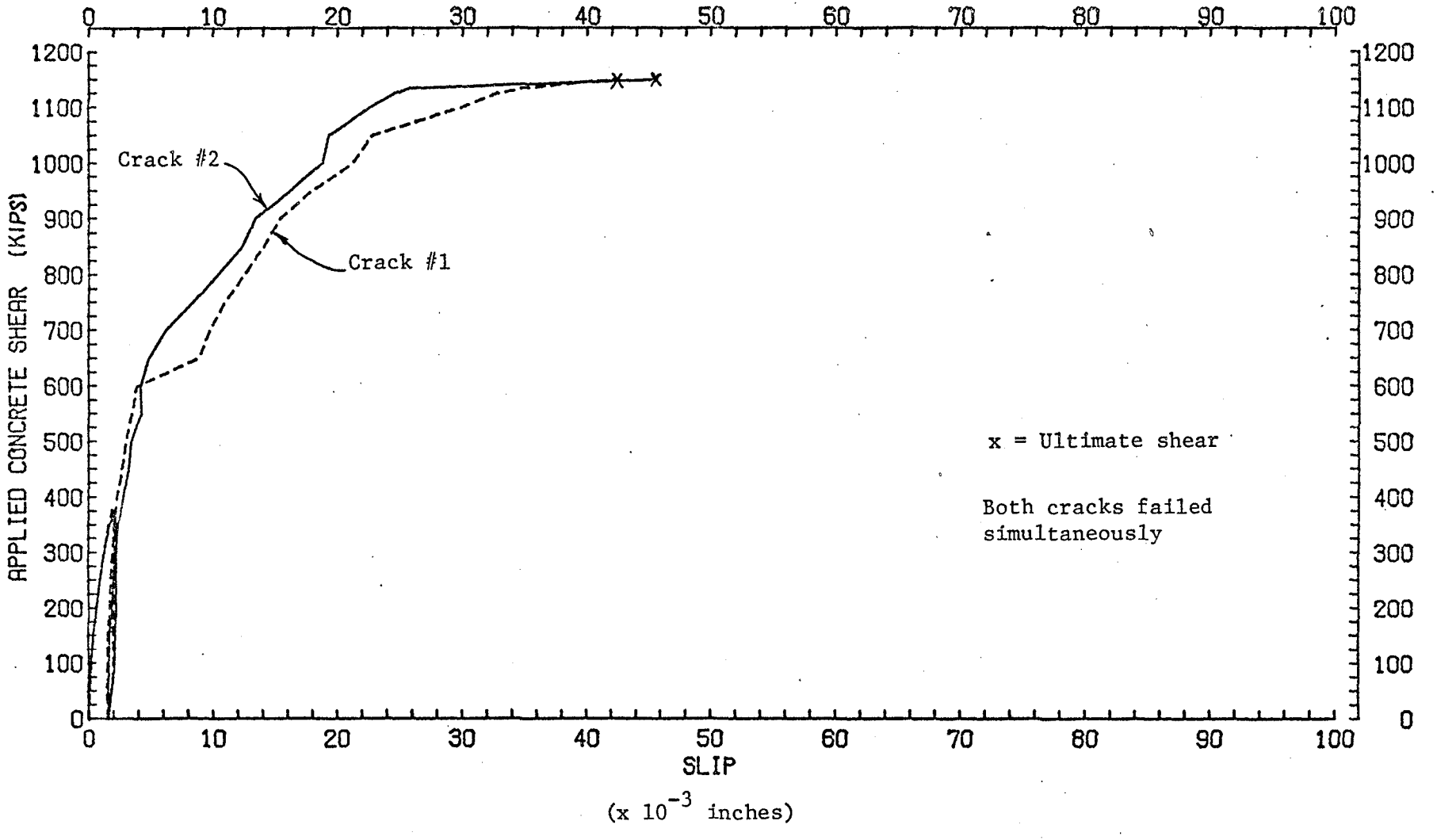

Fig. B4 Applied concrete shear-slip curves, Specimen M9A

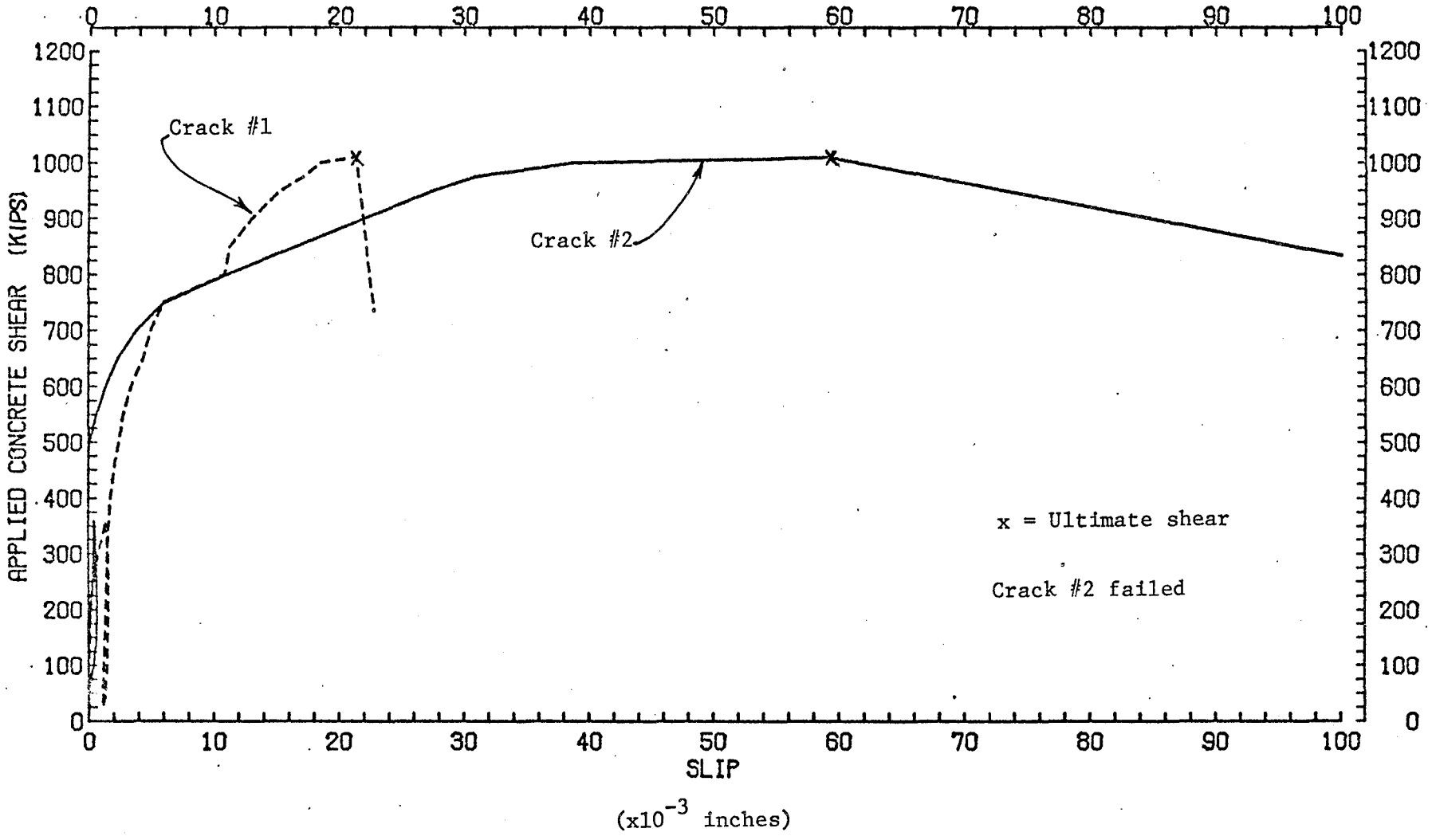

Fig. B5 Applied concrete shear-slip curves, Specimen M10A

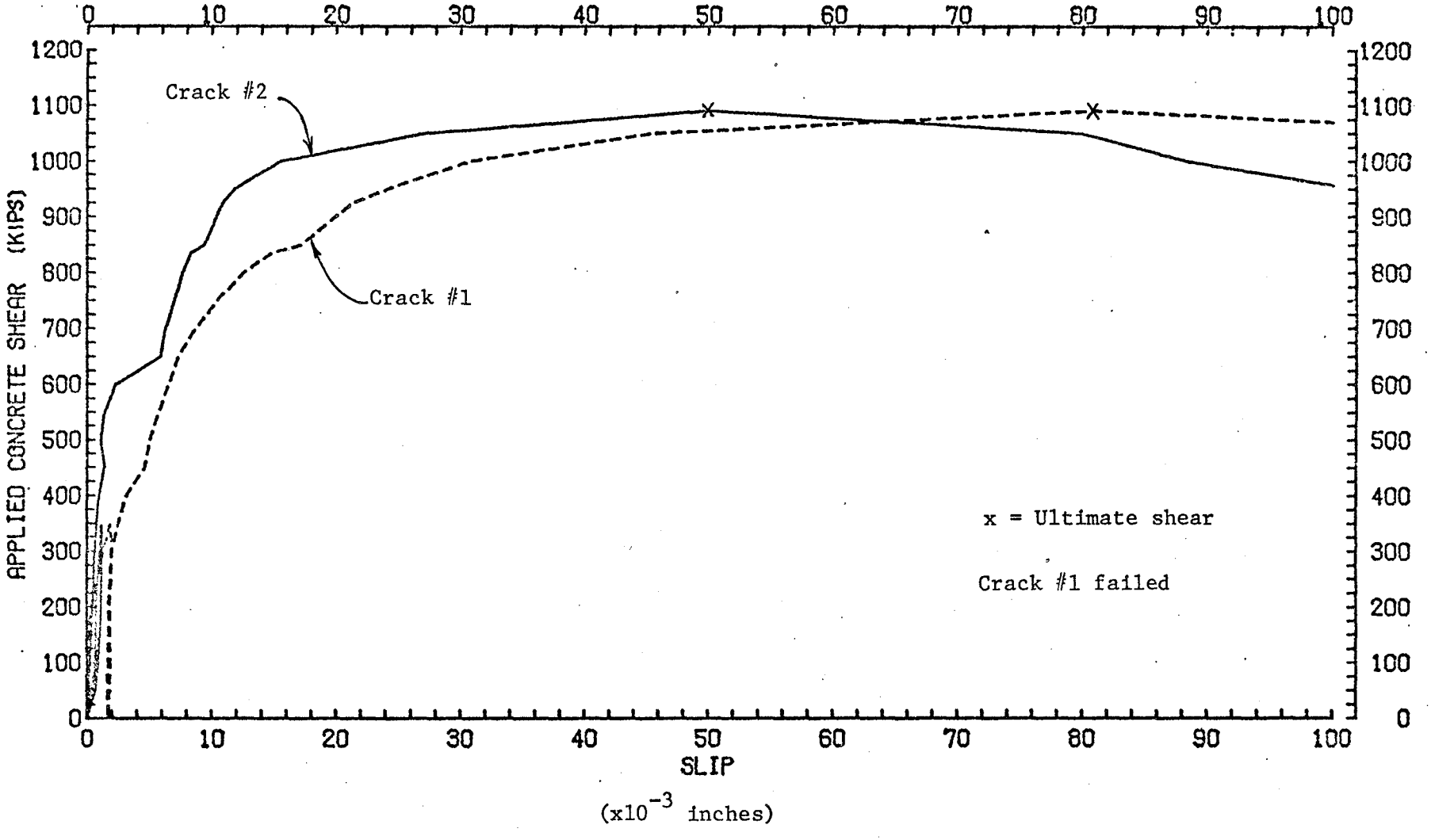

Fig. B6 Applied concrete shear-slip curves, Specimen M11A

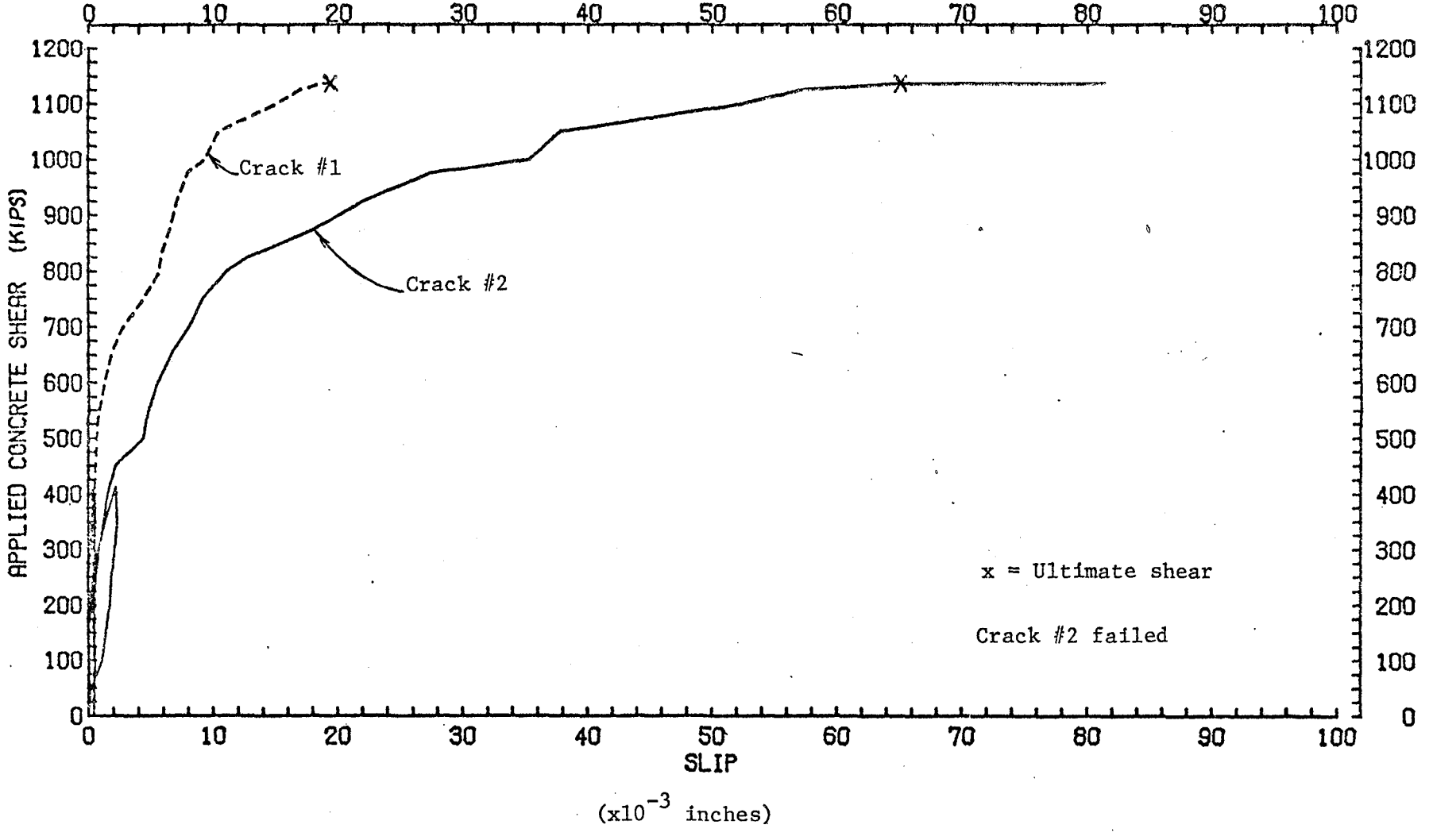

Fig. B7 Applied concrete shear-slip curves, Specimen M14A

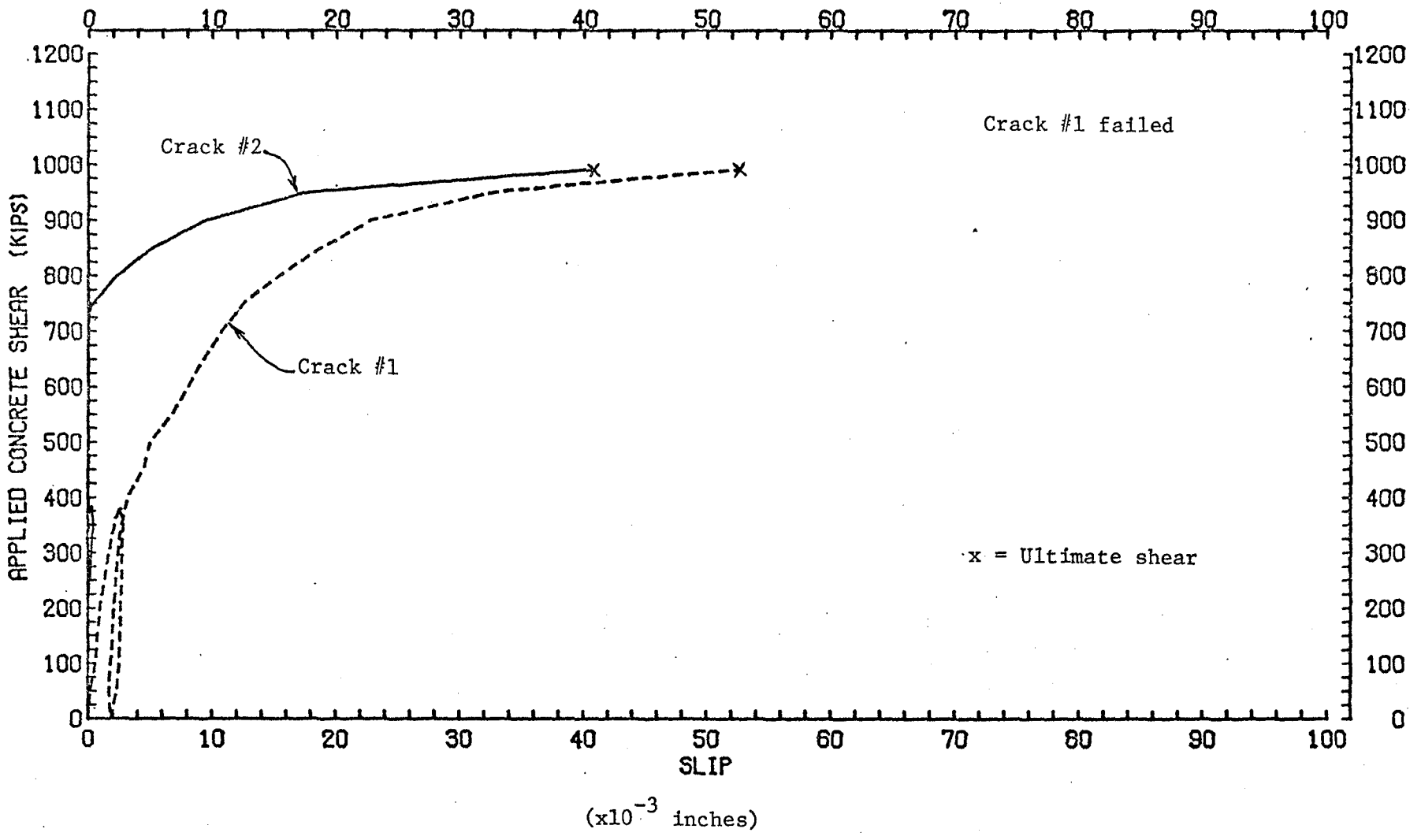

Fig. B8 Applied concrete shear-slip curves, Specimen M18A

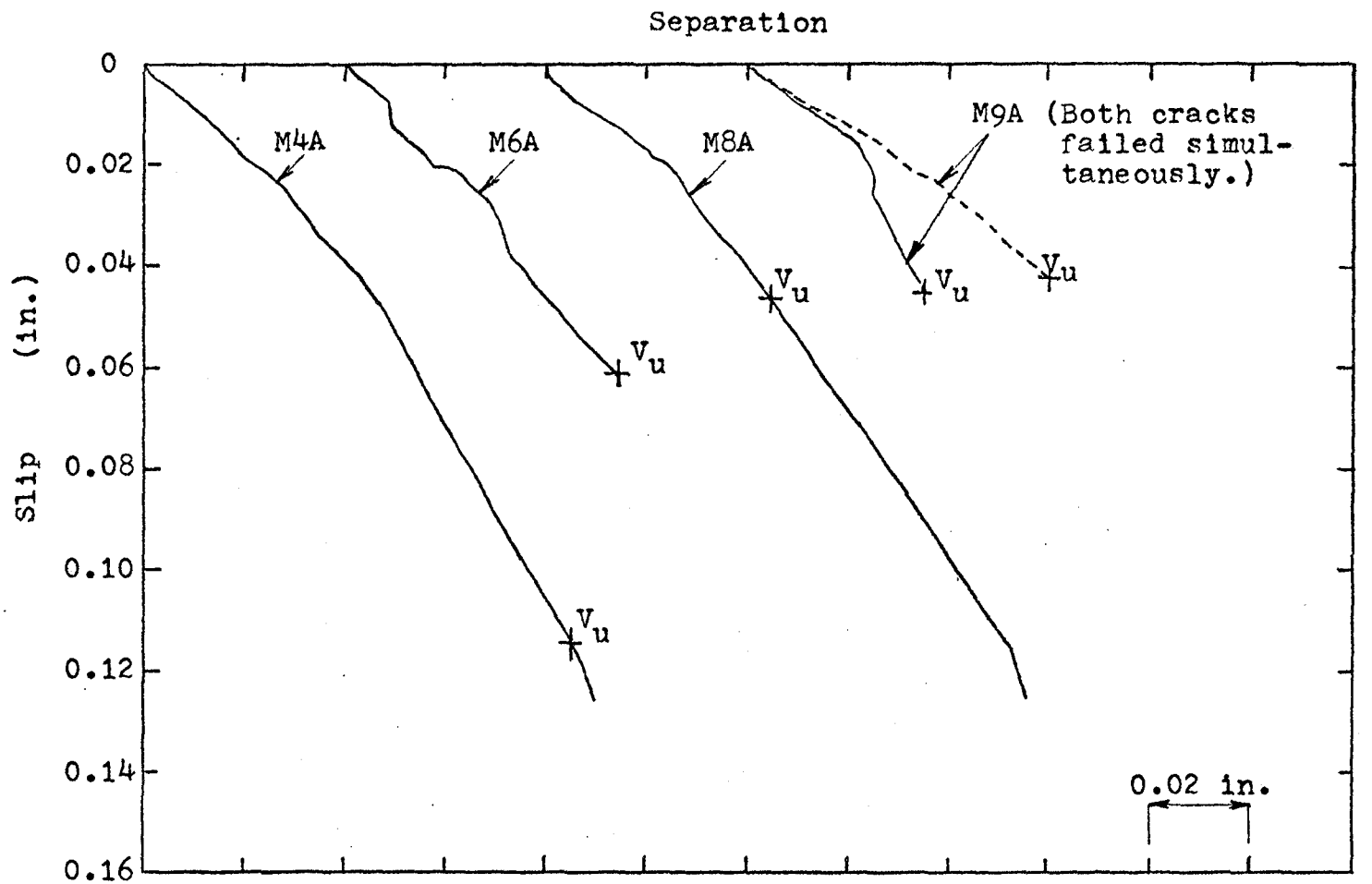

Fig. B9 - Slip - separation curves for crack that failed in Specimens M4A, M6A, M8A, M9A.

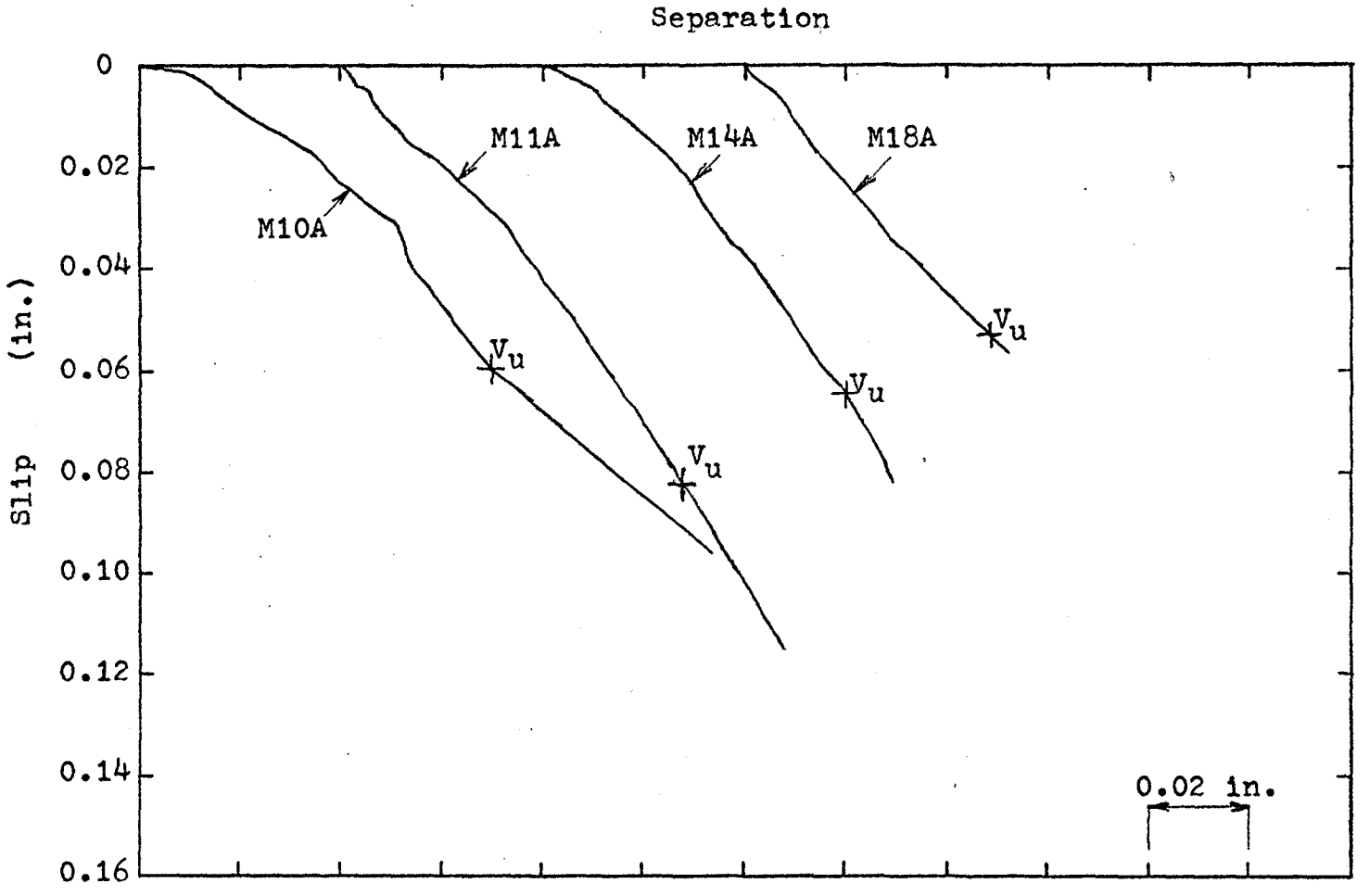

Fig. B10 - Slip - separation curves for crack that failed in Specimens M10A, M11A, M14A, M18A.

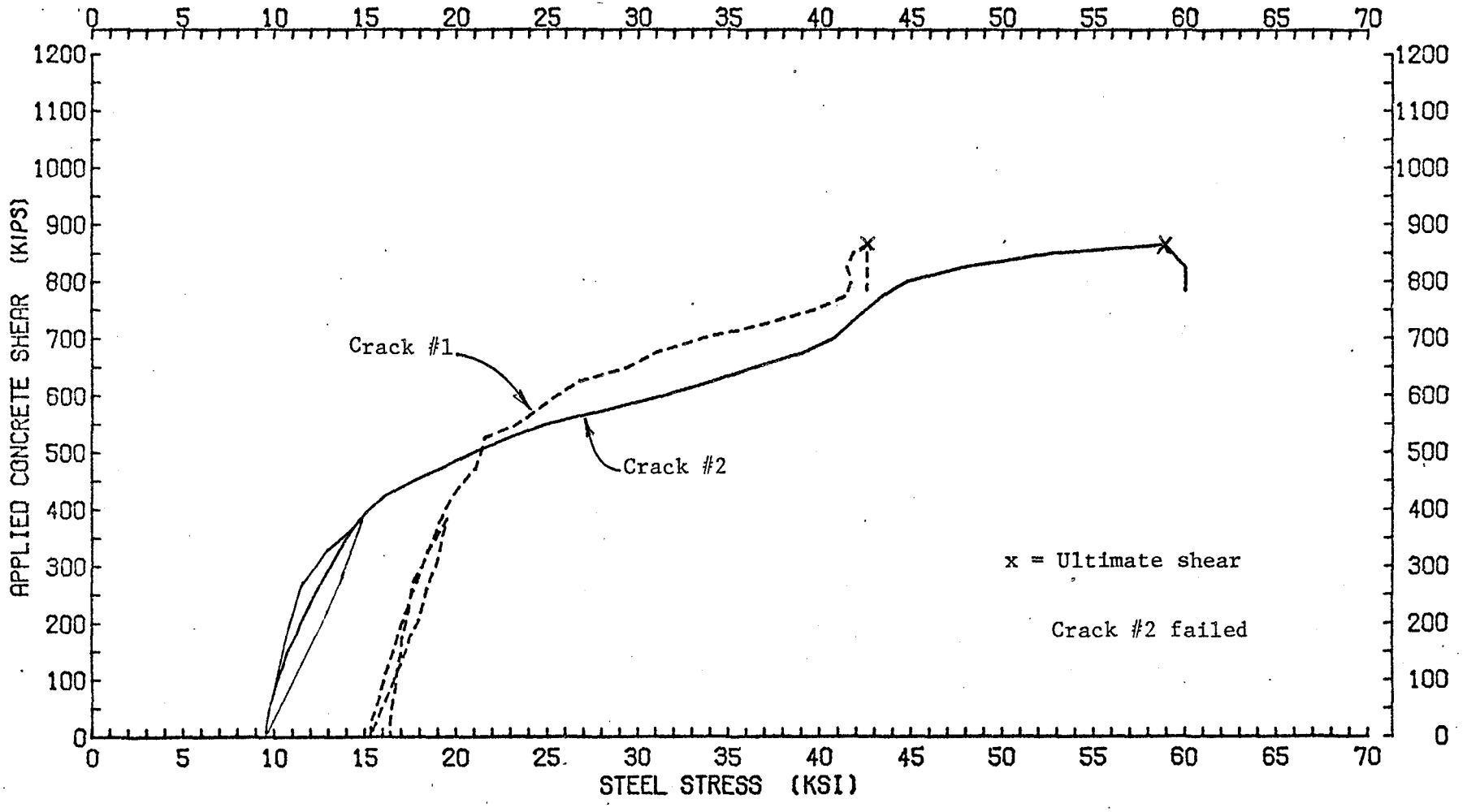

Fig. B11 Applied concrete shear-steel stress curves, Specimen M4A

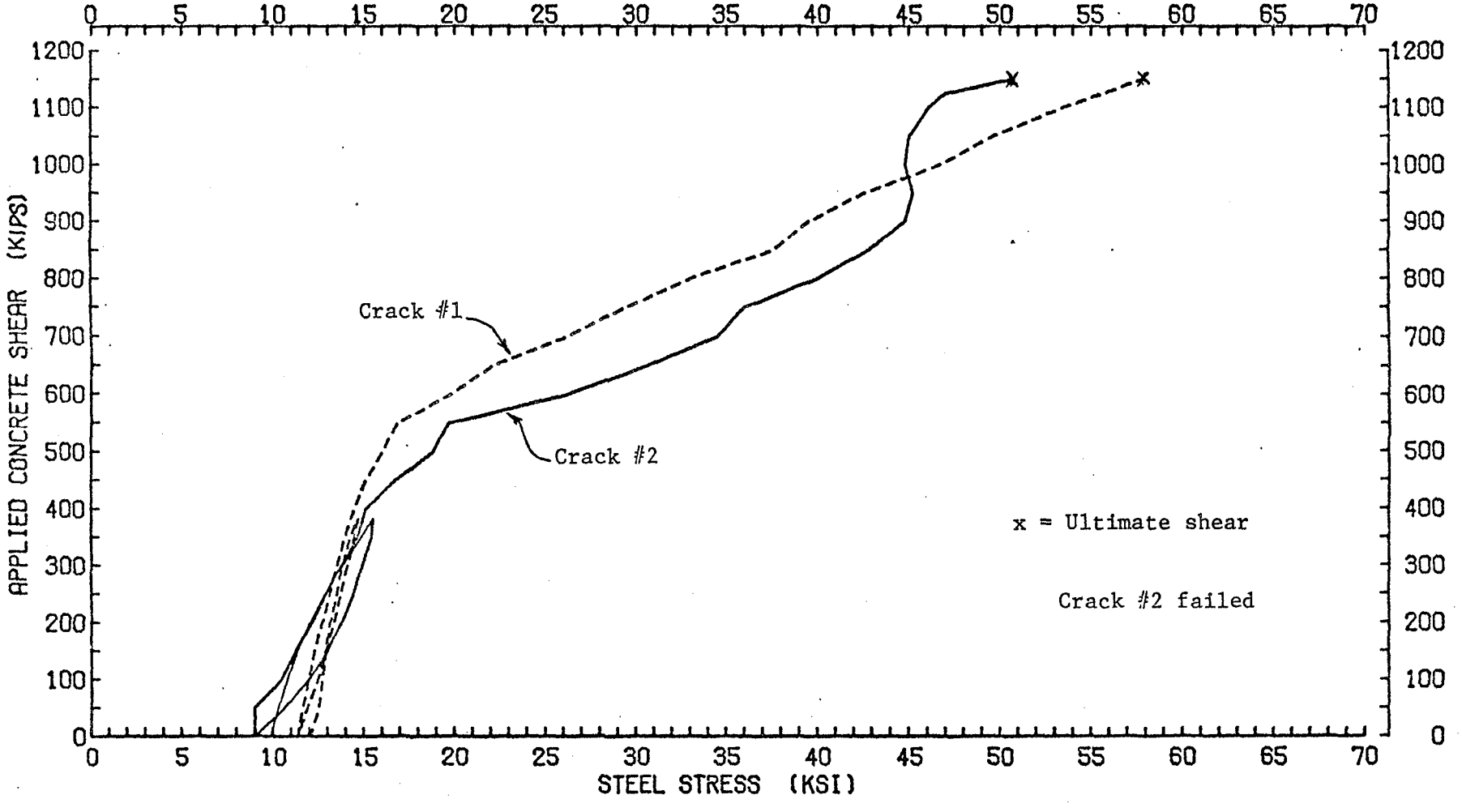

Fig. B12 Applied concrete shear-steel stress curves, Specimen M6A

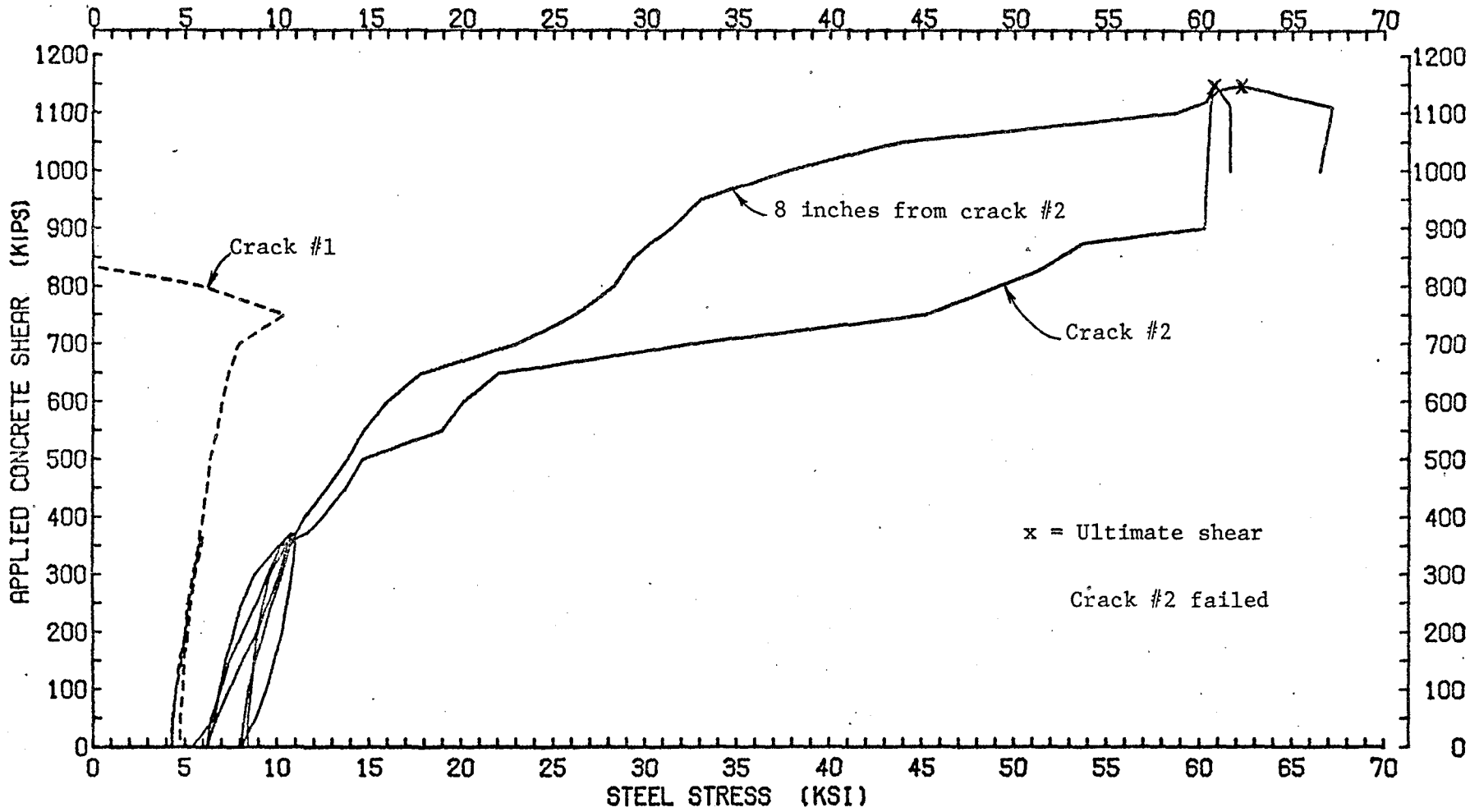

Fig. B13 Applied concrete shear-steel stress curves, Specimen M8A

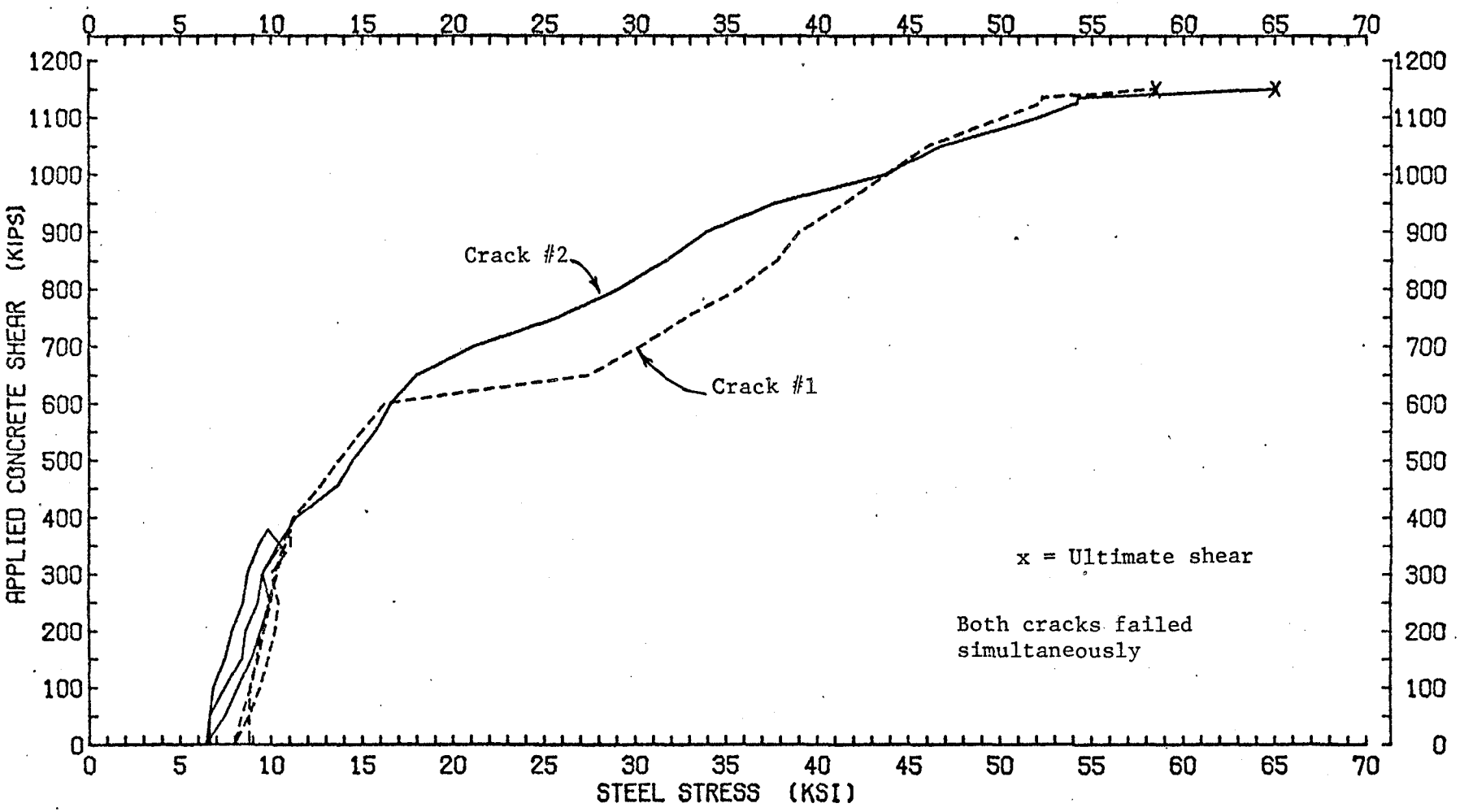

Fig. B14 Applied concrete shear-steel stress curves, Specimen M9A

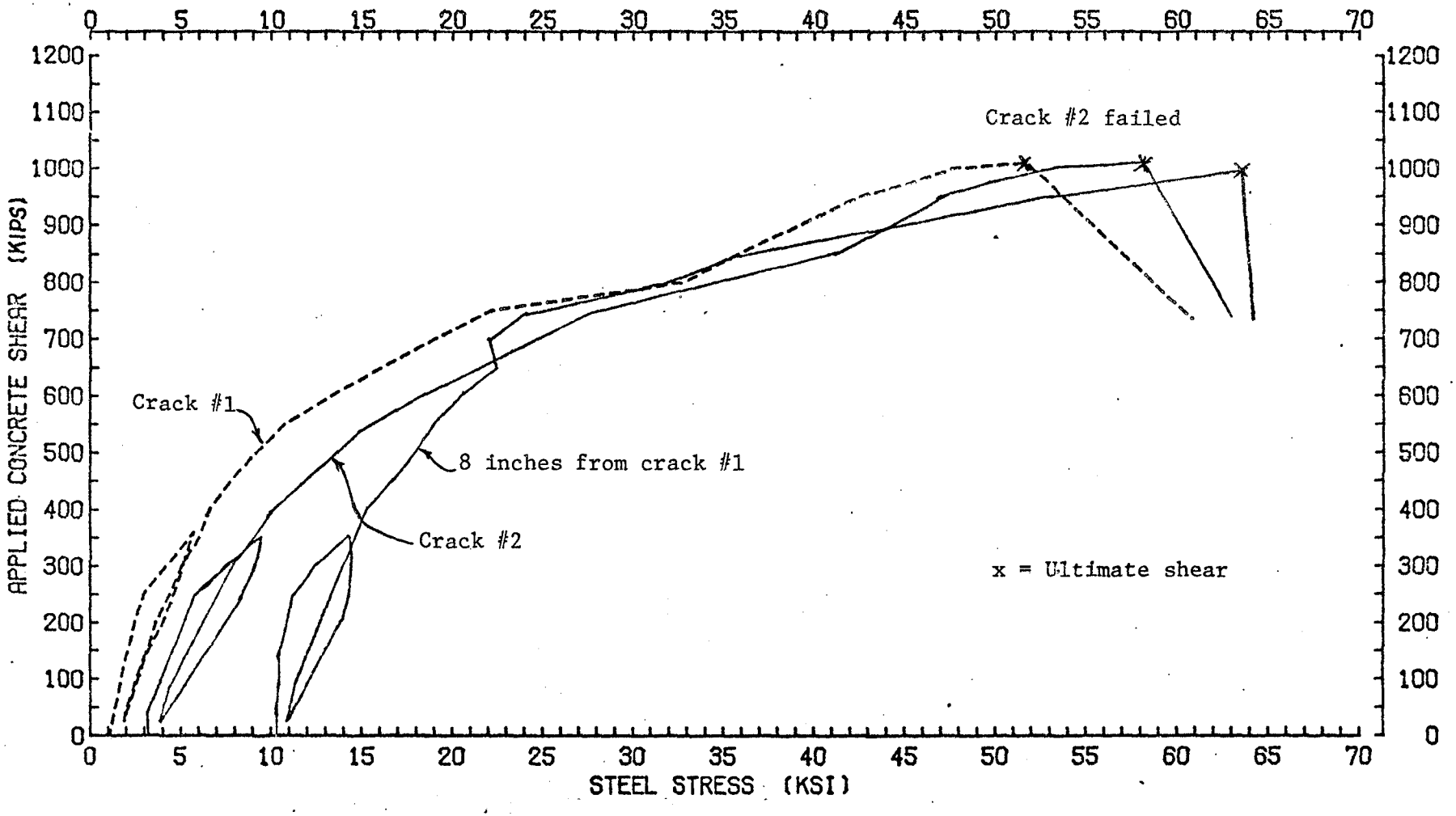

Fig. 815 Applied concrete shear-steel stress curves, Specimen M10A

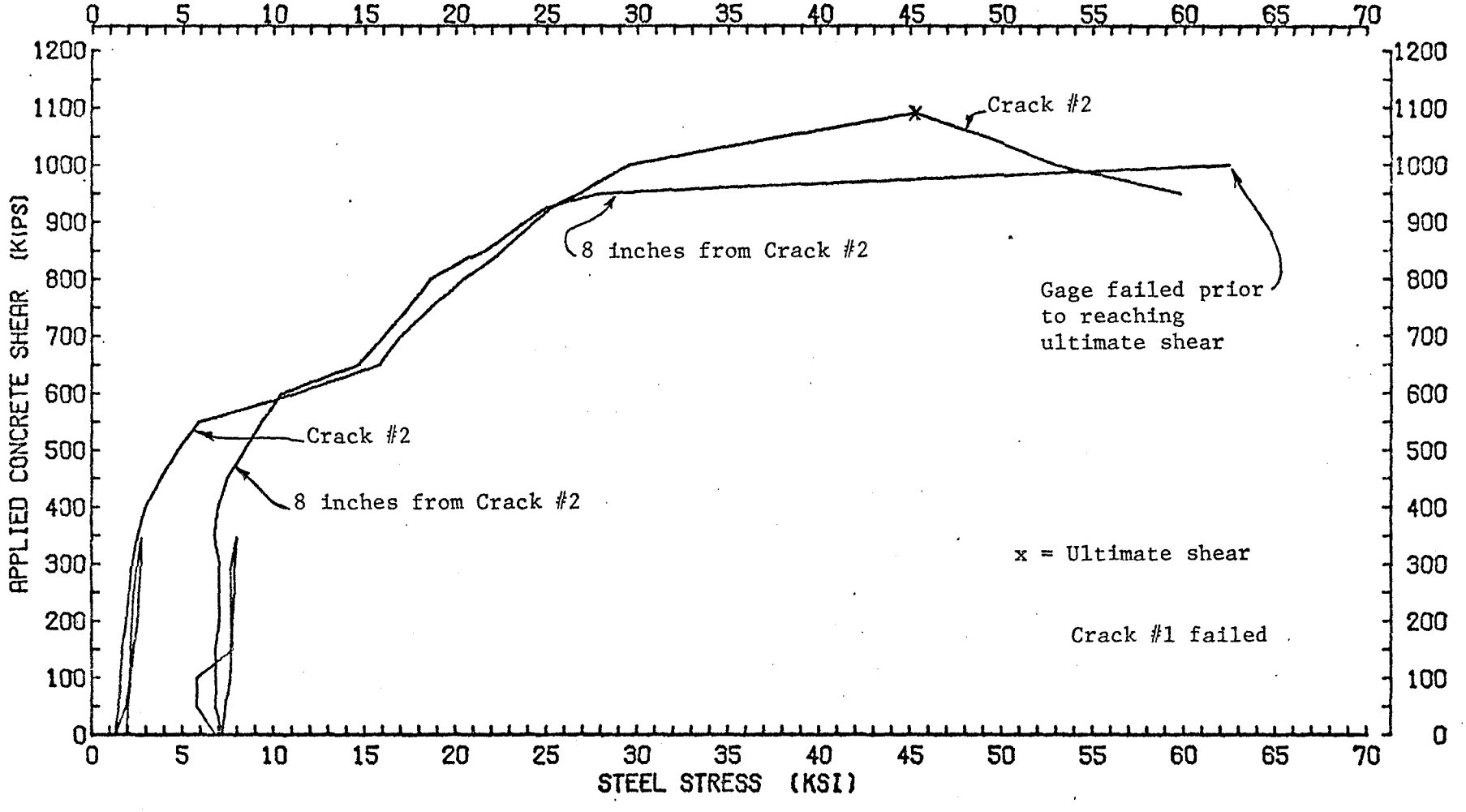

Fig. B16 Applied concrete shear-steel stress curves, Specimen M11A

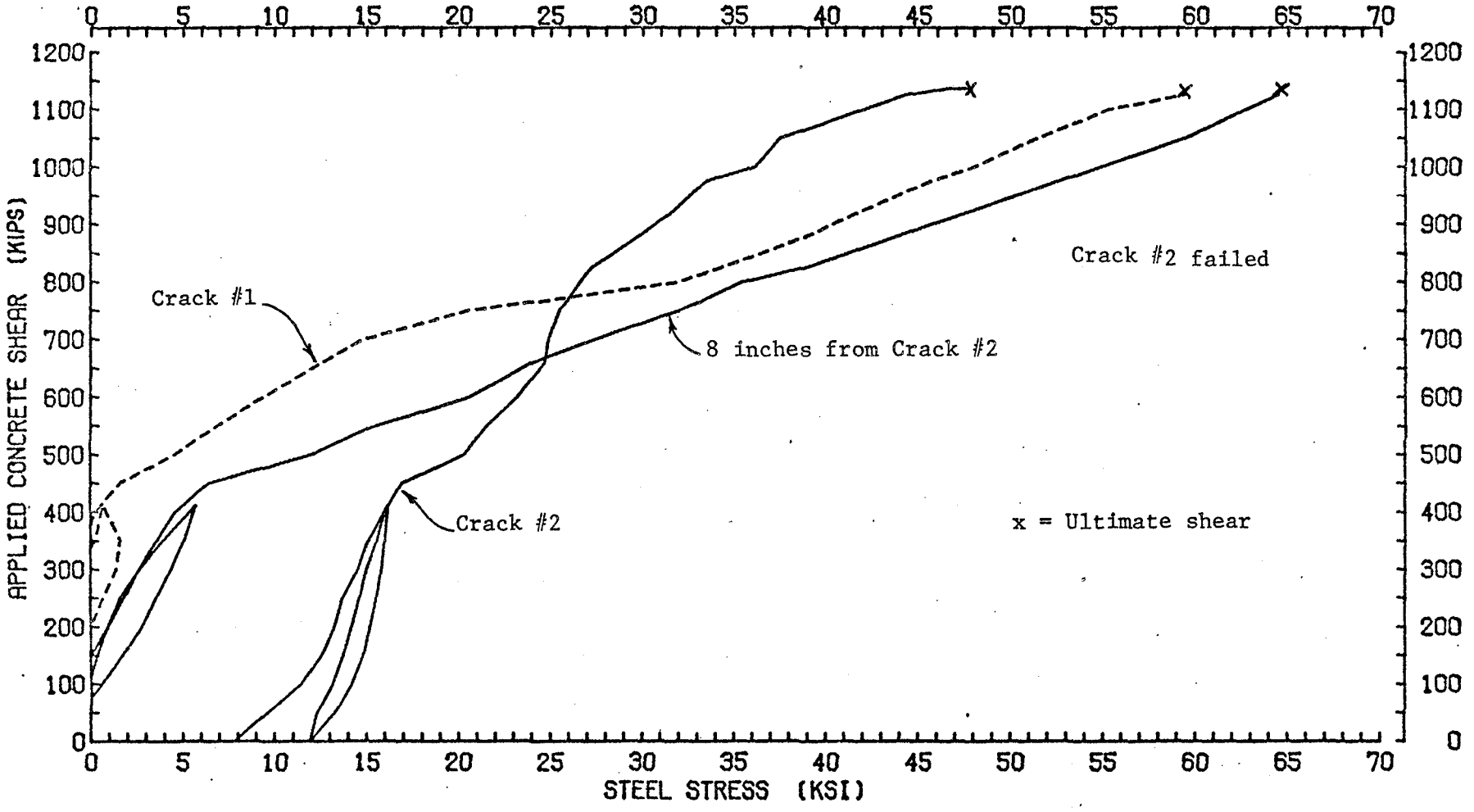

Fig. B17 Applied concrete shear-steel stress curves, Specimen M14A

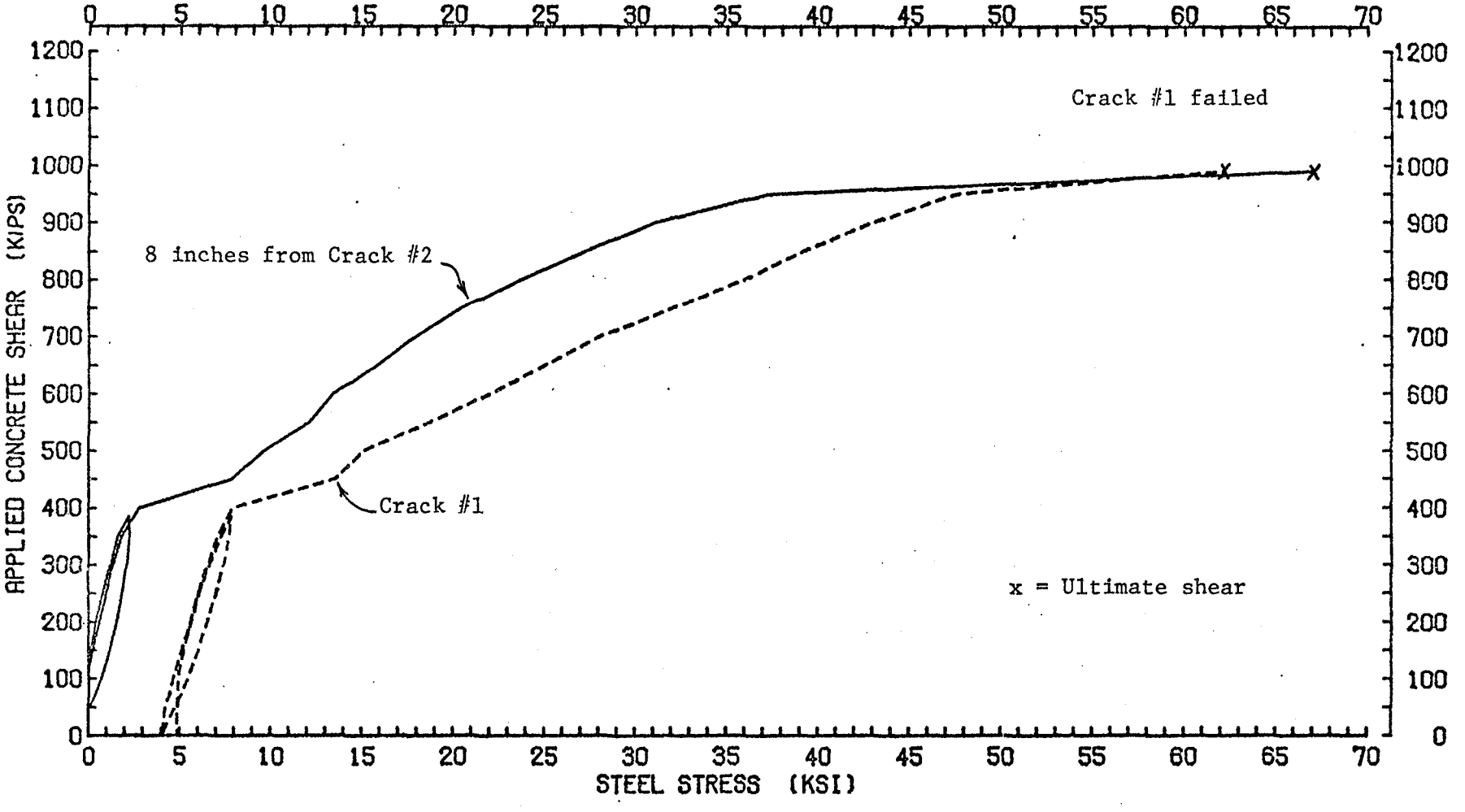

Fig. B18 Applied concrete shear-steel stress curves, Specimen M18A

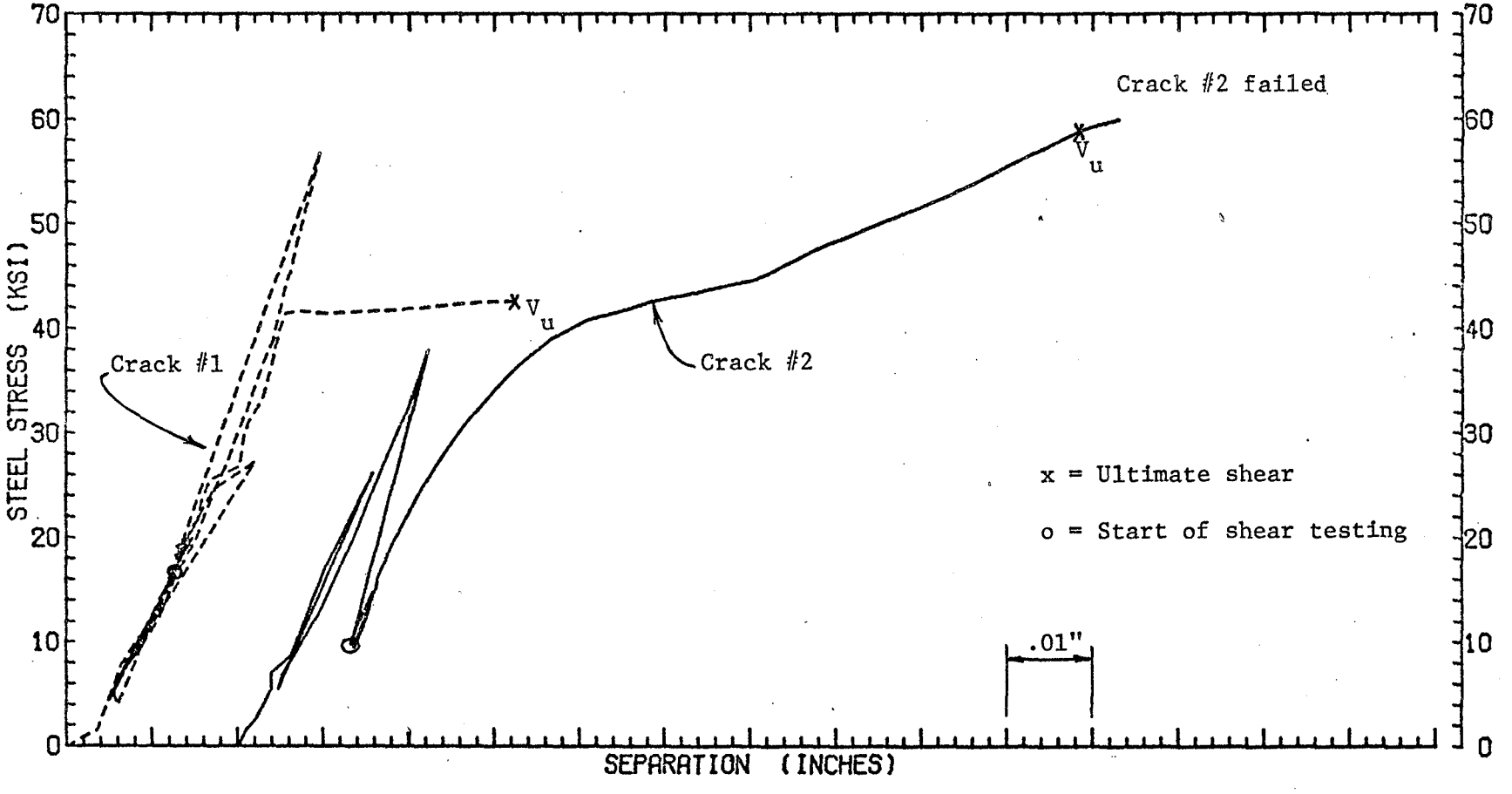

Fig. B19 Steel stress-separation curves, Specimen M4A

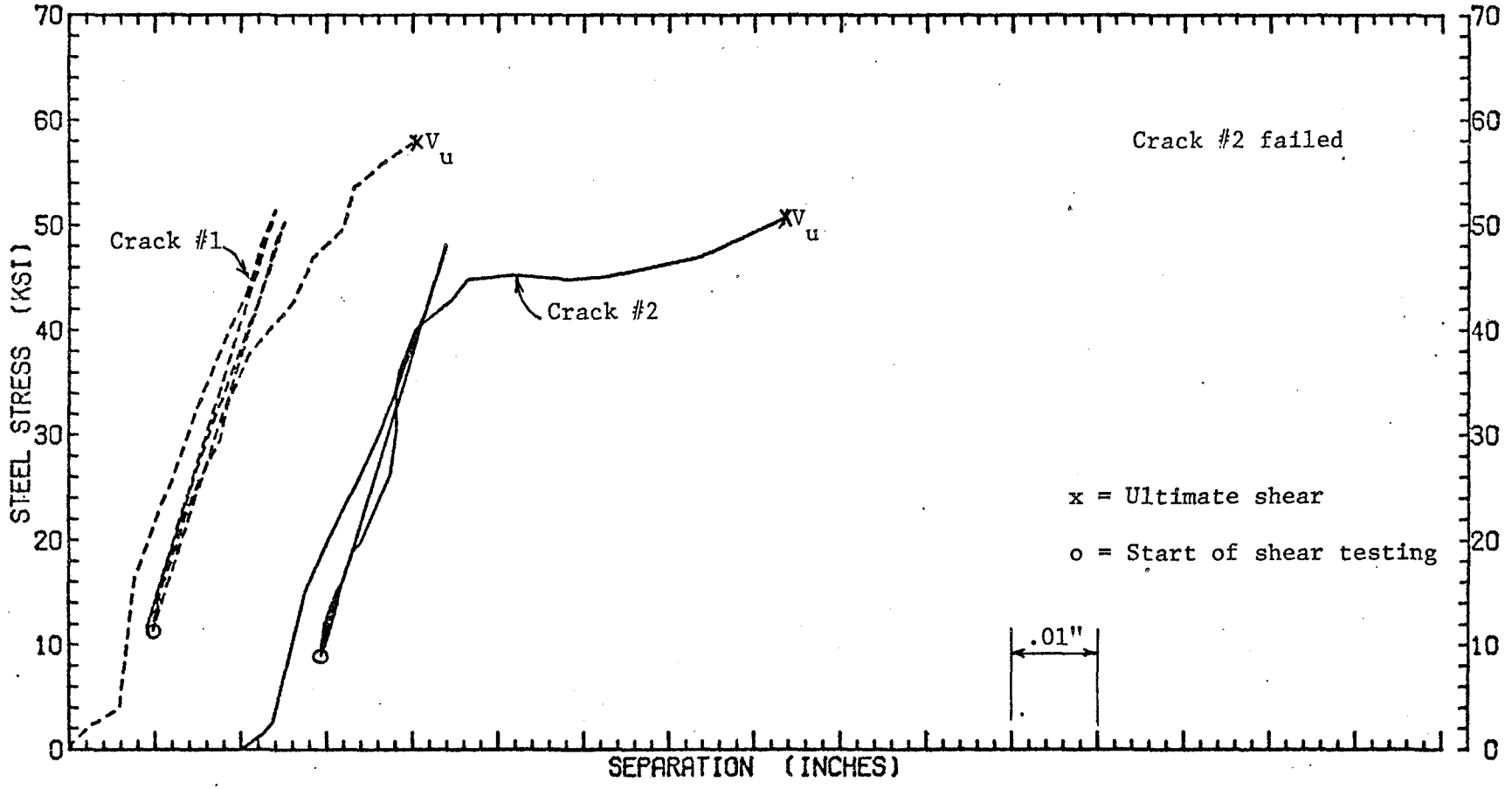

Fig. B20 Steel stress-separation curves, Specimen M6A

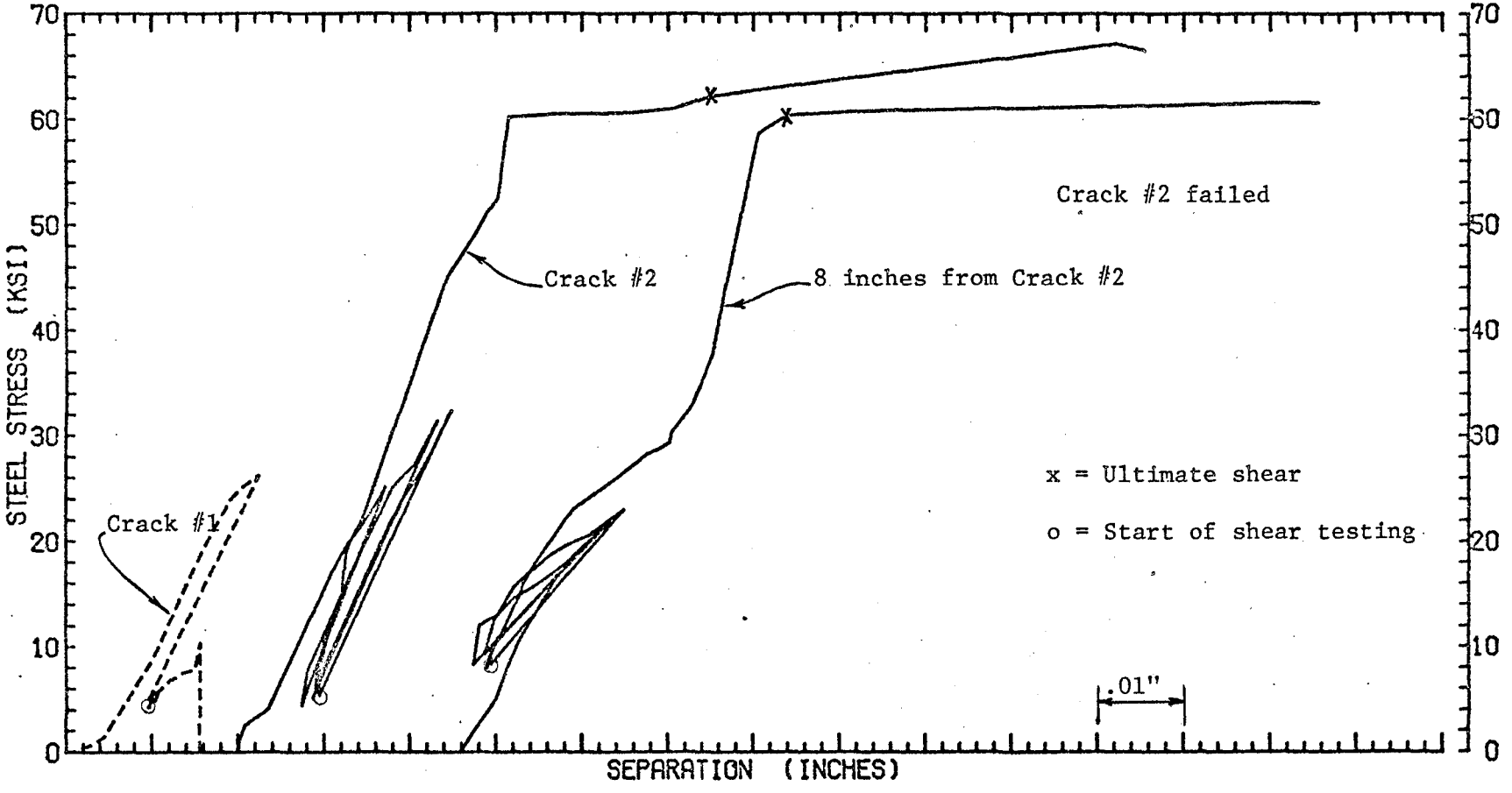

Fig. B21 Steel stress-separation curves, Specimen M8A

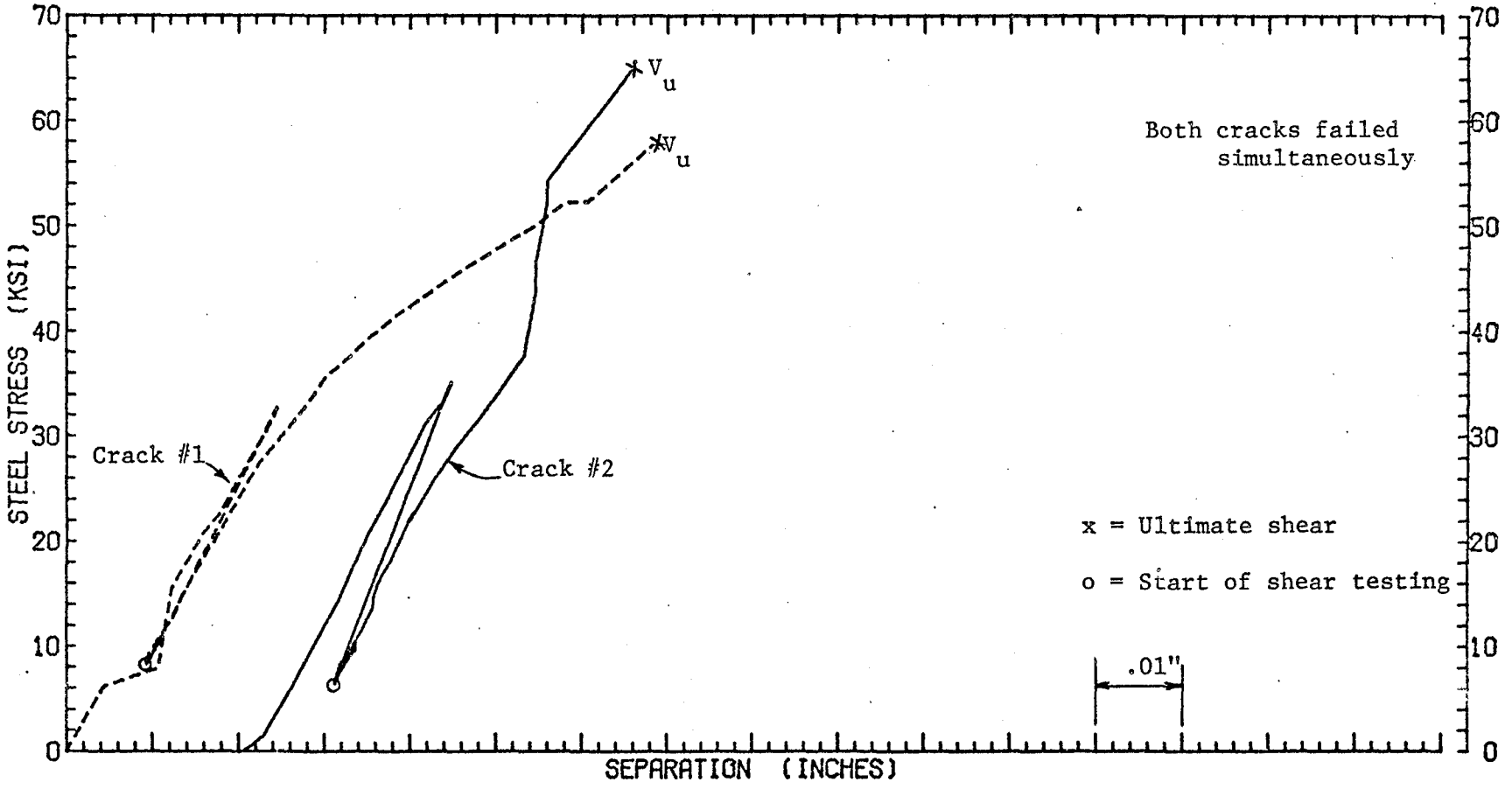

Fig. B22 Steel stress-separation curves, Specimen M9A

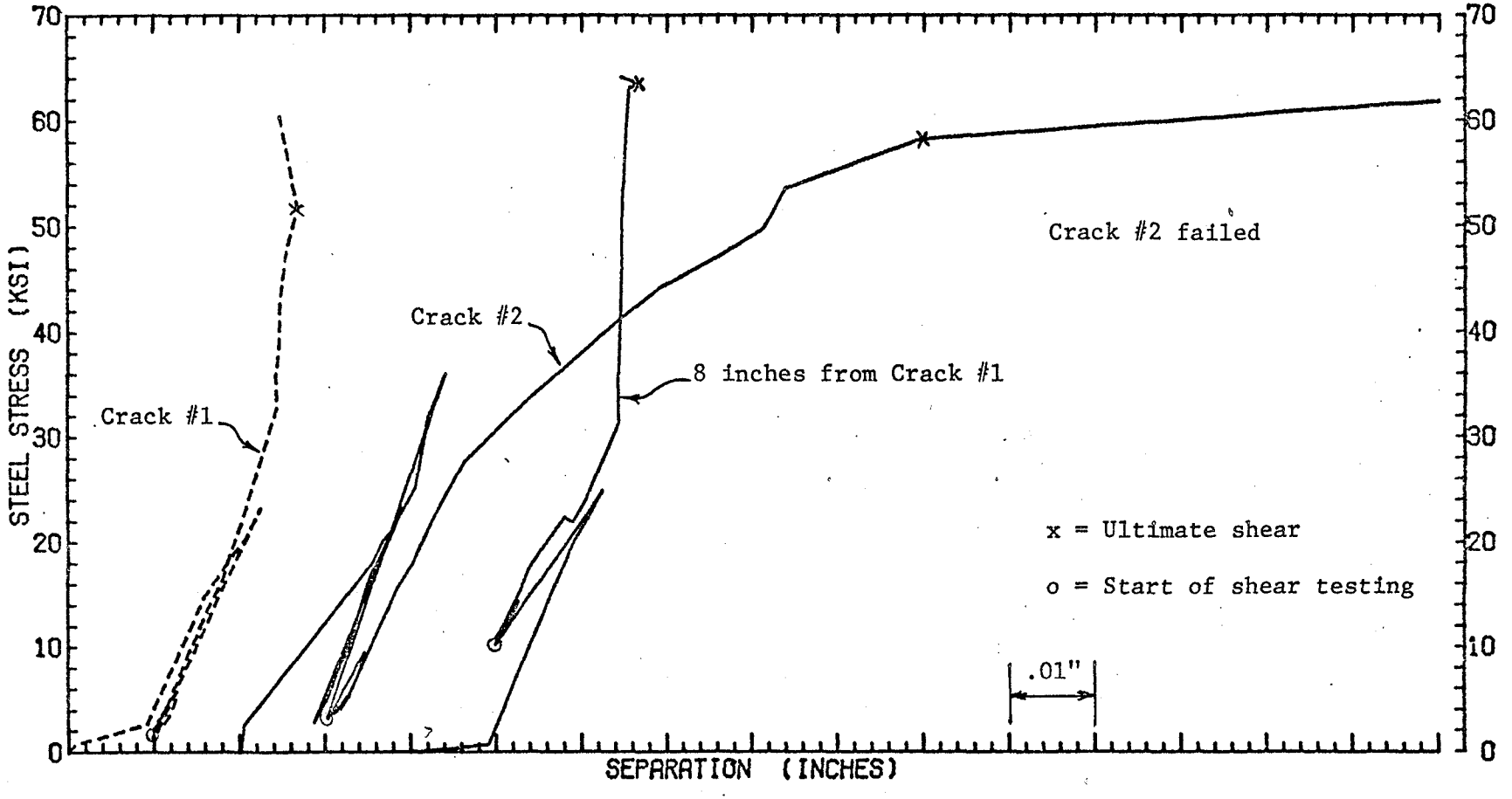

Fig. B23 Steel stress-separation curves, Specimen M10A

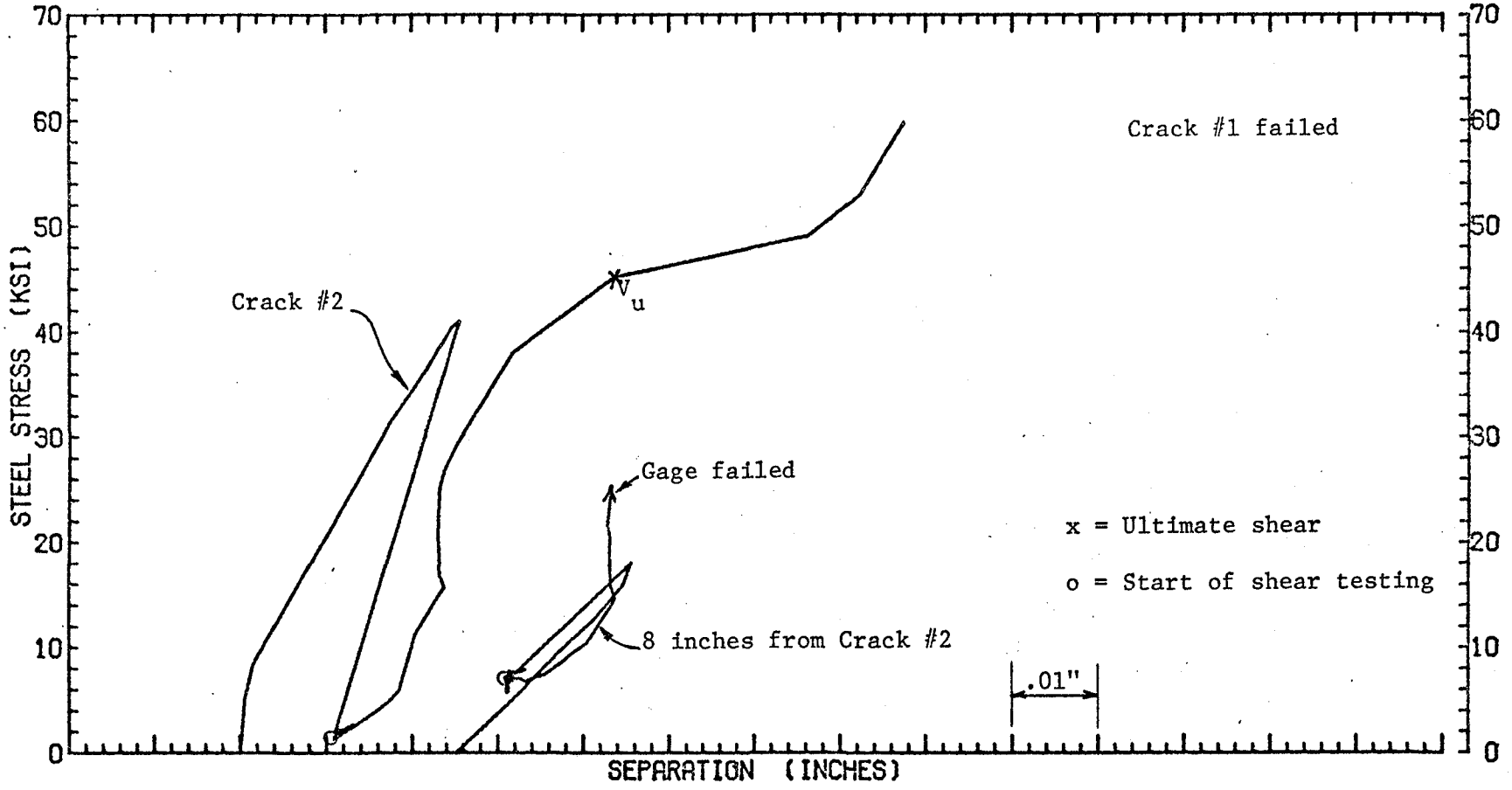

Fig. B24 Steel stress-separation curves, Specimen M11A

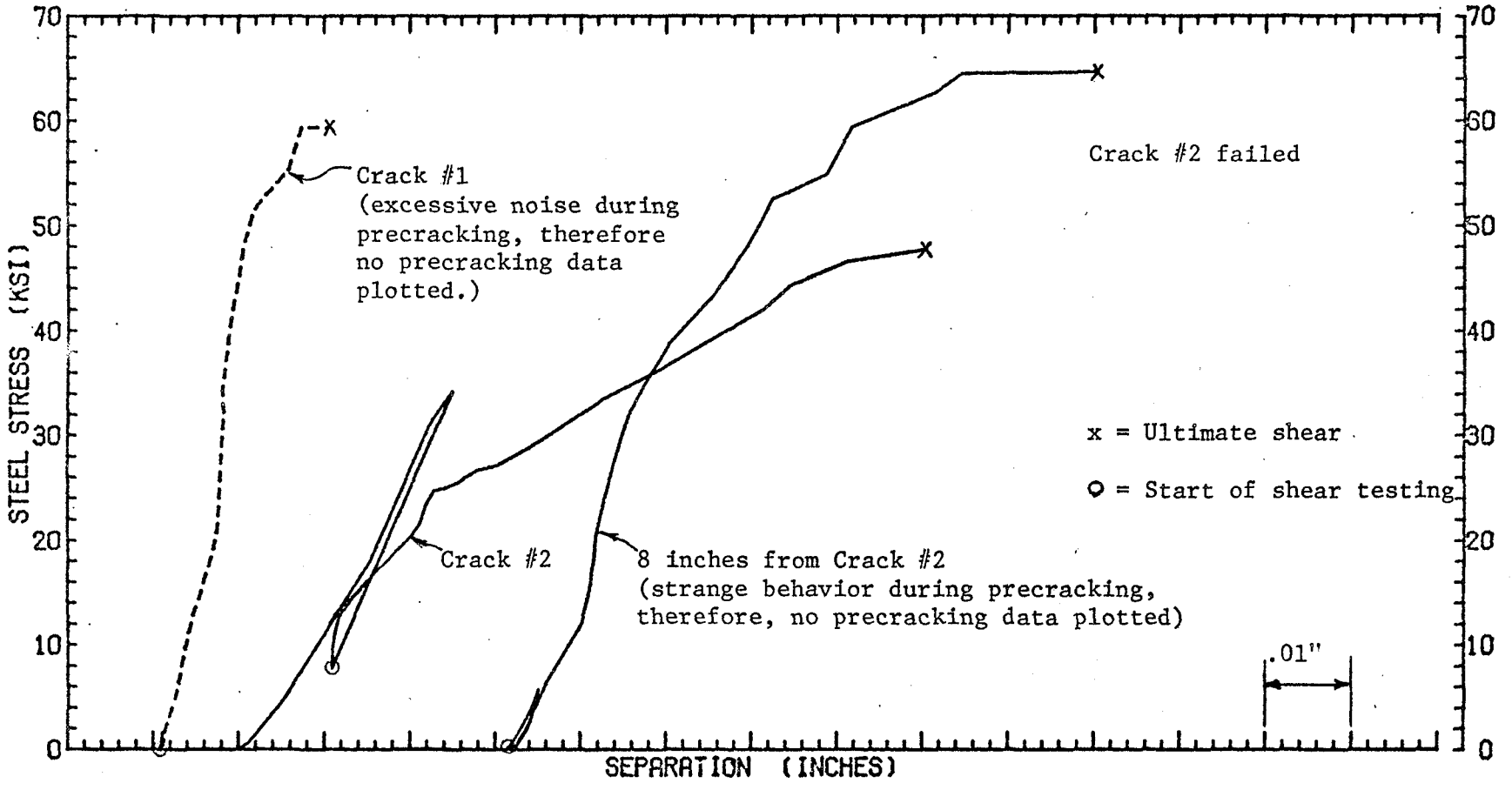

Fig. B25 Steel stress-separation curves, Specimen M14A

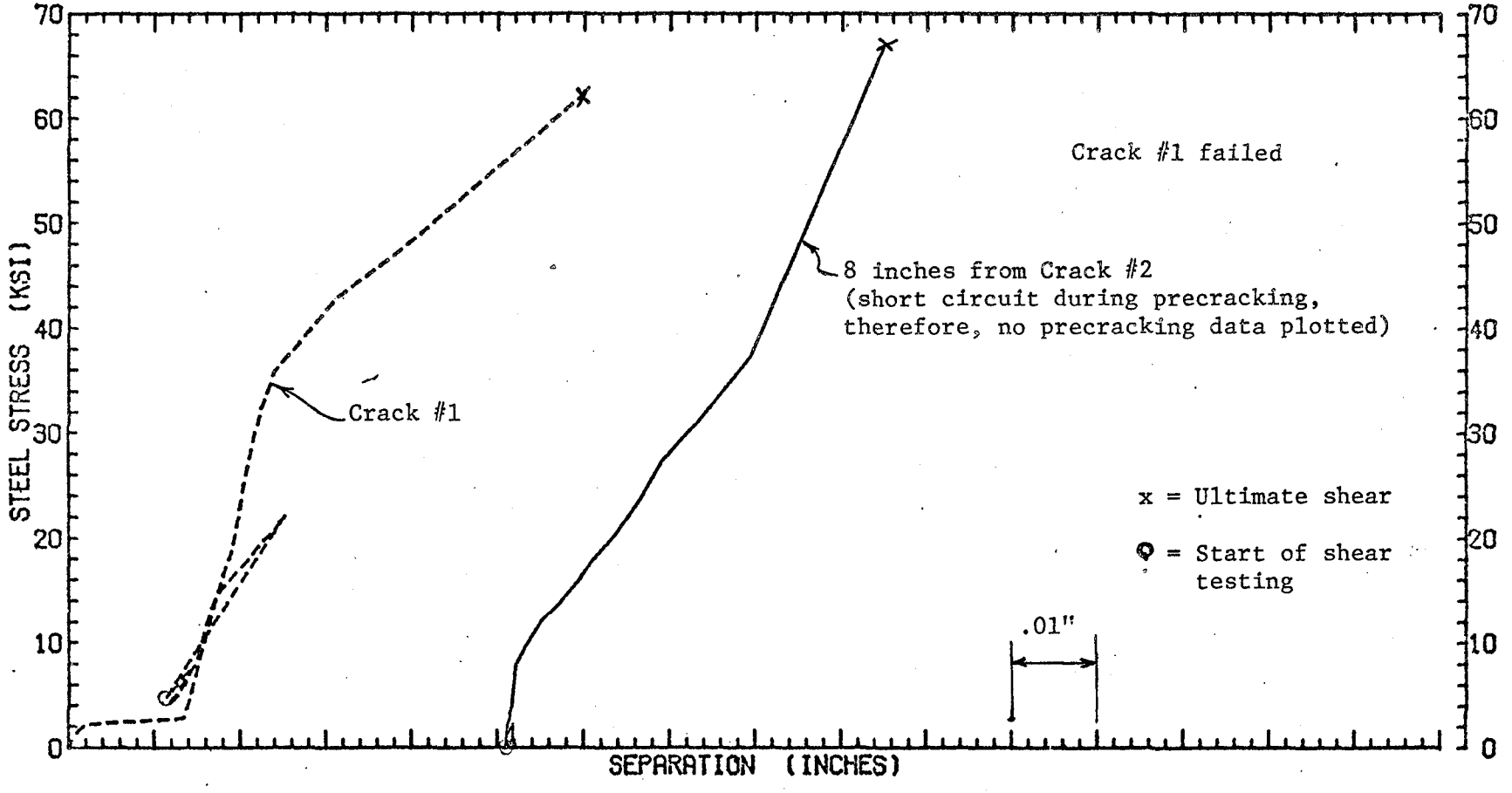

Fig. B26 Steel stress-separation curves, Specimen M18A

APPENDIX C

TYPICAL DATA FROM CYCLIC LOADING TESTS

(Data presented is for the crack in which failure occurred).

Figure	Title
C1	Shear - slip curves, C4A, cycles 1 - 5
C2	Shear - slip curves, C4A, cycles 6 - 10
C3	Shear - slip curves, C4A, cycles 21 - 25
C4	Shear - slip curves, C4A, cycles 36 - 40
C5	Shear - slip curves, C4A, cycles 41 - 42
C6	Shear - slip curves, C8A, cycles 1 - 5
C7	Shear - slip curves, C8A, cycles 6 - 10
C8	Shear - slip curves, C8A, cycles 21 - 25
C9	Shear - slip curves, C8A, cycles 46 - 50
C10	Shear - slip curves, C8A, cycles 51 - 56
C11	Shear - slip curves, C10A, cycles 1 - 5
C12	Shear - slip curves, C10A, cycles 6 - 10
C13	Shear - slip curves, C10A, cycles 21 - 25
C14	Shear - slip curves, C10A, cycles 41 - 45
C15	Shear - slip curves, C10A, cycles 46 - 49
C16	Shear - slip curves, C14A, cycles 1 - 5
C17	Shear - slip curves, C14A, cycles 6 - 10
C18	Shear - slip curves, C14A, cycles 21 - 25
C19	Shear - slip curves, C14A, cycles 41 - 45
C20	Shear - slip curves, C14A, cycles 46 - 48

Figure	Title
C21	Slip - separation curves, C4A, cycles 1 - 5
C22	Slip - separation curves, C4A, cycles 6 - 10
C23	Slip - separation curves, C4A, cycles 21 - 25
C24	Slip - separation curves, C4A, cycles 36 - 40
C25	Slip - separation curves, C4A, cycles 41 - 42
C26	Slip - separation curves, C8A, cycles 1 - 5
C27	Slip - separation curves, C8A, cycles 6 - 10
C28	Slip - separation curves, C8A, cycles 21 - 25
C29	Slip - separation curves, C8A, cycles 46 - 50
C30	Slip - separation curves, C8A, cycles 51 - 56
C31	Slip - separation curves, C10A, cycles 1 - 5
C32	Slip - separation curves, C10A, cycles 6 - 10
C33	Slip - separation curves, C10A, cycles 21 - 25
C34	Slip - separation curves, C10A, cycles 41 - 45
C35	Slip - separation curves, C10A, cycles 46 - 49
C36	Slip - separation curves, C14A, cycles 1 - 5
C37	Slip - separation curves, C14A, cycles 6 - 10
C38	Slip - separation curves, C14A, cycles 21 - 25
C39	Slip - separation curves, C14A, cycles 41 - 45
C40	Slip - separation curves, C14A, cycles 46 - 48
C41	Shear - steel stress curves, C4A, cycles 21 - 42
C42	Shear - steel stress curves, C8A, cycles 1 - 25
C43	Shear - steel stress curves, C8A, cycles 30 - 56
C44	Shear - steel stress curves, C10A, cycles 1 - 25
C45	Shear - steel stress curves, C10A, cycles 30 - 49

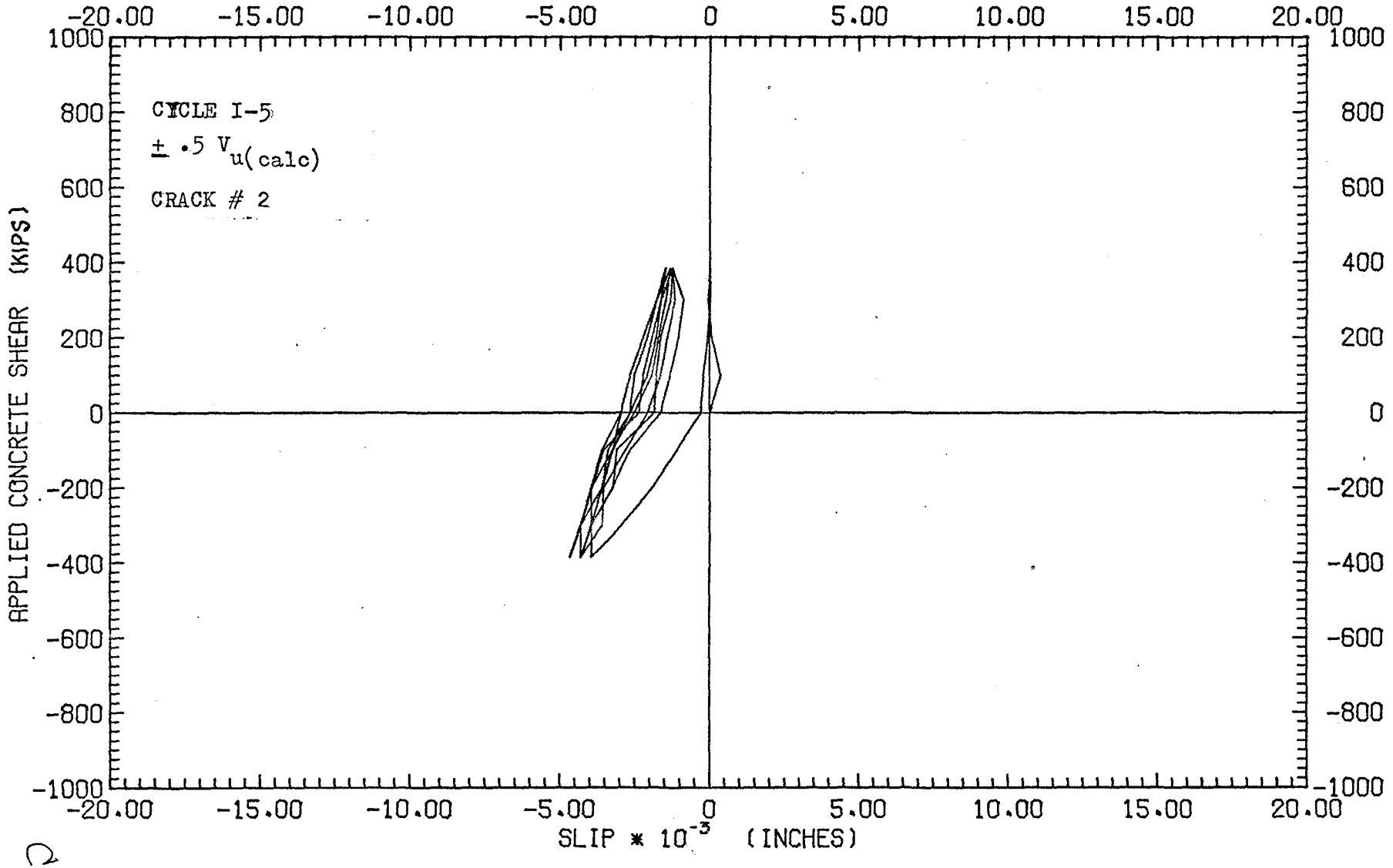

FIG.- C1, SHEAR-SLIP CURVES, C4A

42

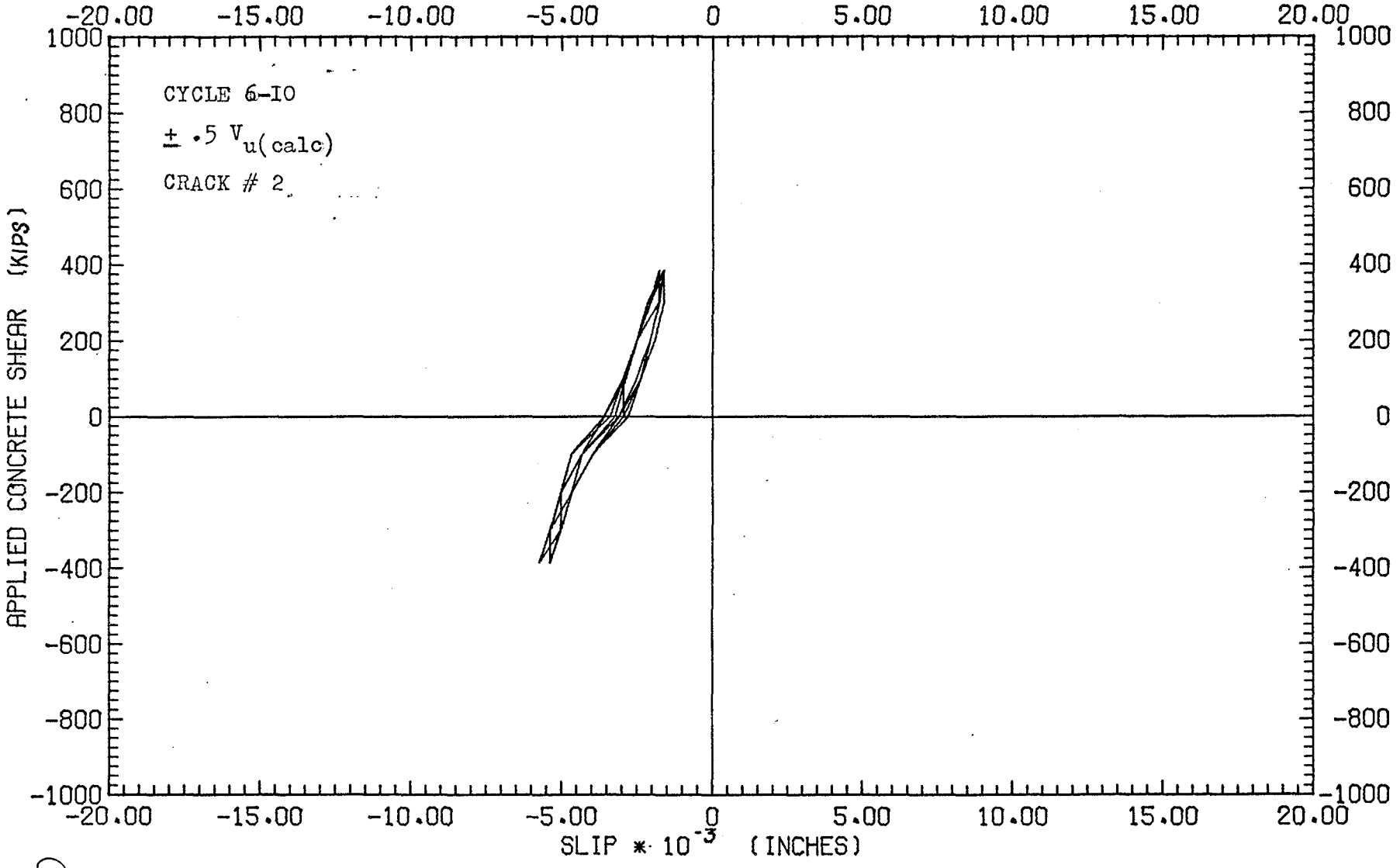

FIG.-C2, SHEAR-SLIP CURVES, C4A

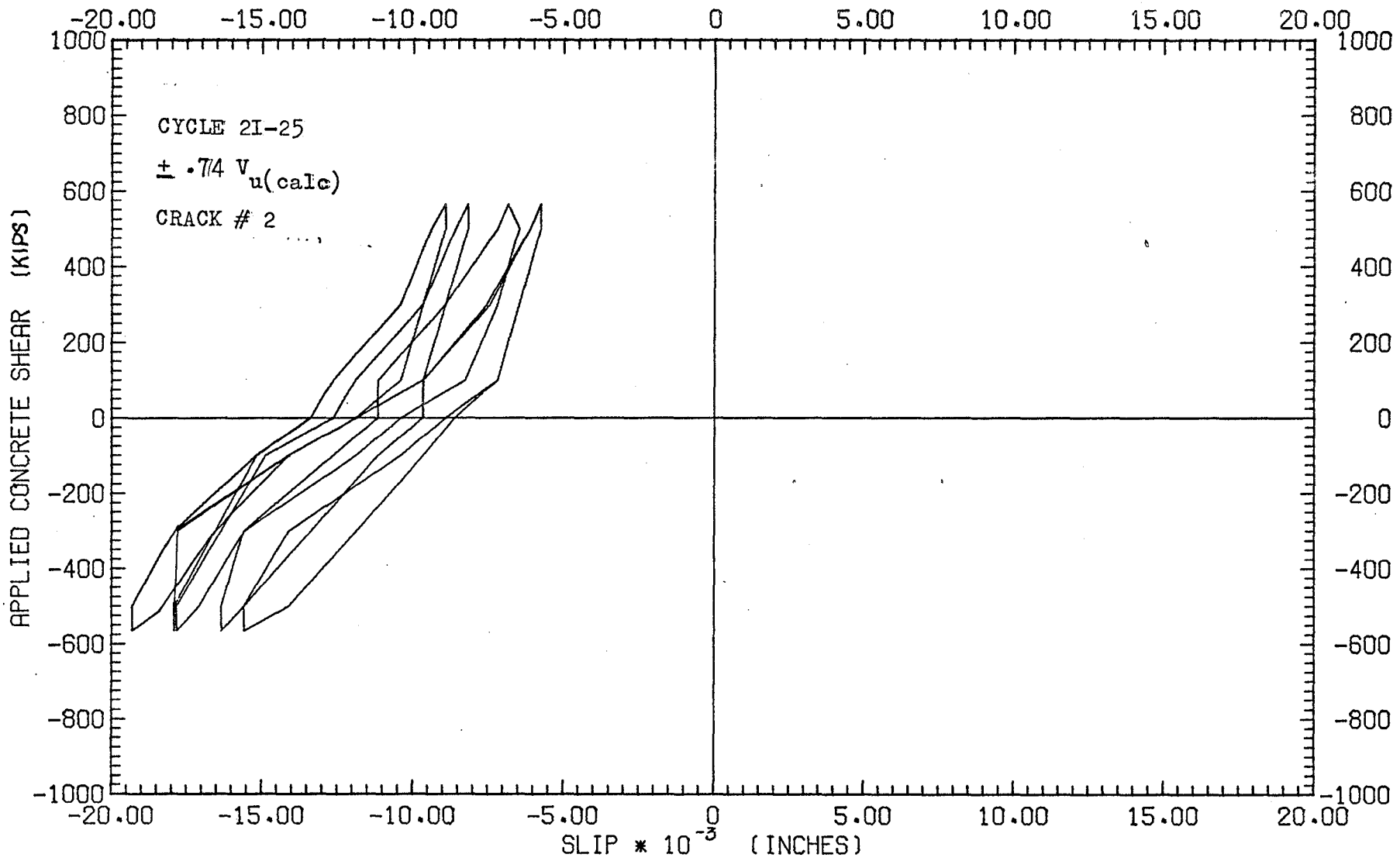

FIG.-C3, SHEAR-SLIP CURVES, C4A

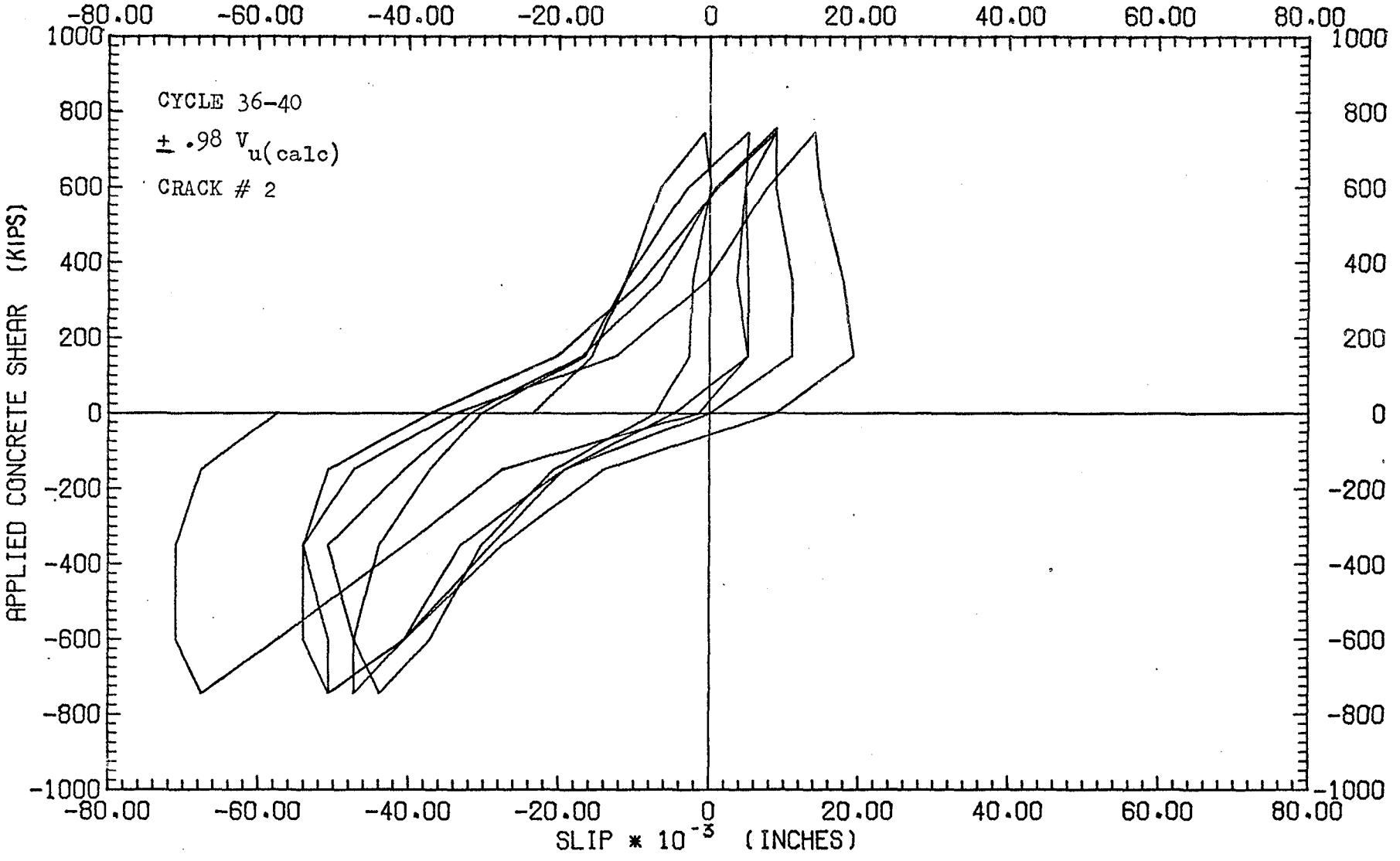

FIG.-C4, SHEAR-SLIP CURVES, C4A

42

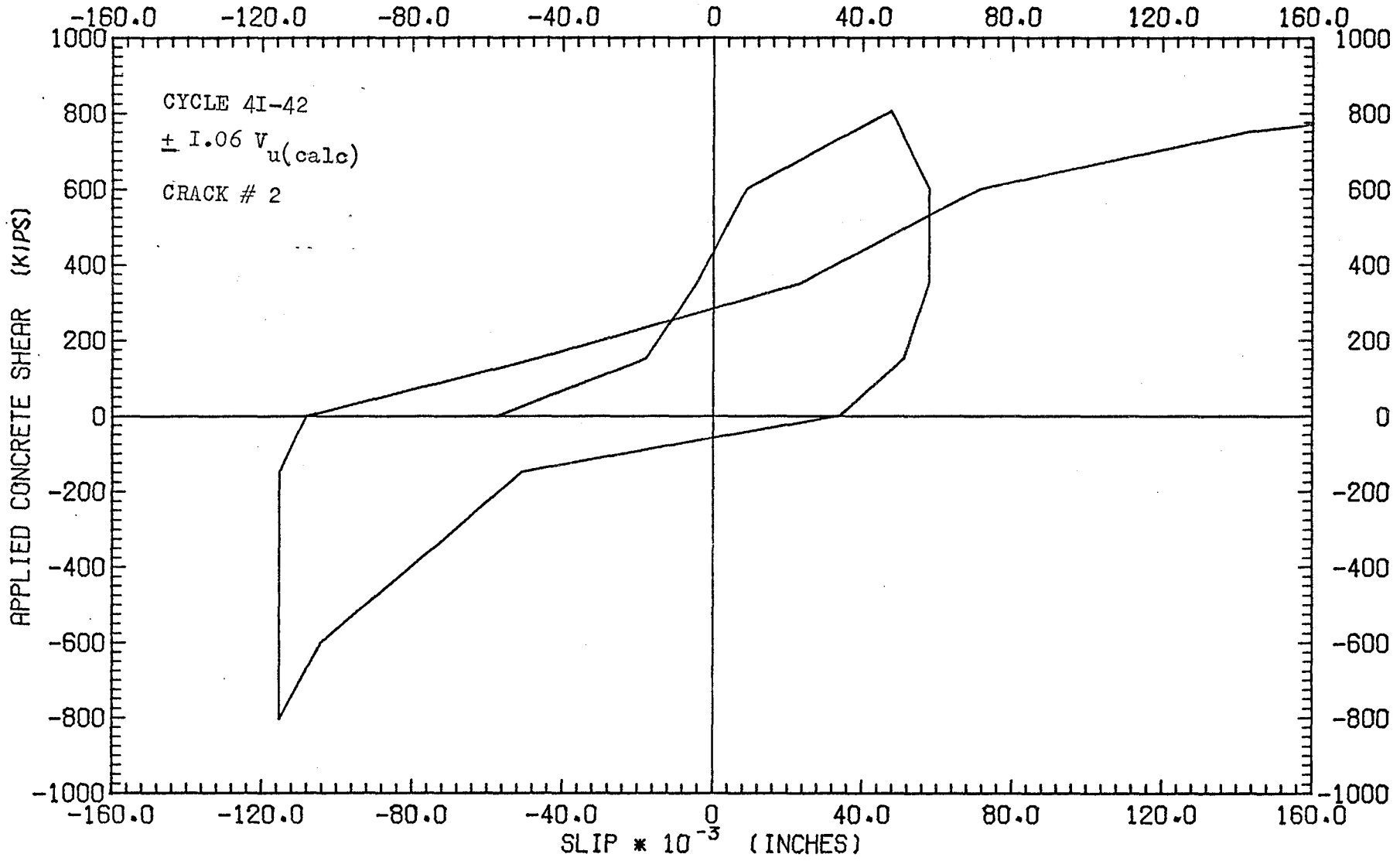

FIG.-C5, SHEAR-SLIP CURVES, C4A

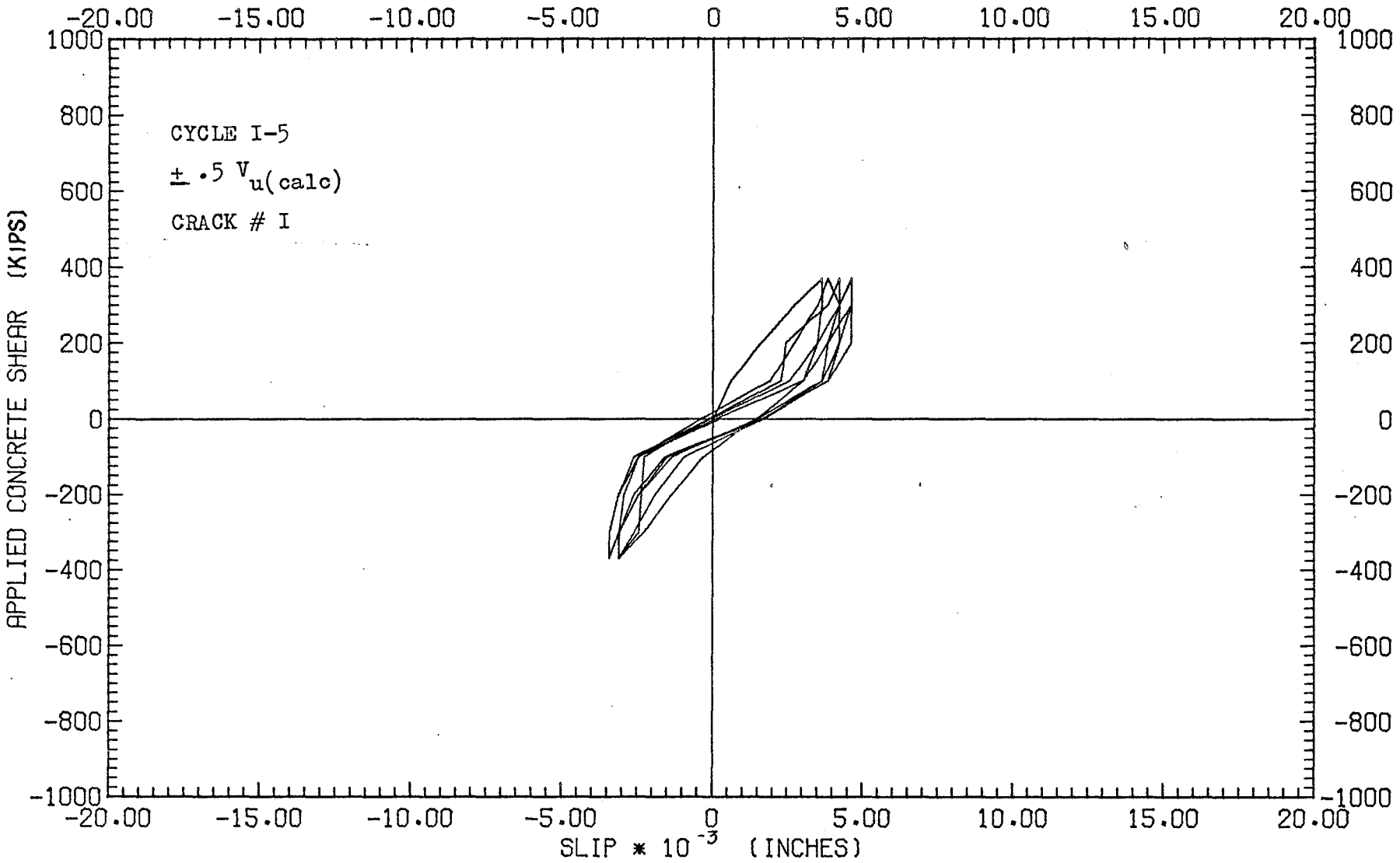

FIG.-C6, SHEAR-SLIP CURVES, C8A

62

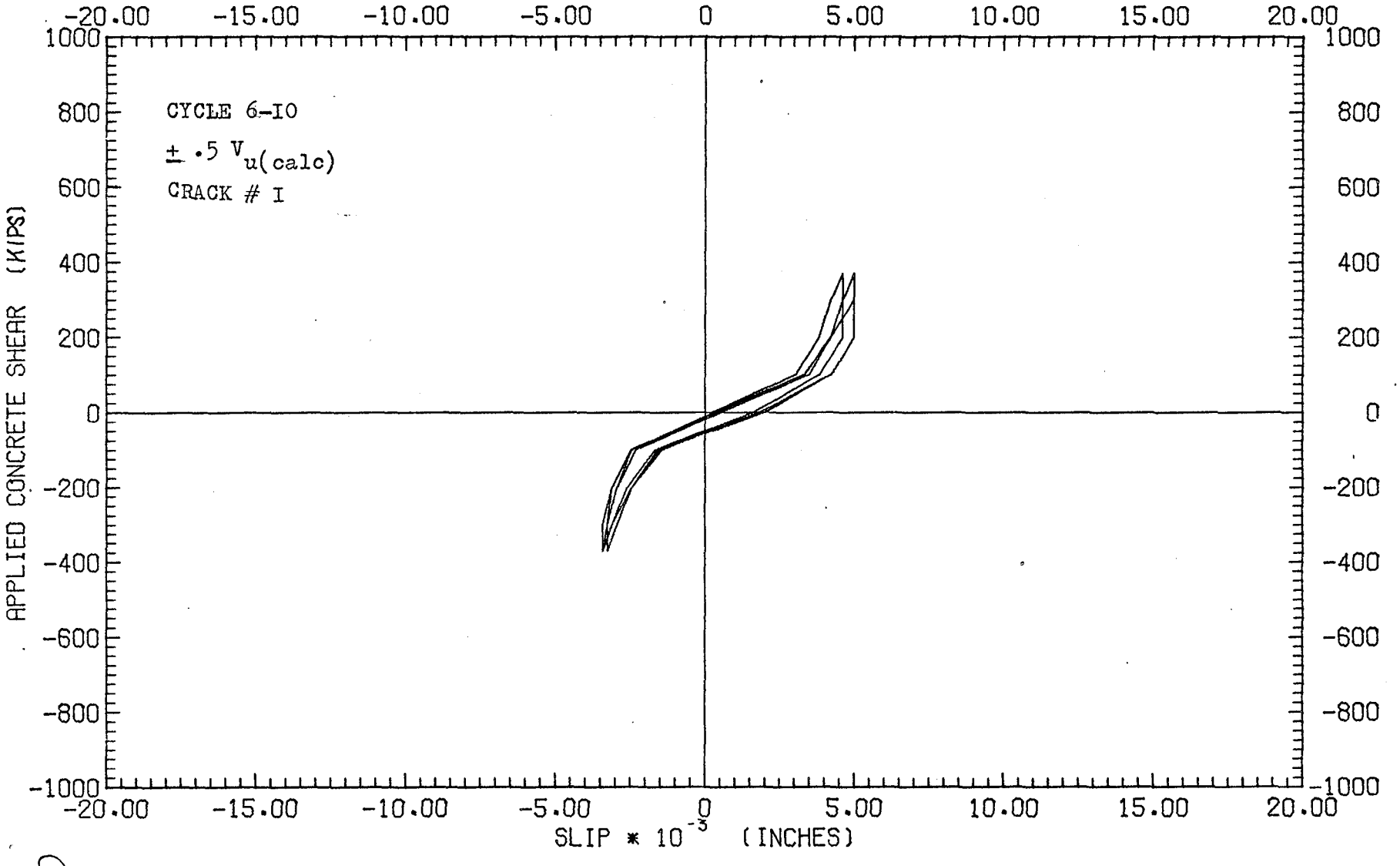

FIG.-C7, SHEAR-SLIP CURVES, C8A

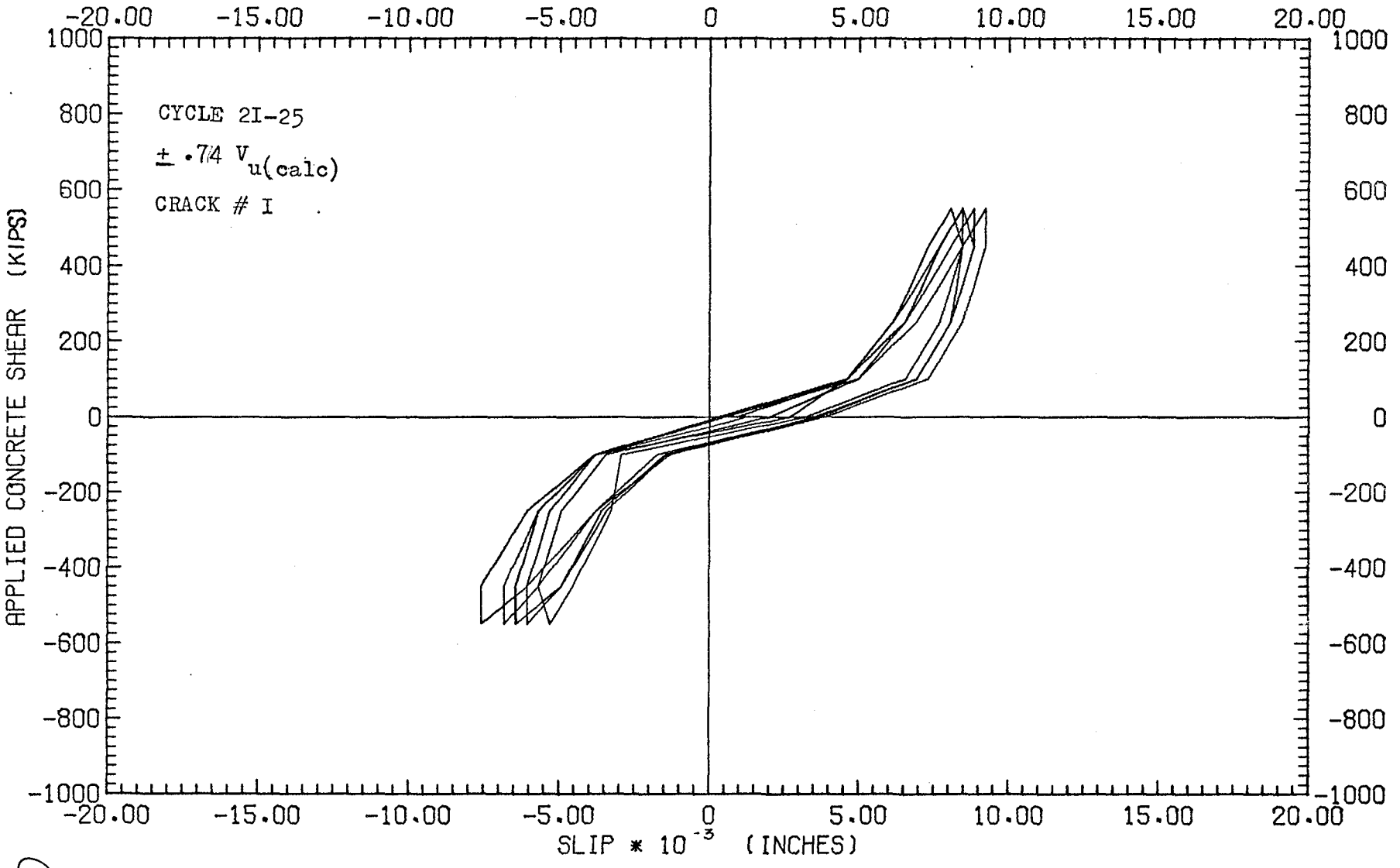

FIG.-C8, SHEAR-SLIP CURVES, C8A

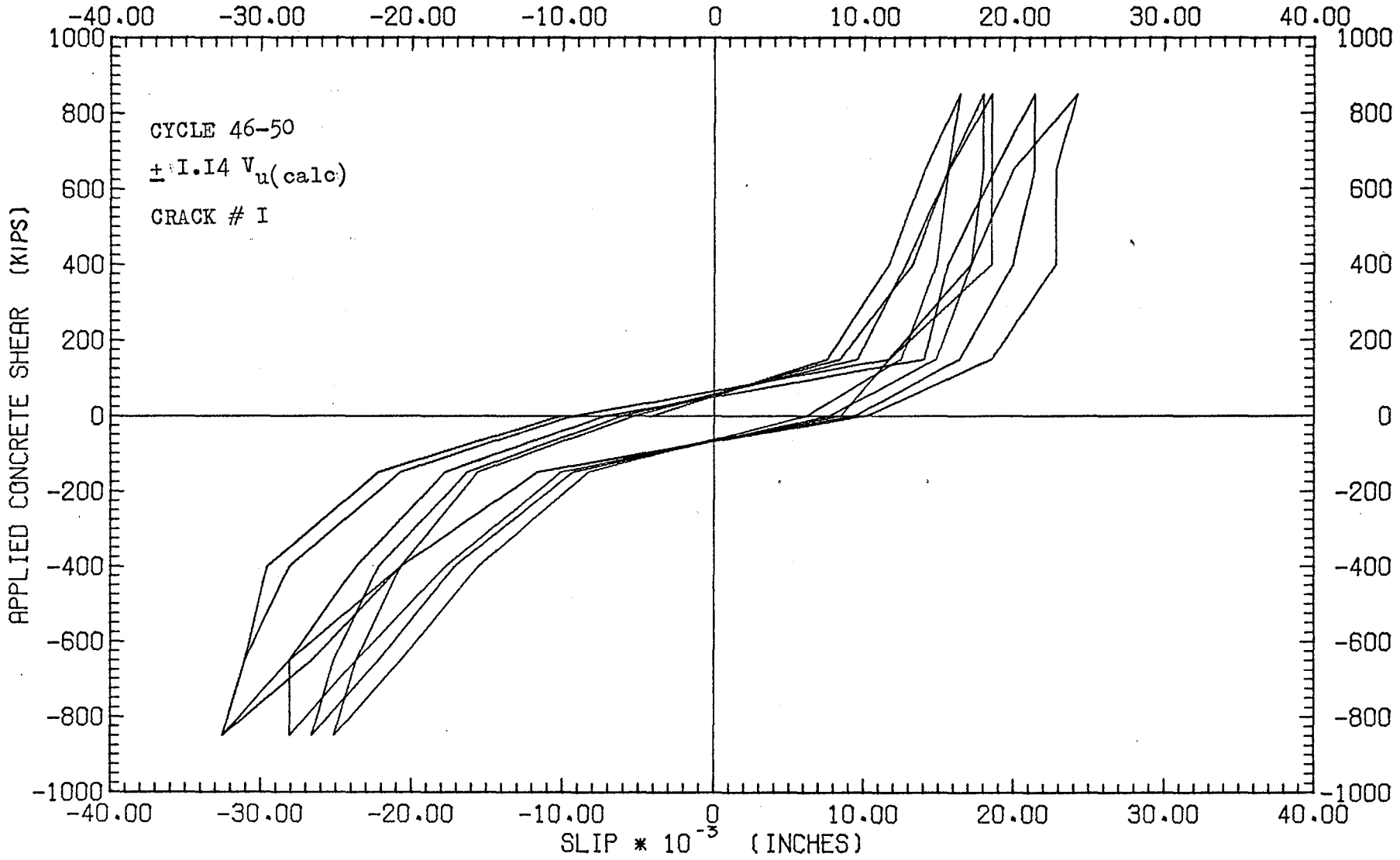

FIG.-C9, SHEAR-SLIP CURVES, C8A

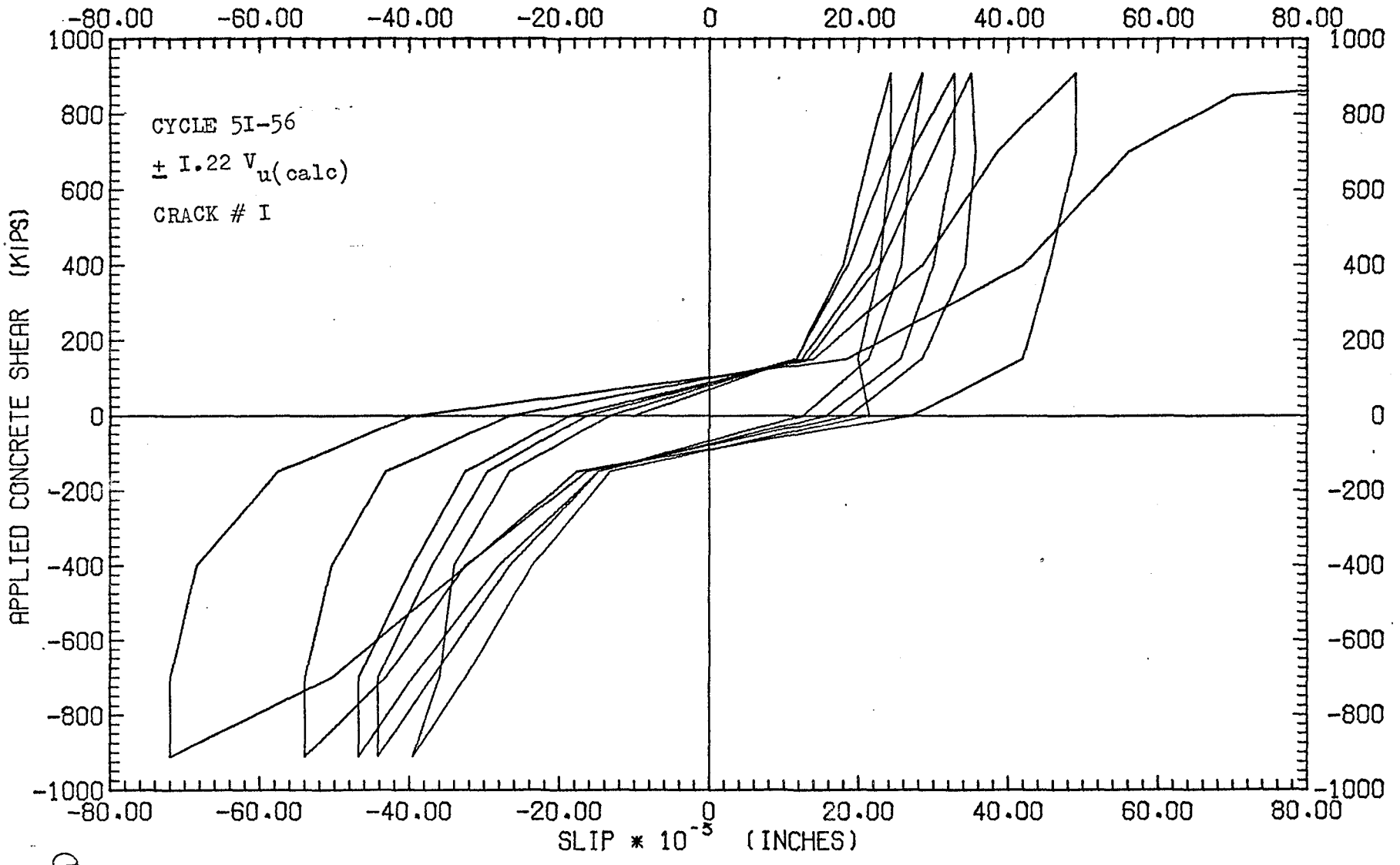

FIG.-C10, SHEAR-SLIP CURVES, C8A

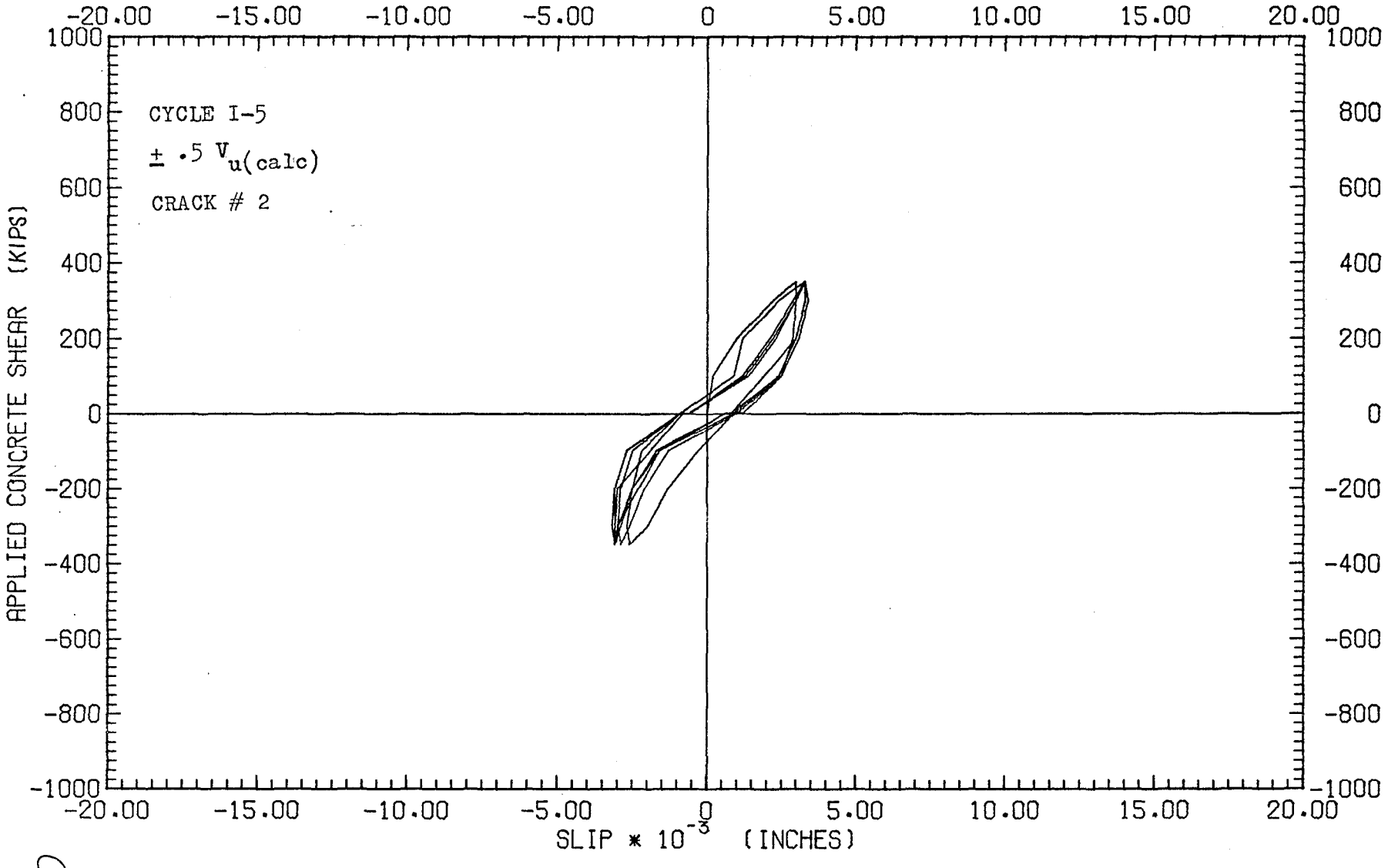

FIG.-C11, SHEAR-SLIP CURVES, C10A

12

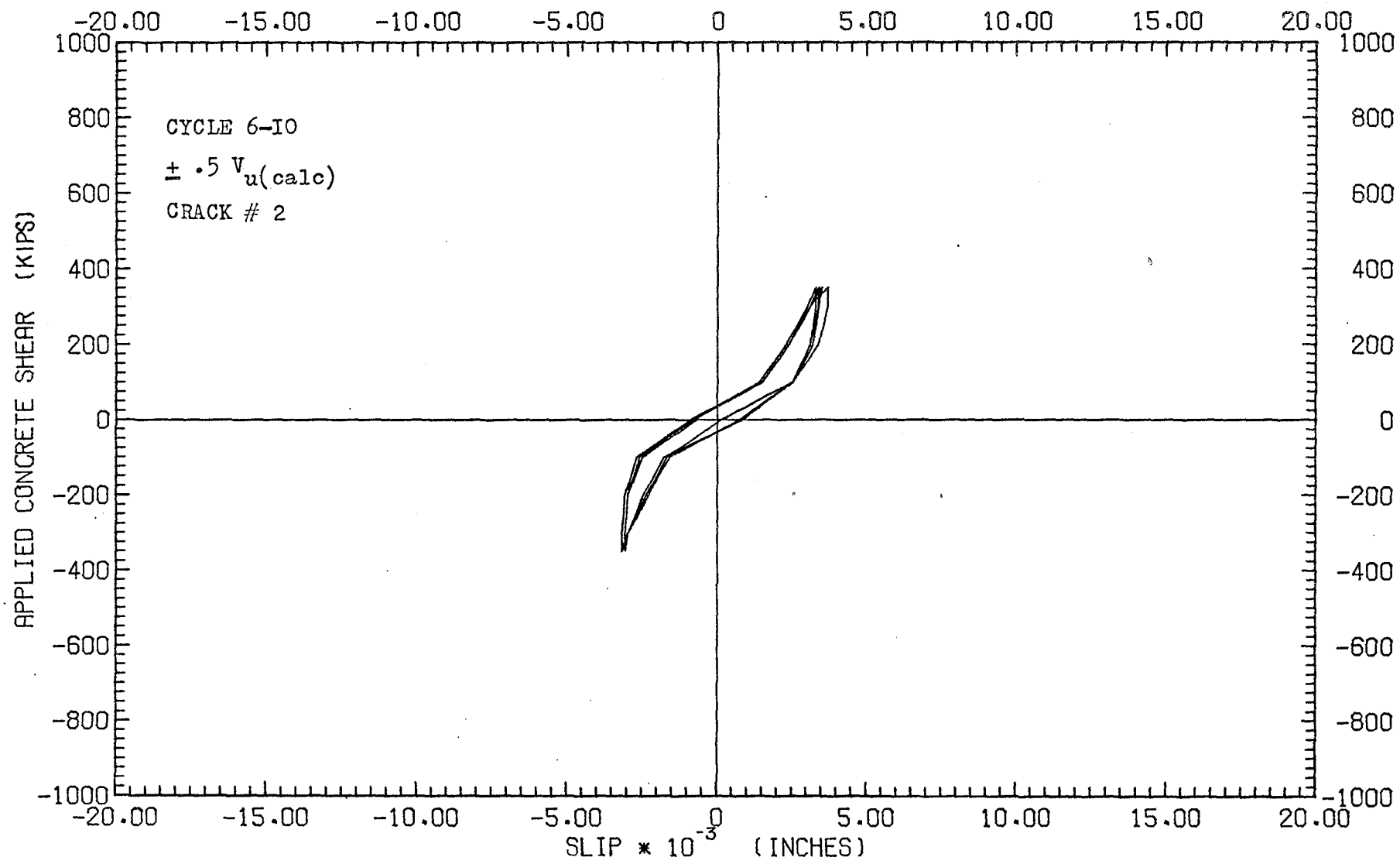

FIG.-C12, SHEAR-SLIP CURVES, C10A

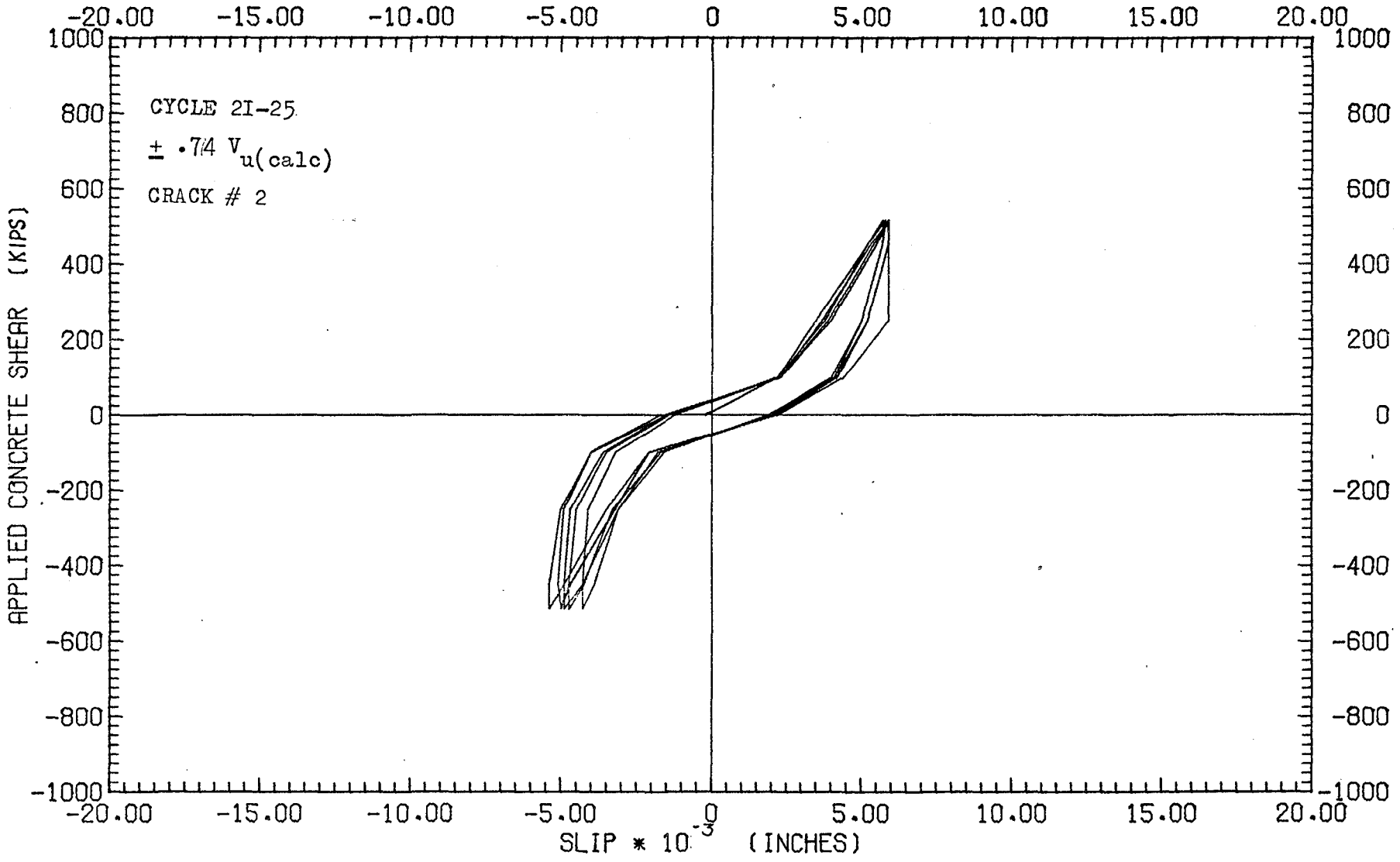

FIG.-C13, SHEAR-SLIP CURVES, C10A

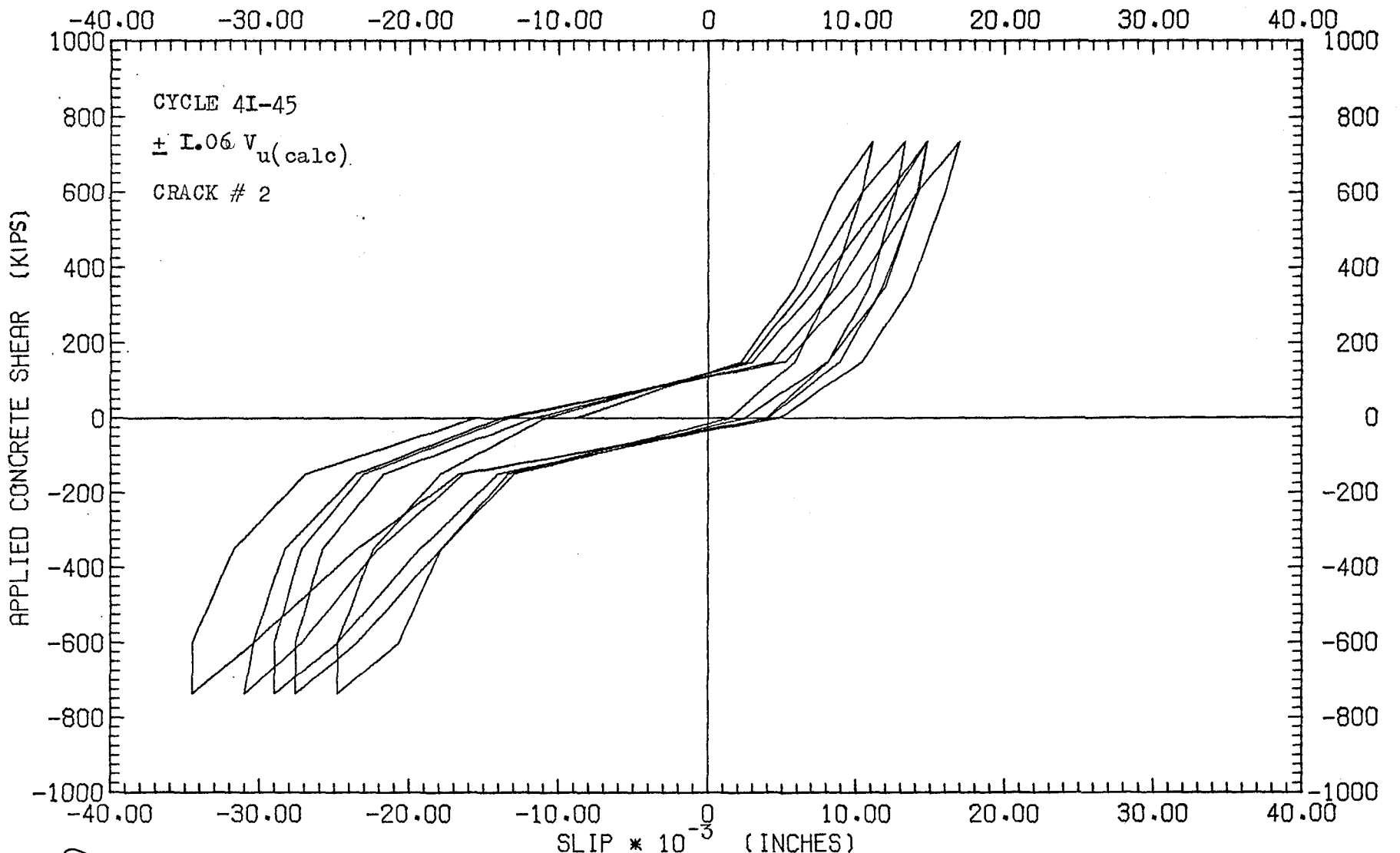

FIG.-C14, SHEAR-SLIP CURVES, C10A

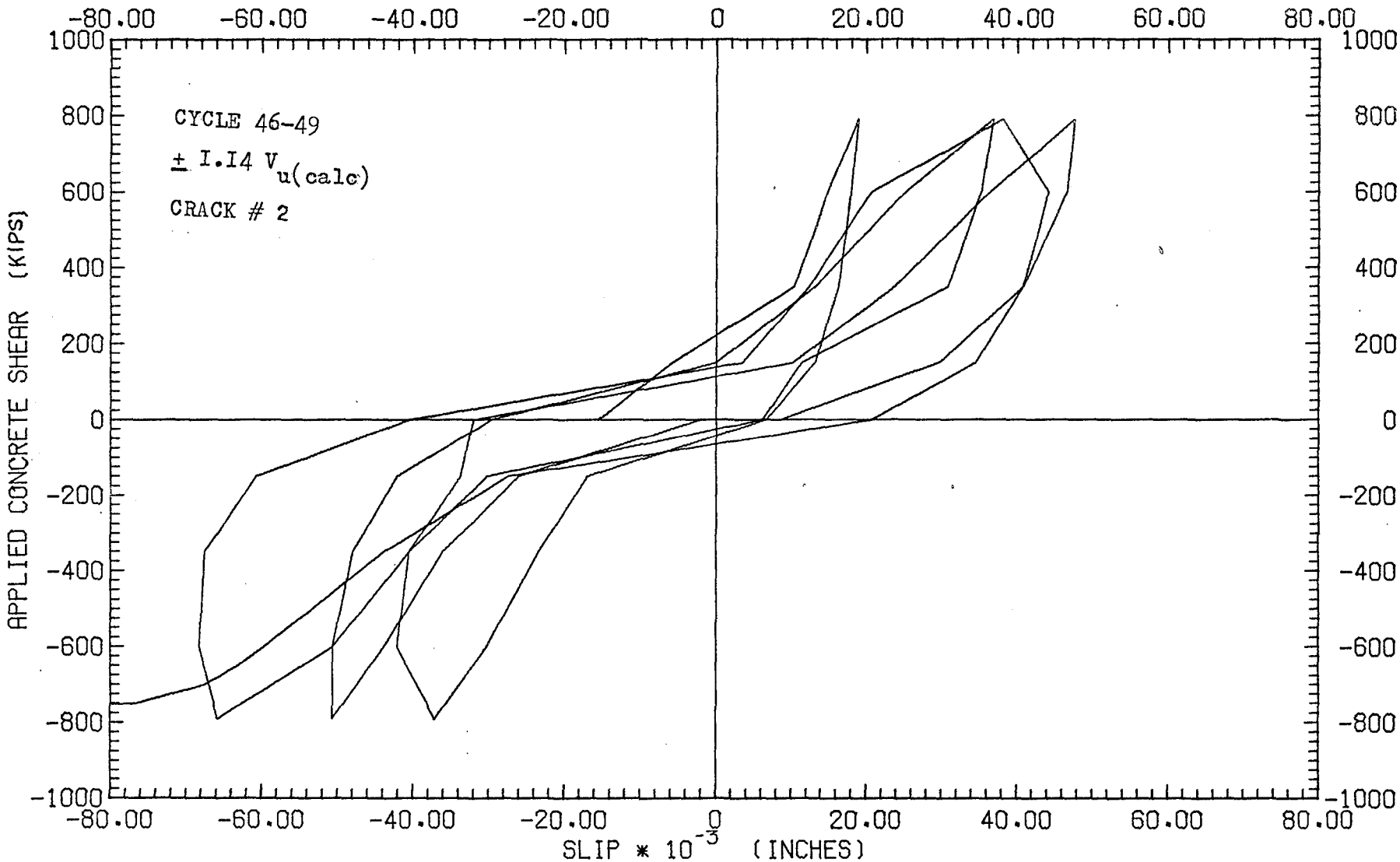

FIG.-C15, SHEAR-SLIP CURVES, C10A

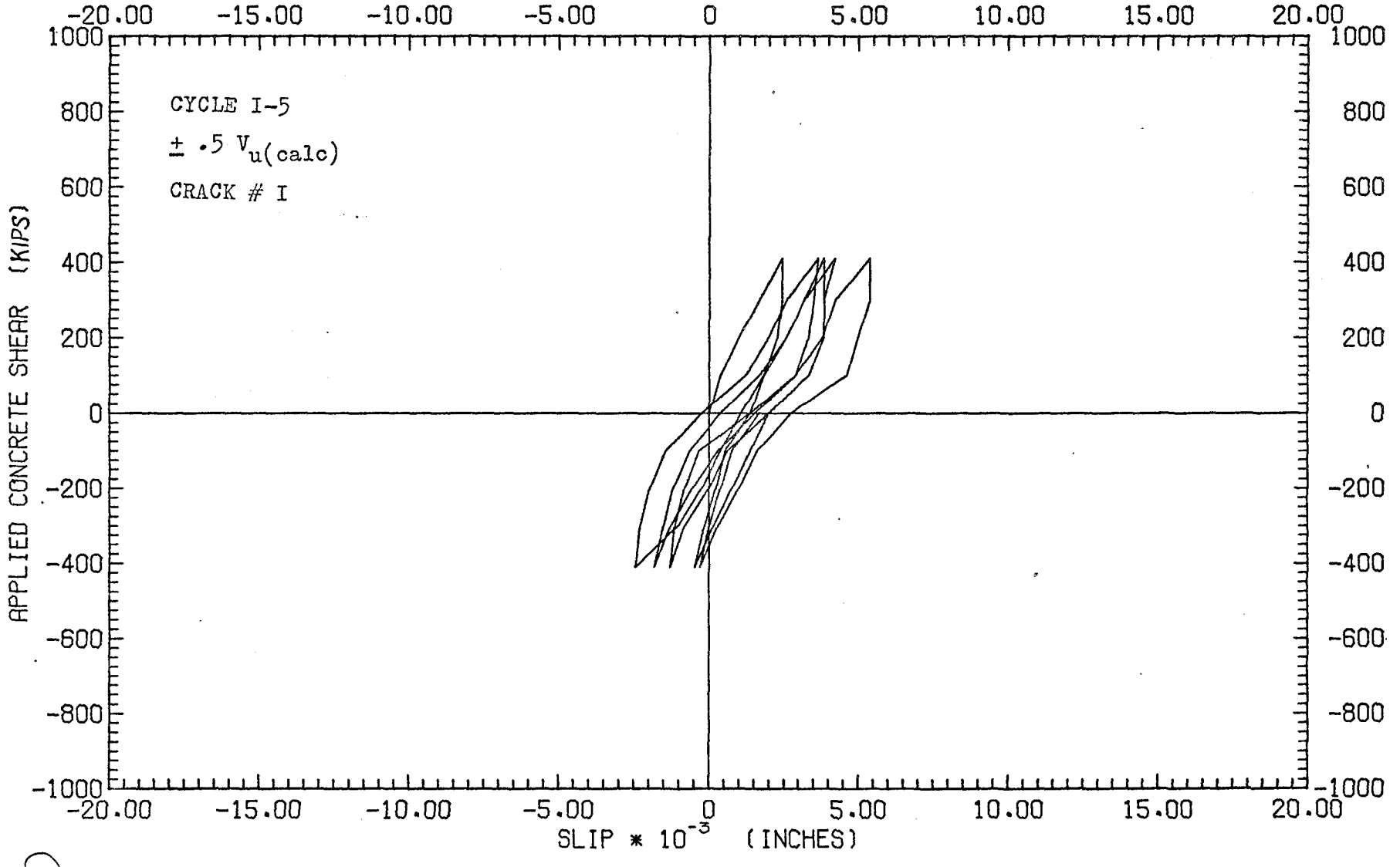

FIG.-C16, SHEAR-SLIP CURVES, C14A

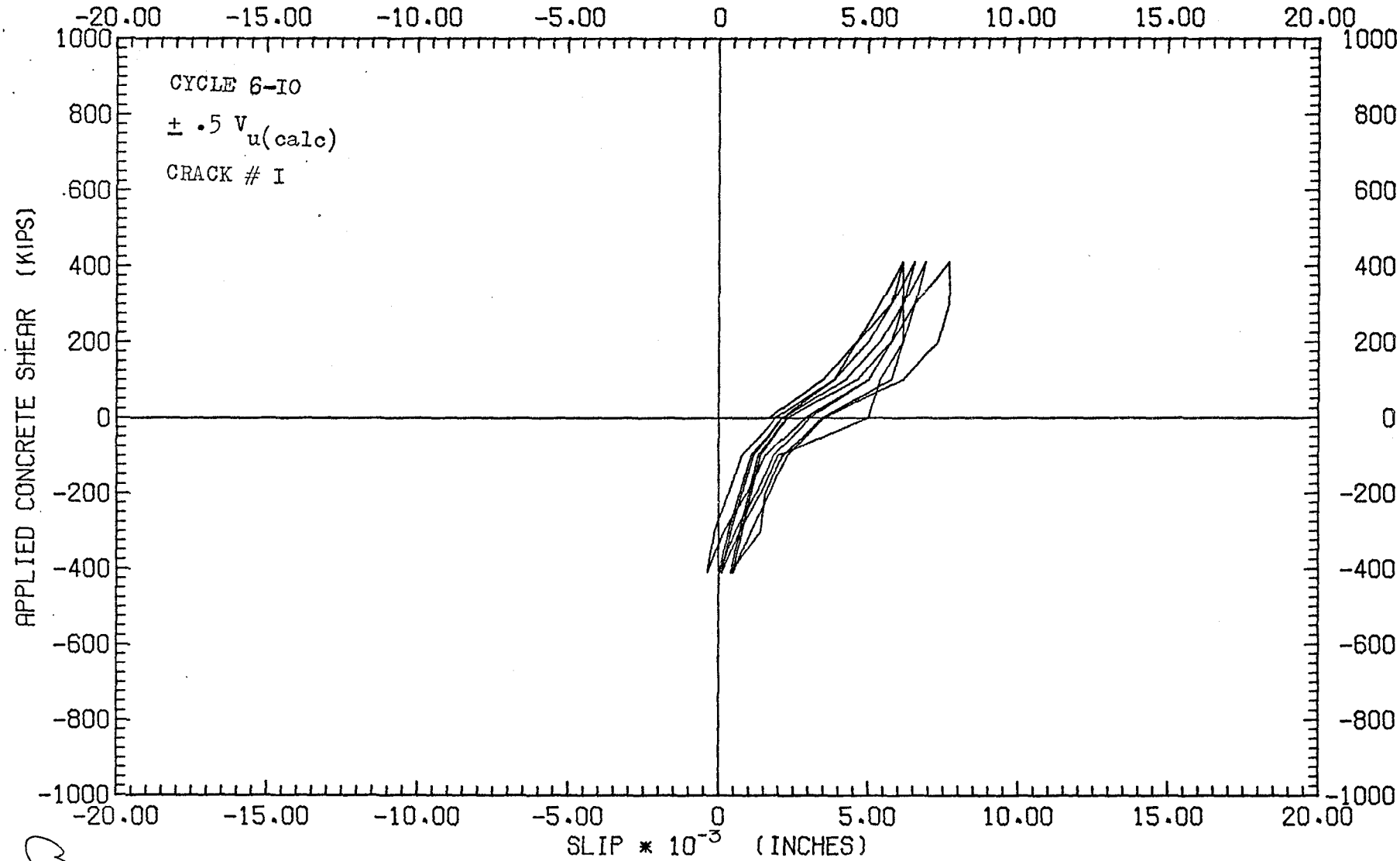

FIG.-C17, SHEAR-SLIP CURVES, C14A

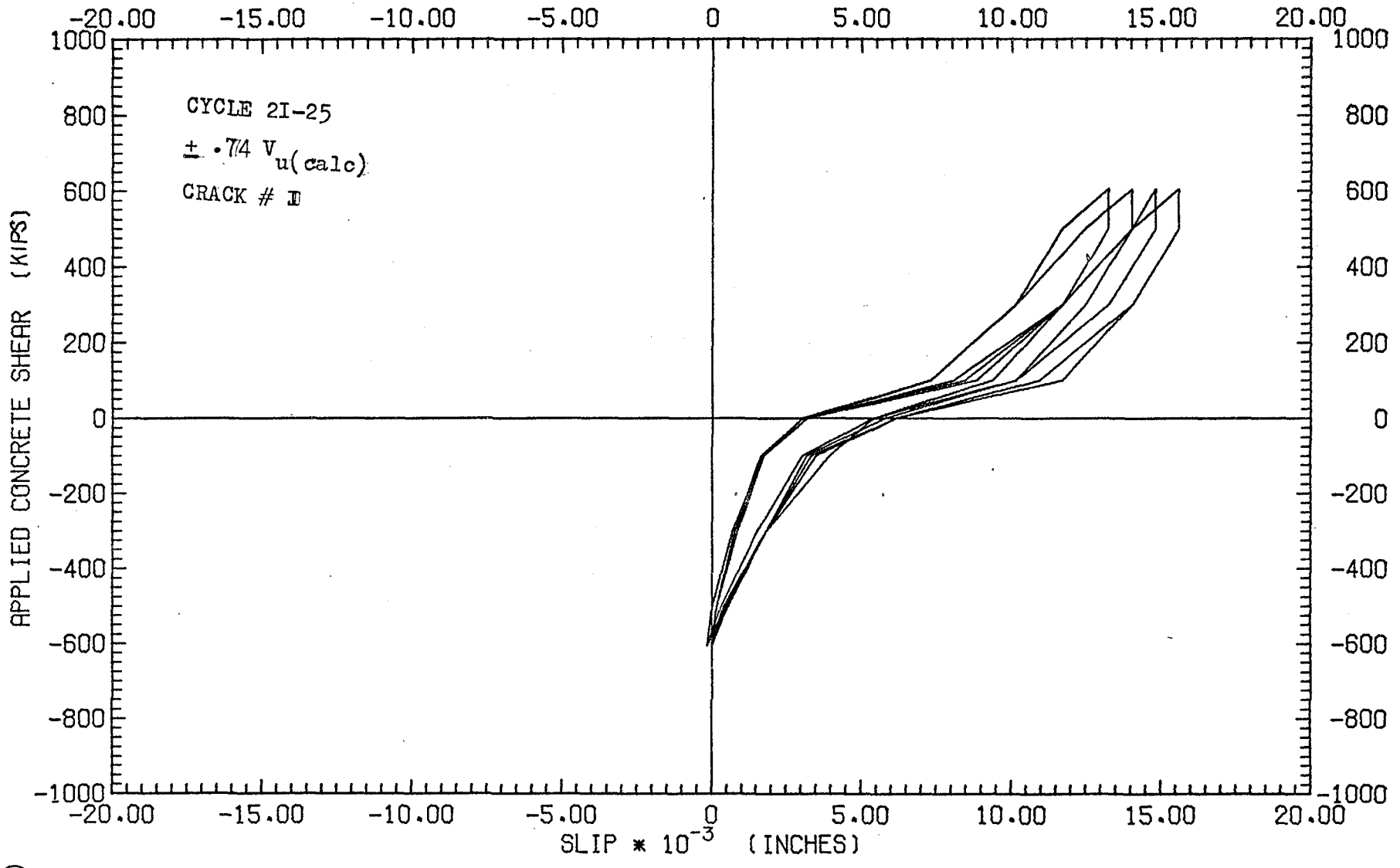

FIG.-C18, SHEAR-SLIP CURVES, C14A

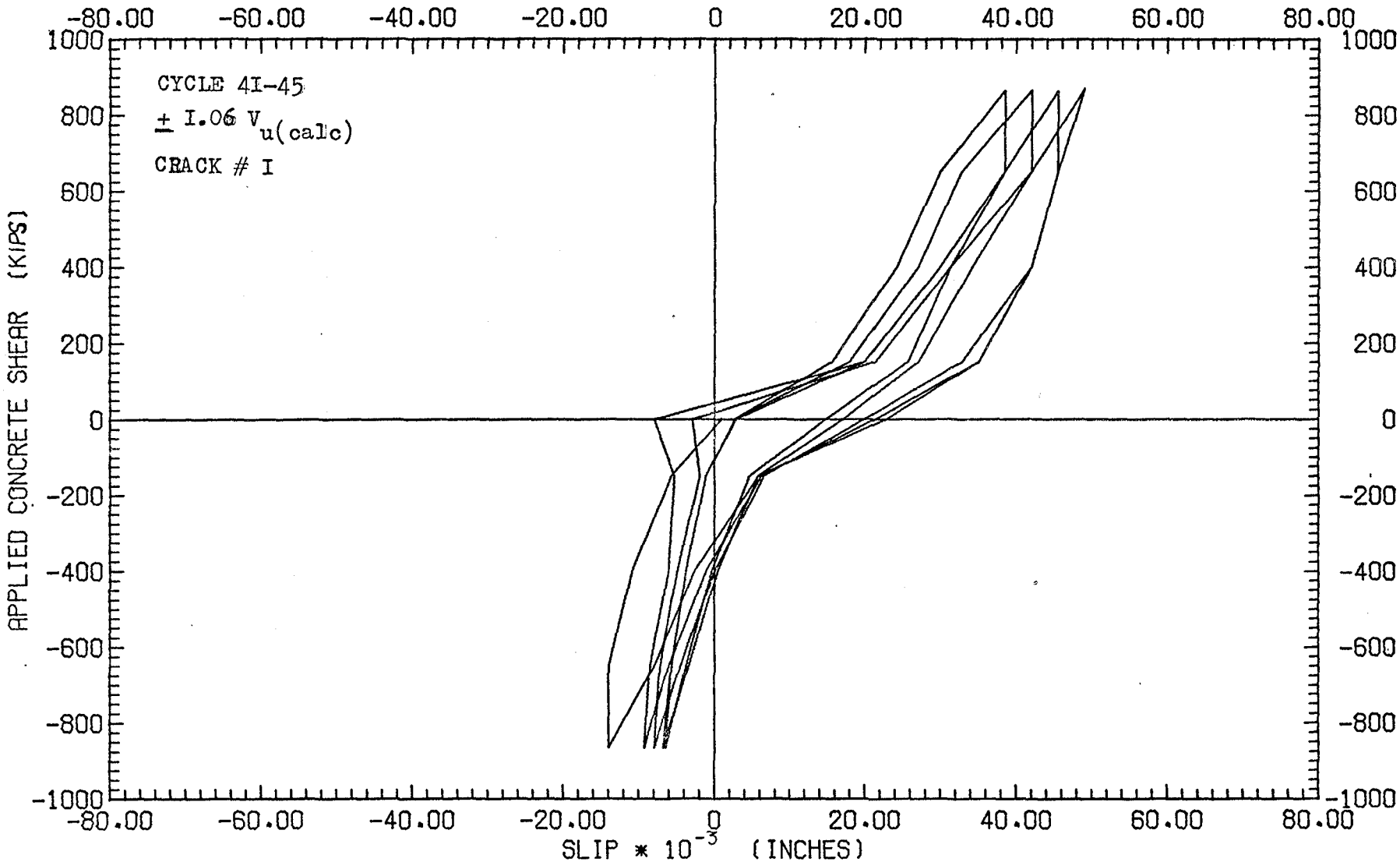

FIG.-C19, SHEAR-SLIP CURVES, C14A

C22

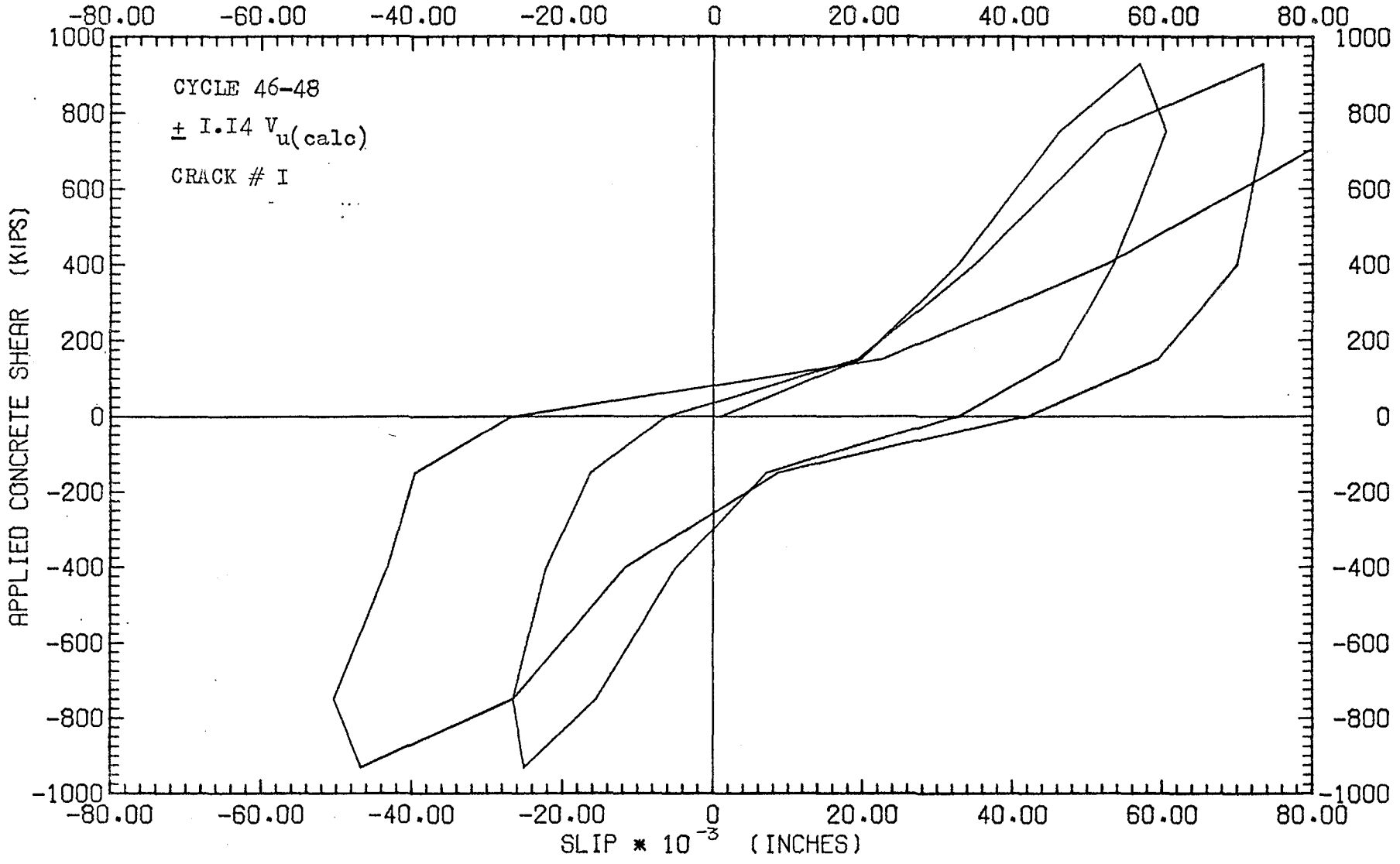

FIG.-C20, SHEAR-SLIP CURVES, C14A

C22

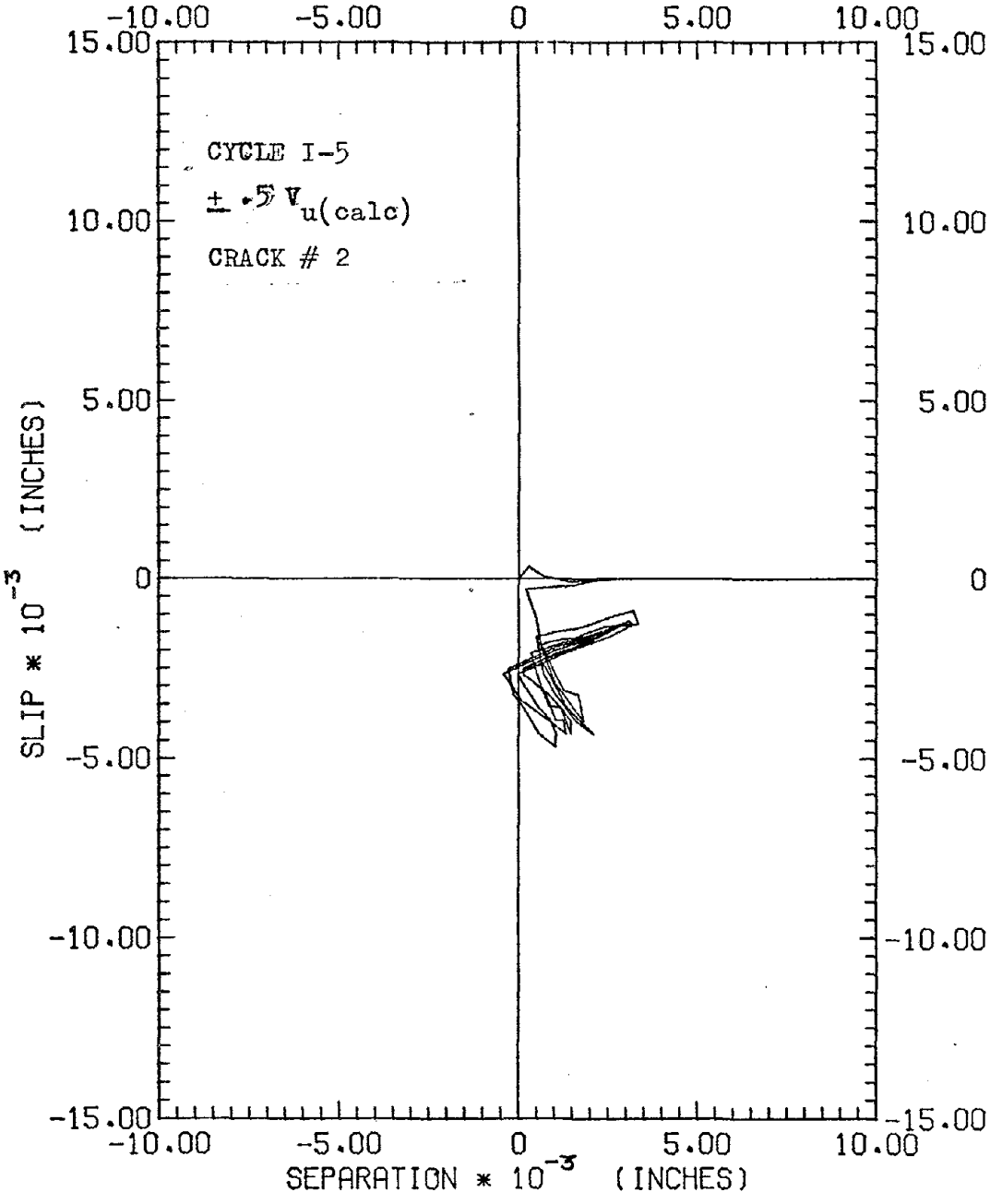

FIG.-C21, SLIP-SEPARATION CURVES, C4A

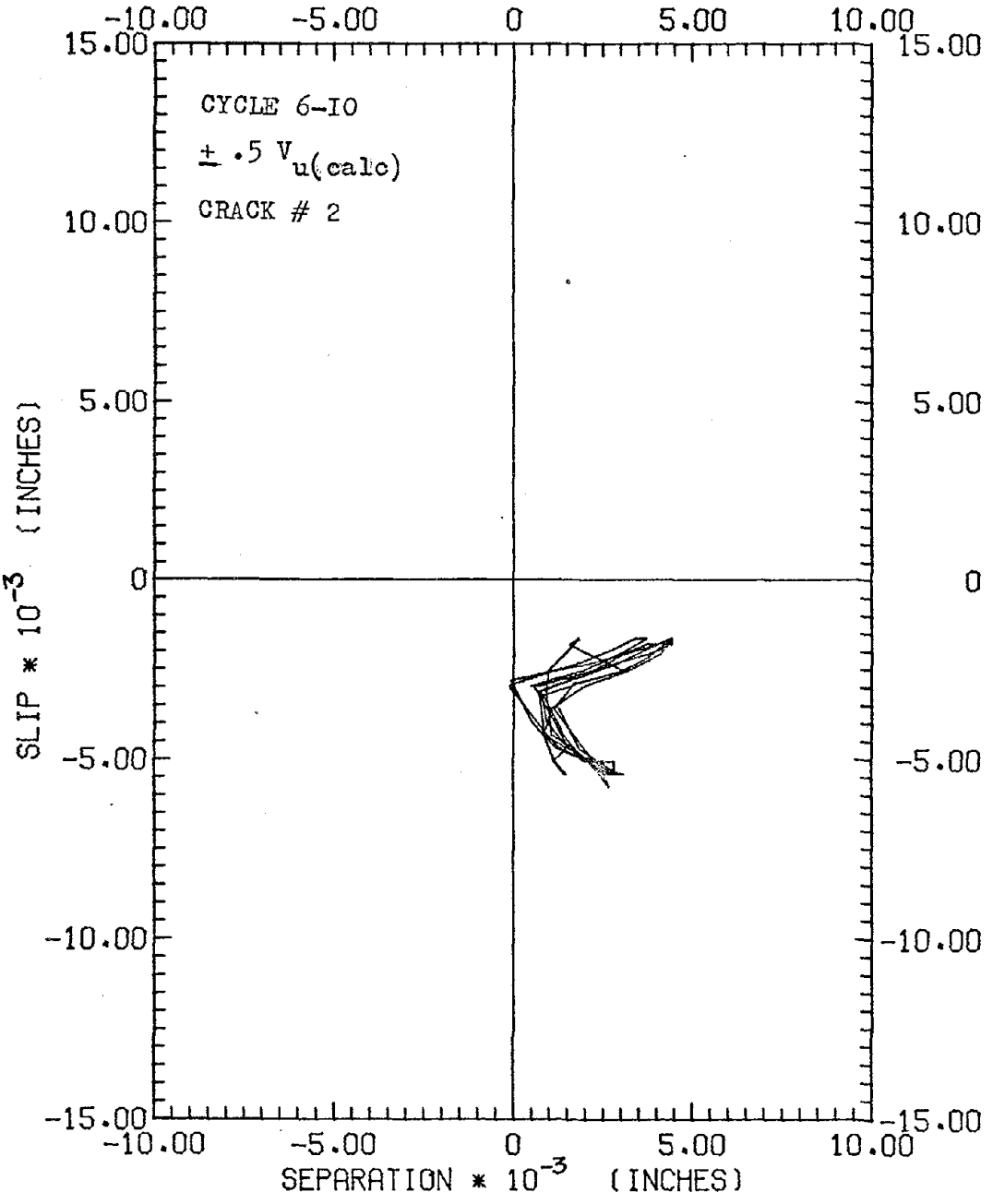

FIG.-C22, SLIP-SEPARATION CURVES, C4A

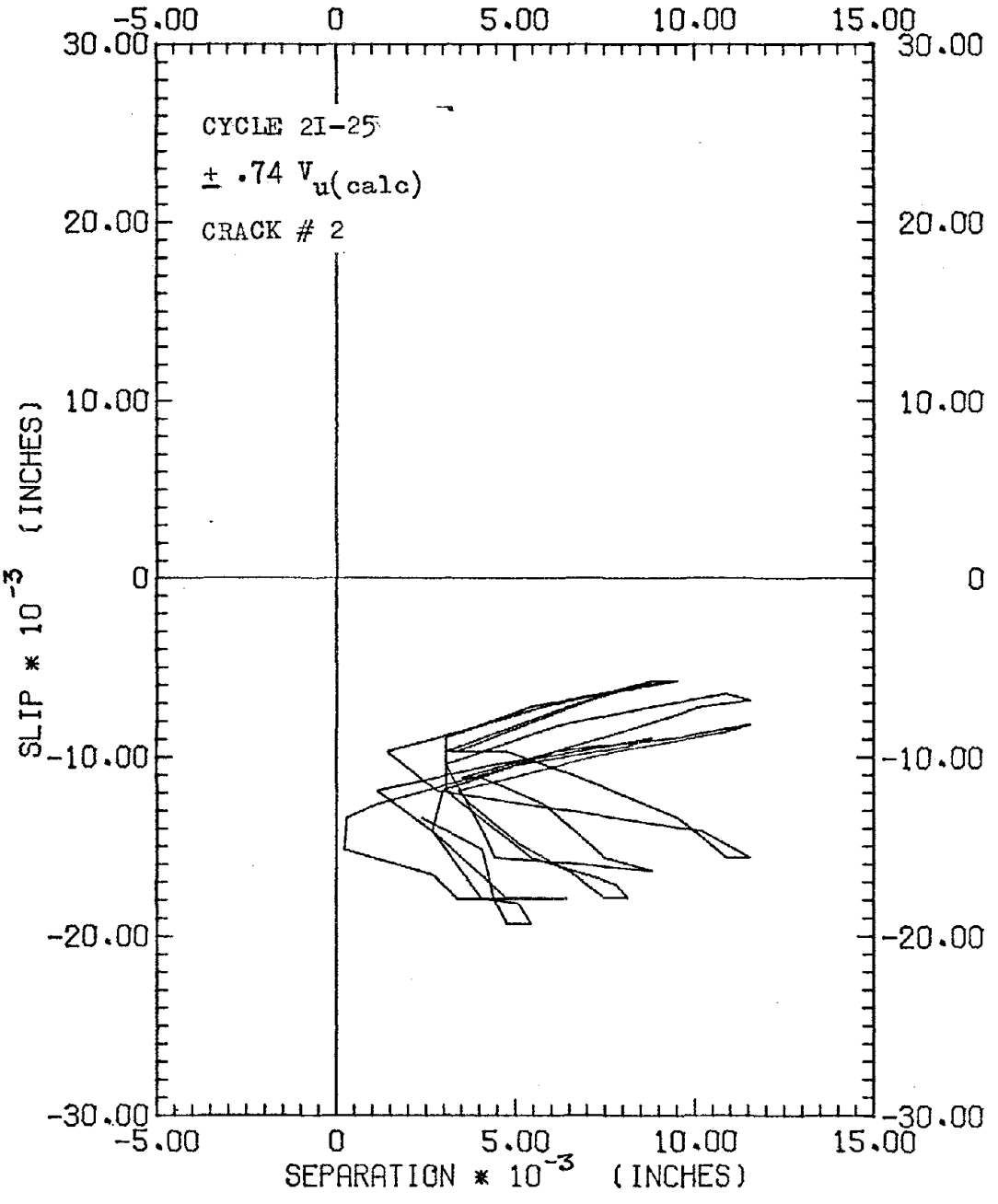

FIG.-C23, SLIP-SEPARATION CURVES, C4A

C26

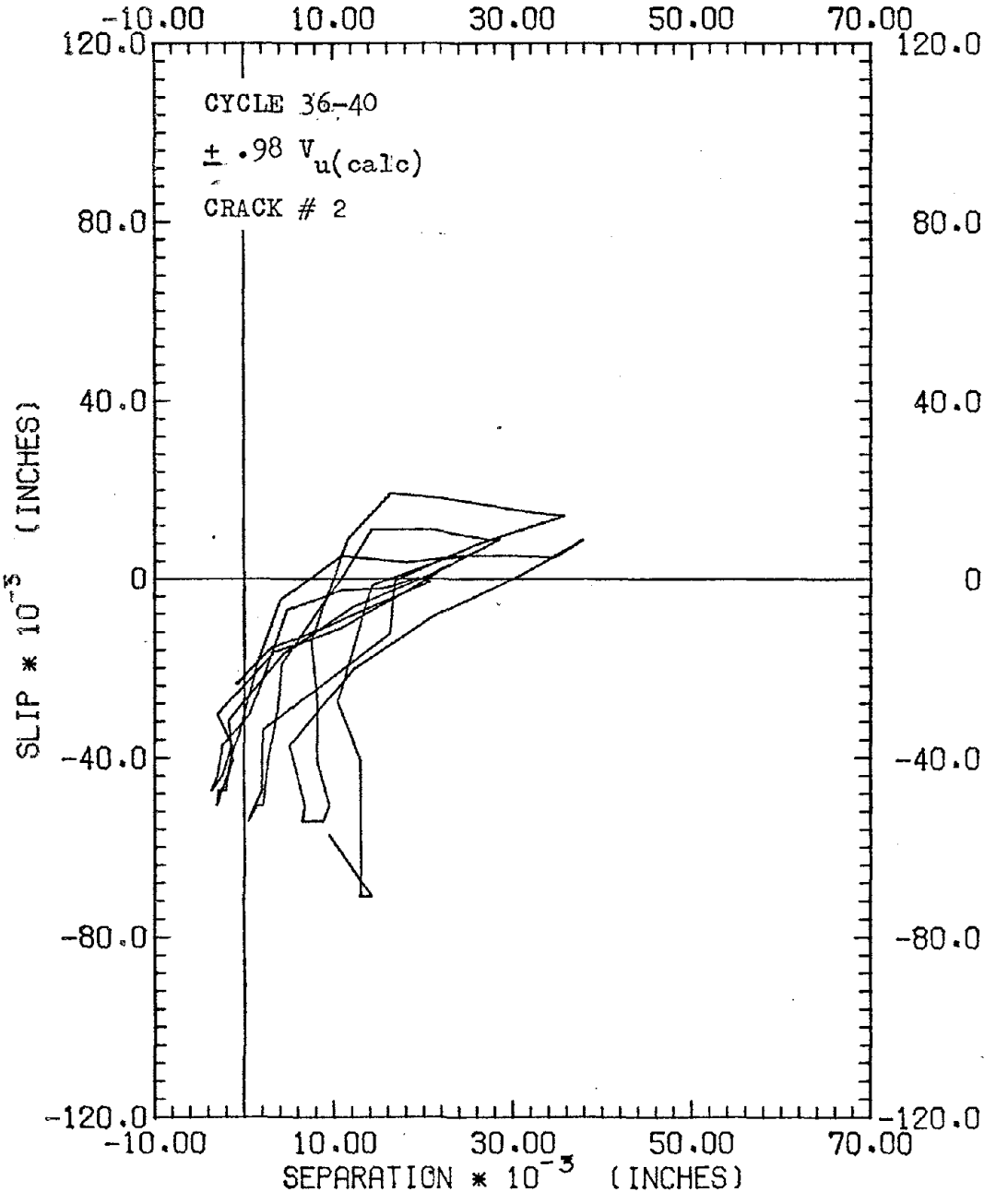

FIG.-C24, SLIP-SEPARATION CURVES, C4A

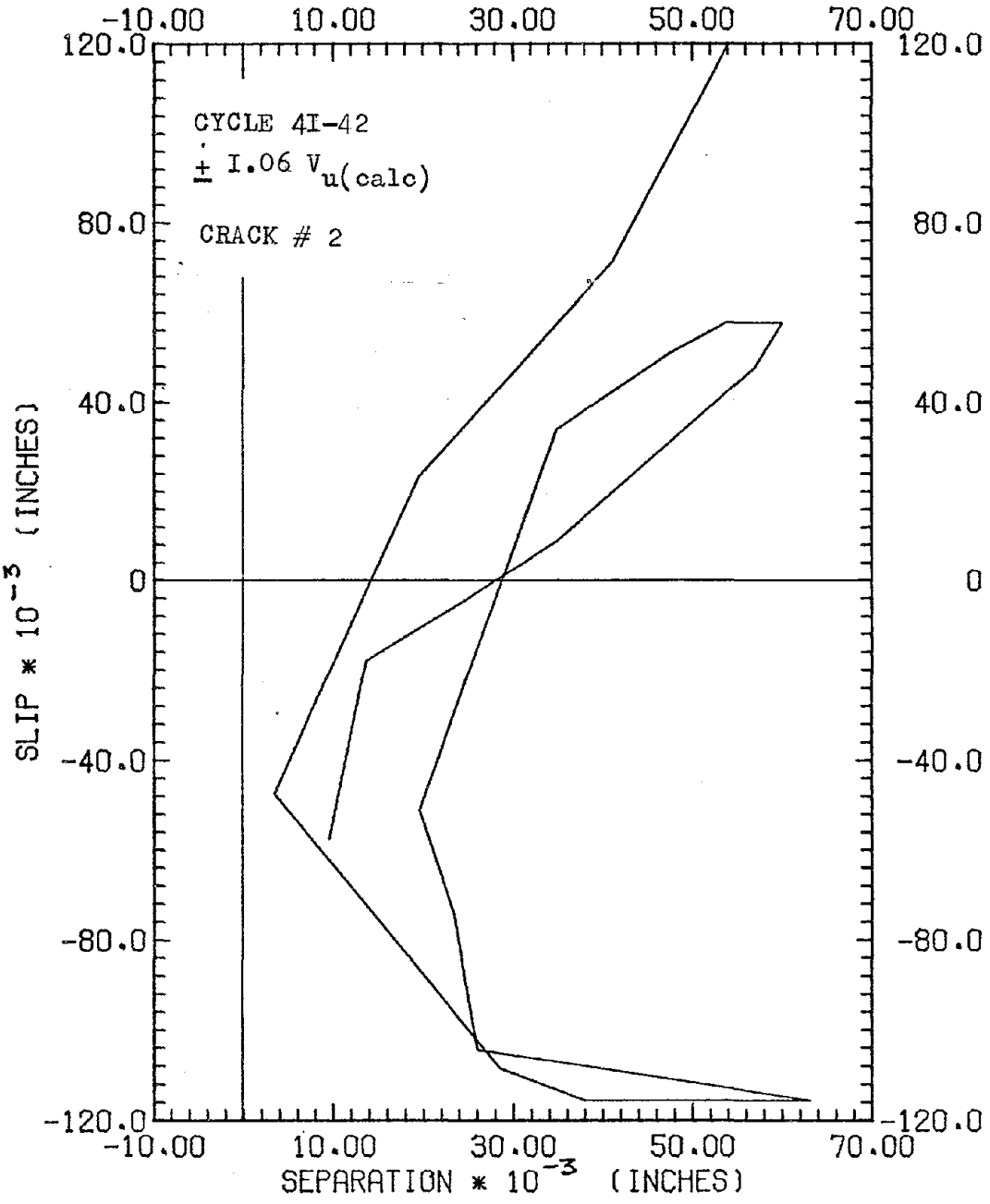

FIG.-C25, SLIP-SEPARATION CURVES, C4A

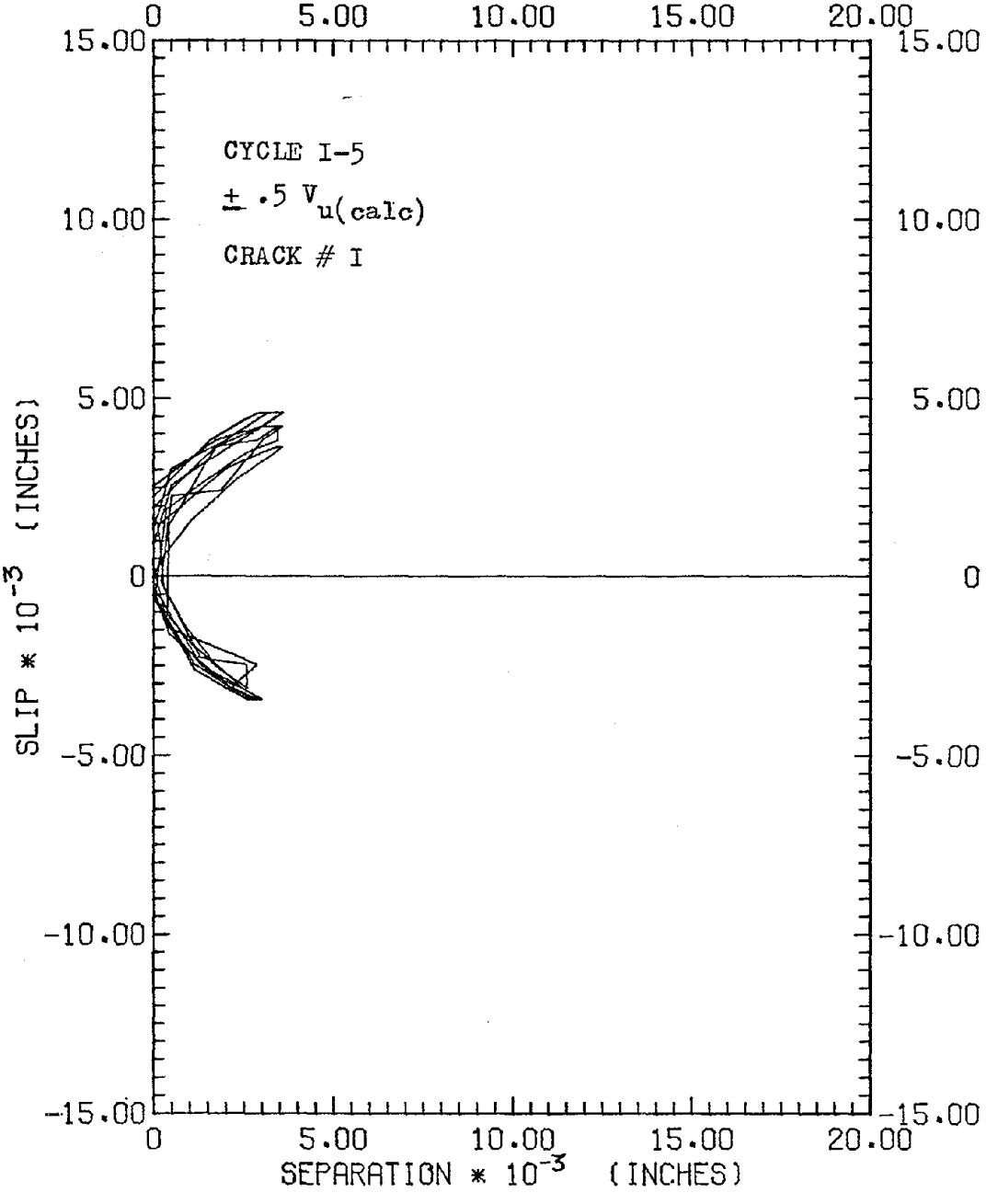

FIG.-C26, SLIP-SEPARATION CURVES, C8A

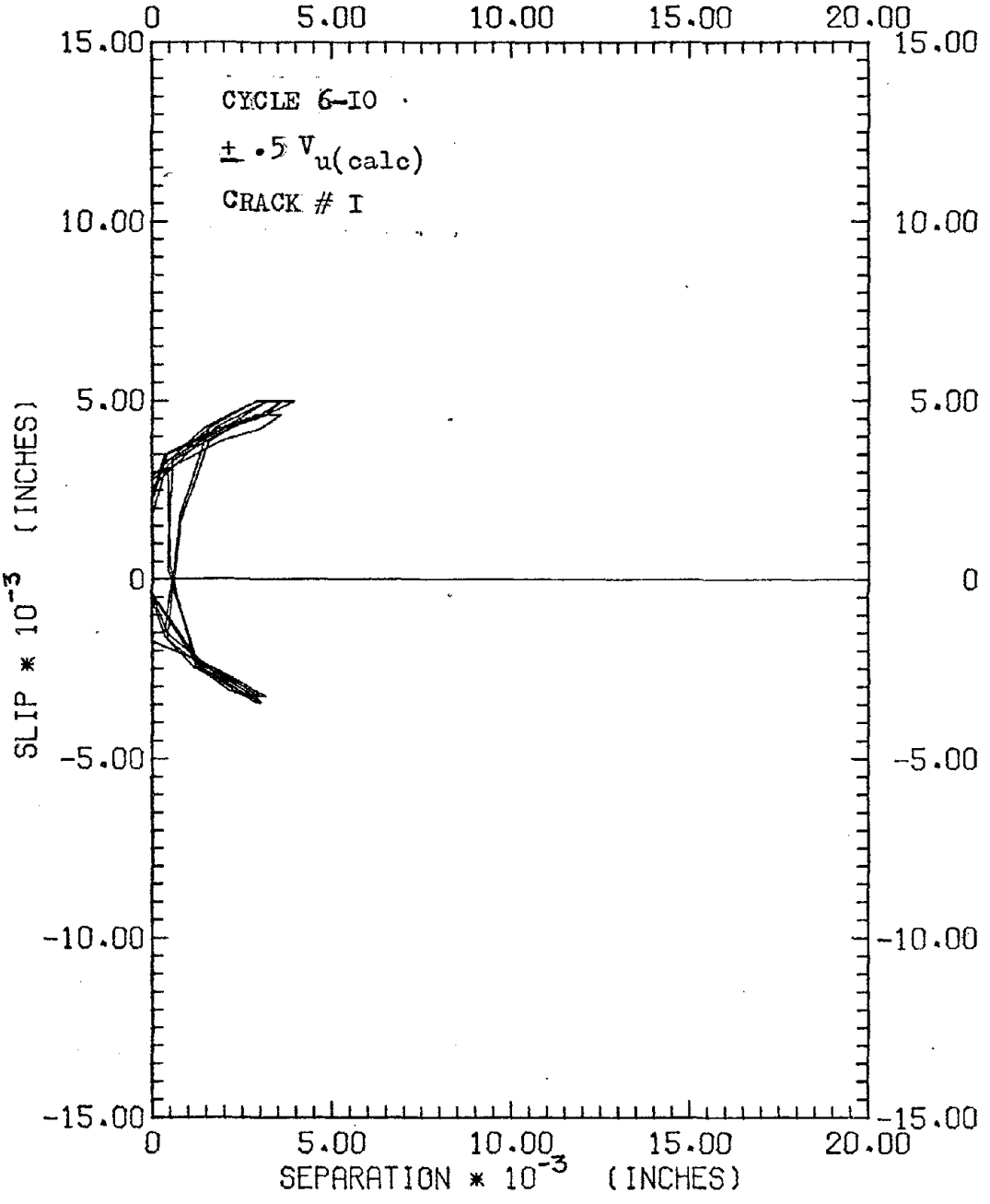

FIG.-C27, SLIP-SEPARATION CURVES, C8A

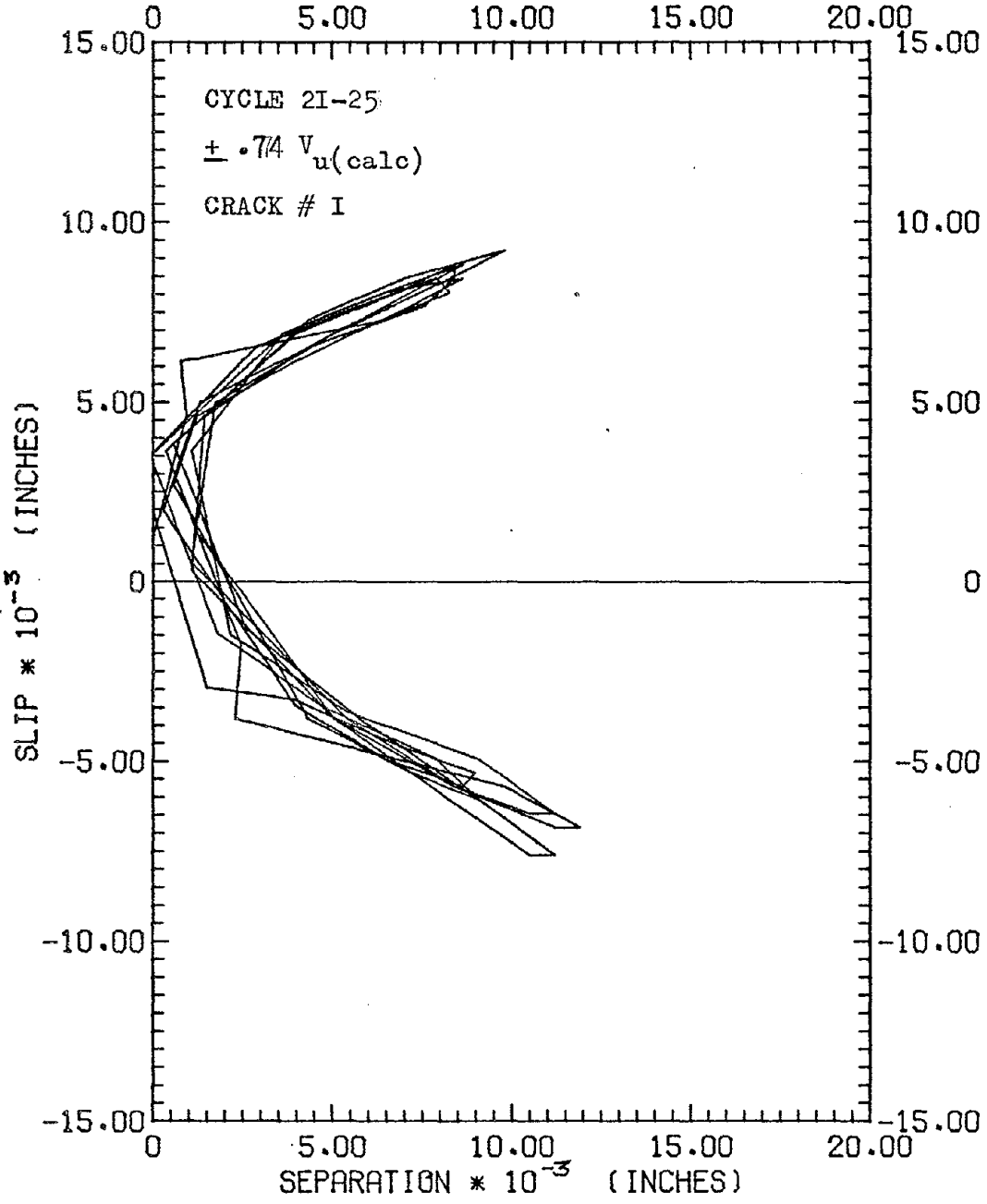

FIG.-C28, SLIP-SEPARATION CURVES, C8A

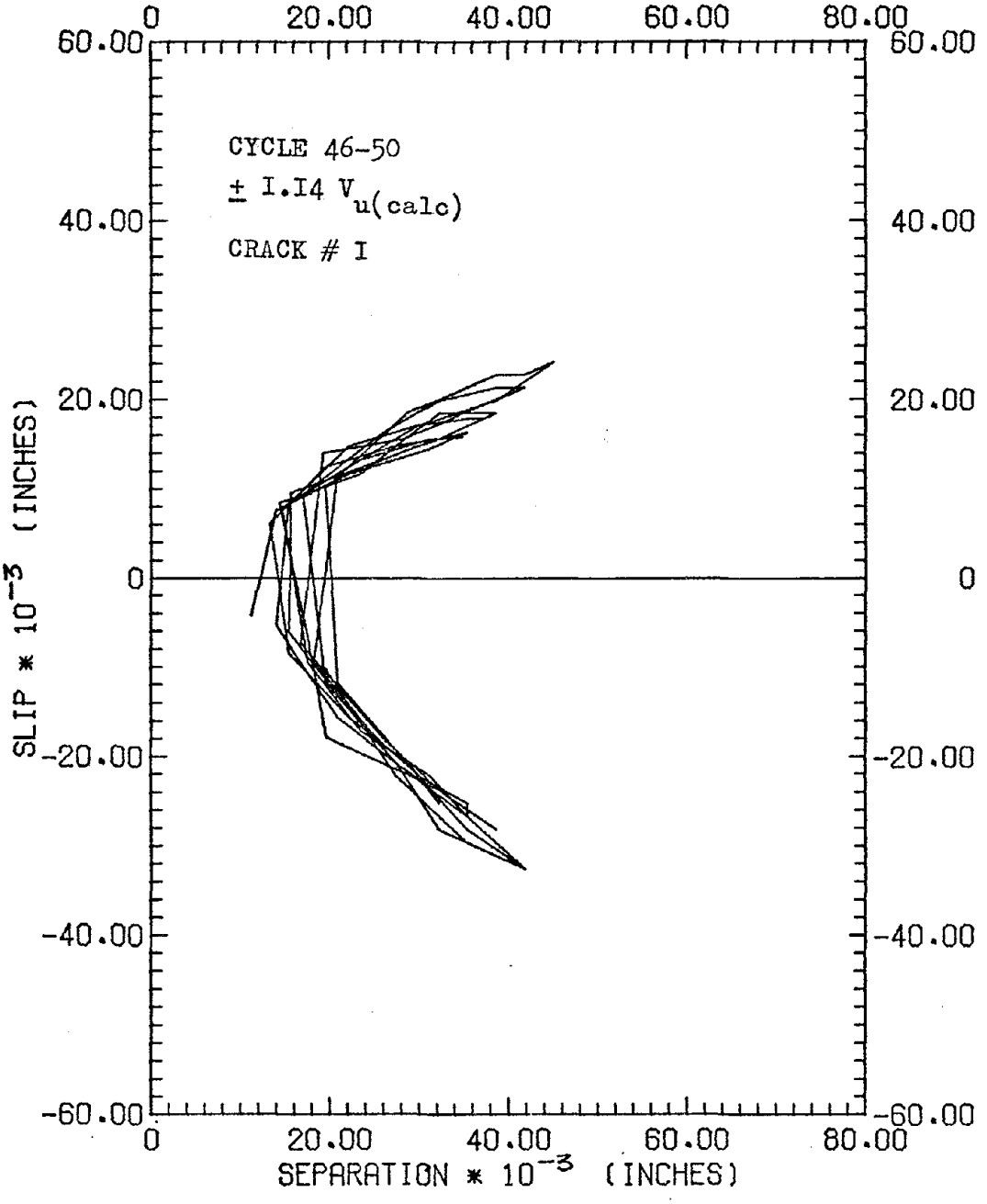

FIG.-C29, SLIP-SEPARATION CURVES, C8A

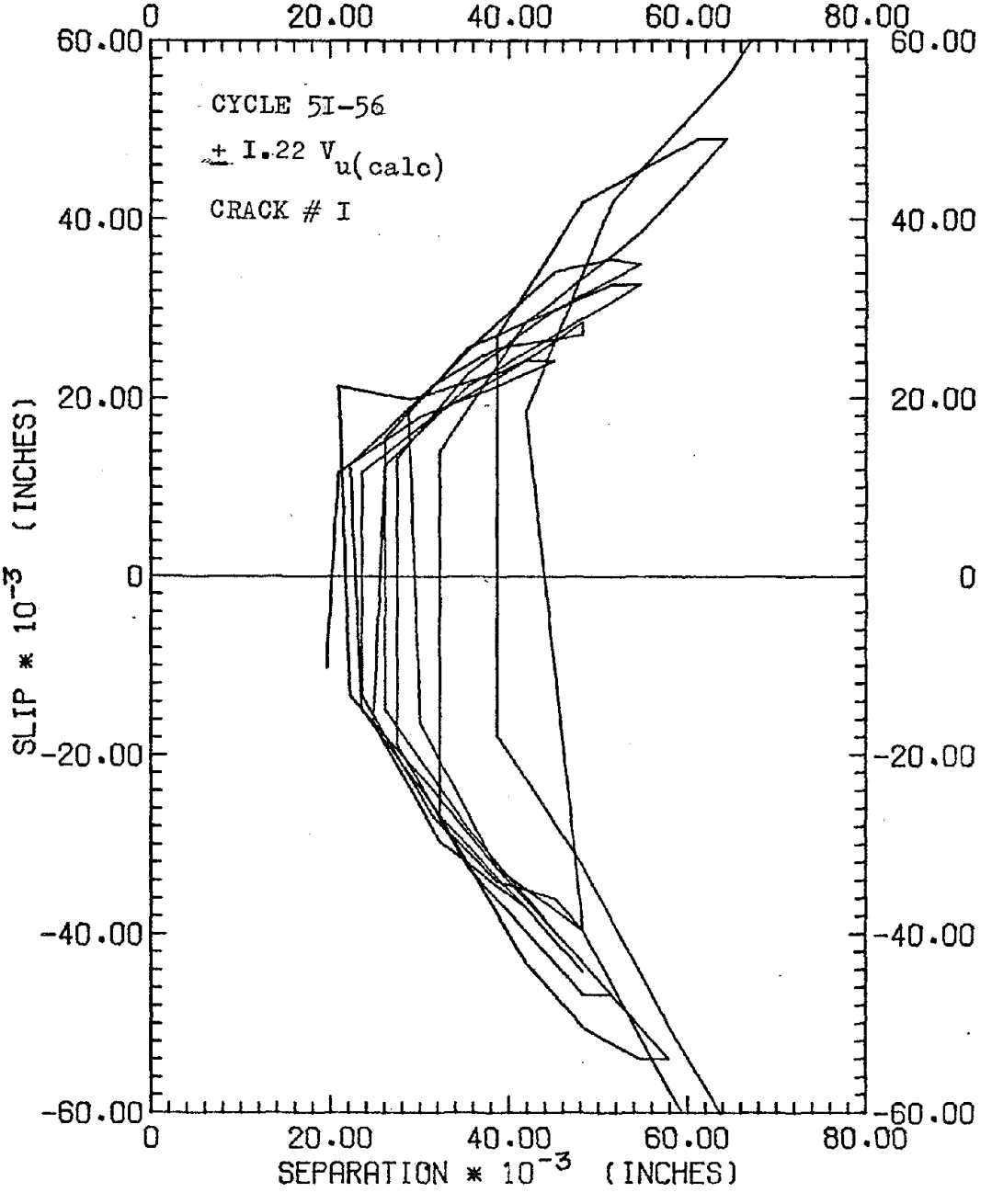

FIG.-C30, SLIP-SEPARATION CURVES, C8A

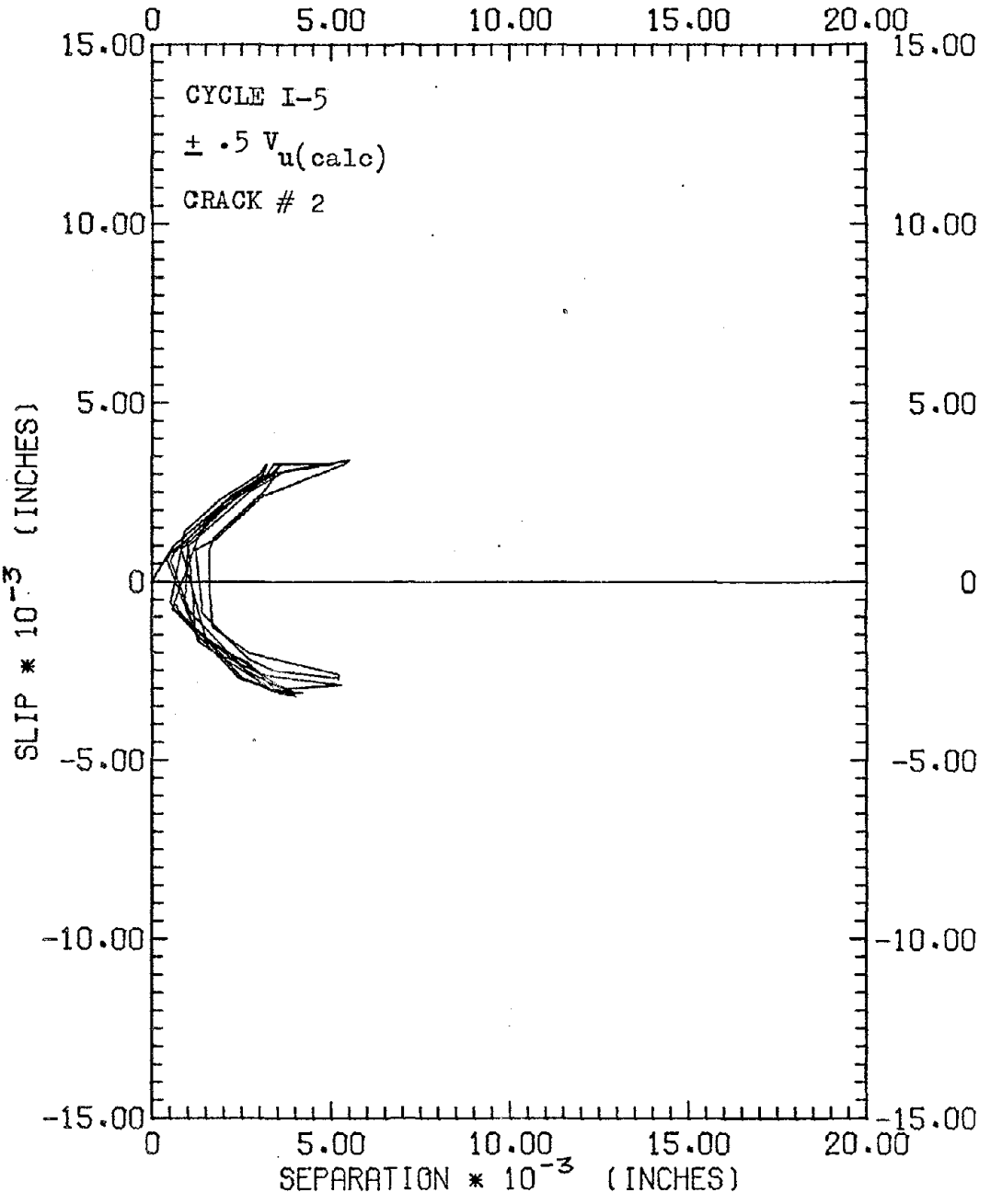

FIG.-C31, SLIP-SEPARATION CURVES, C10A

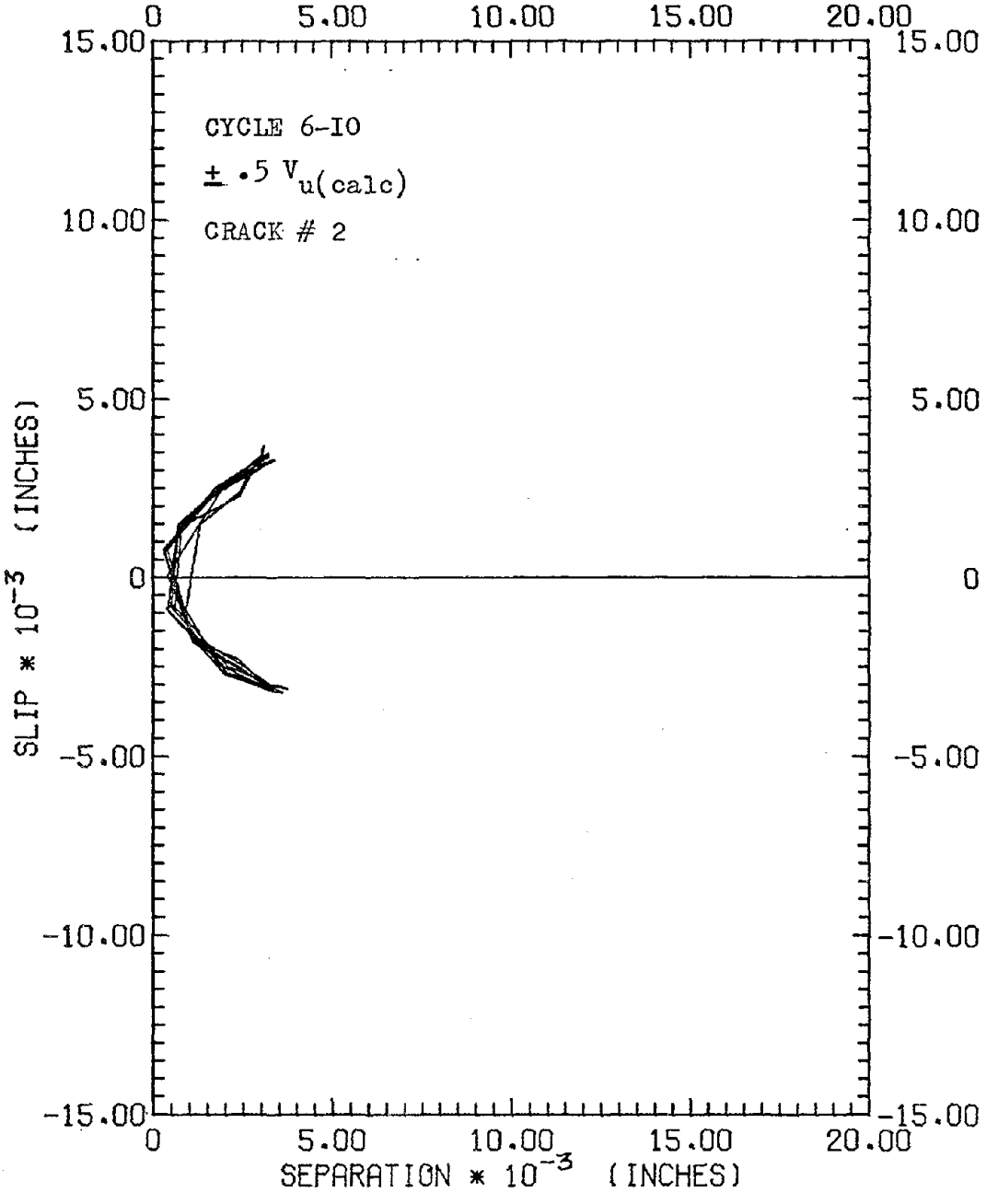

FIG.-C32, SLIP-SEPARATION CURVES, C10A

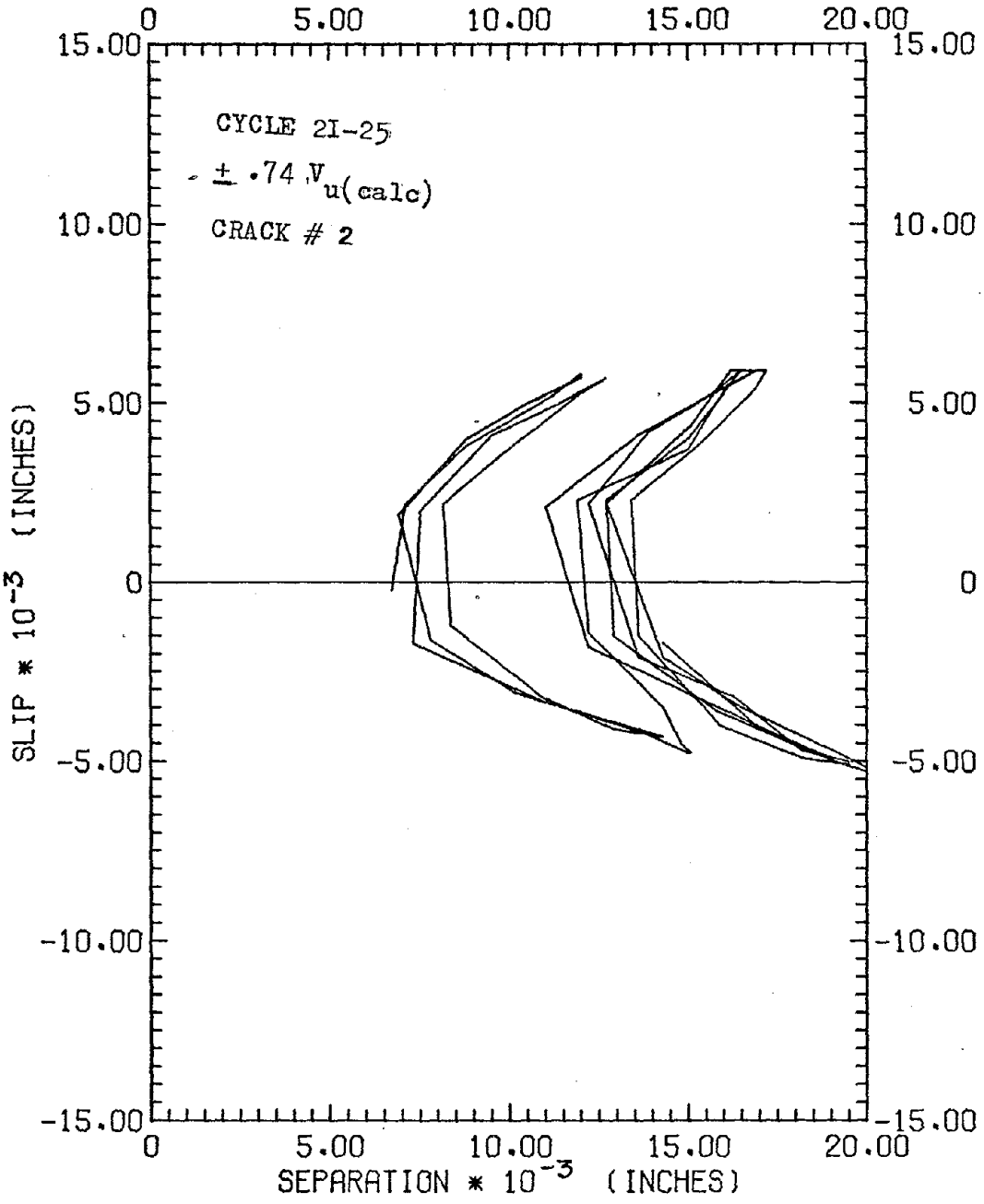

FIG.-C33, SLIP-SEPARATION CURVES, C10A

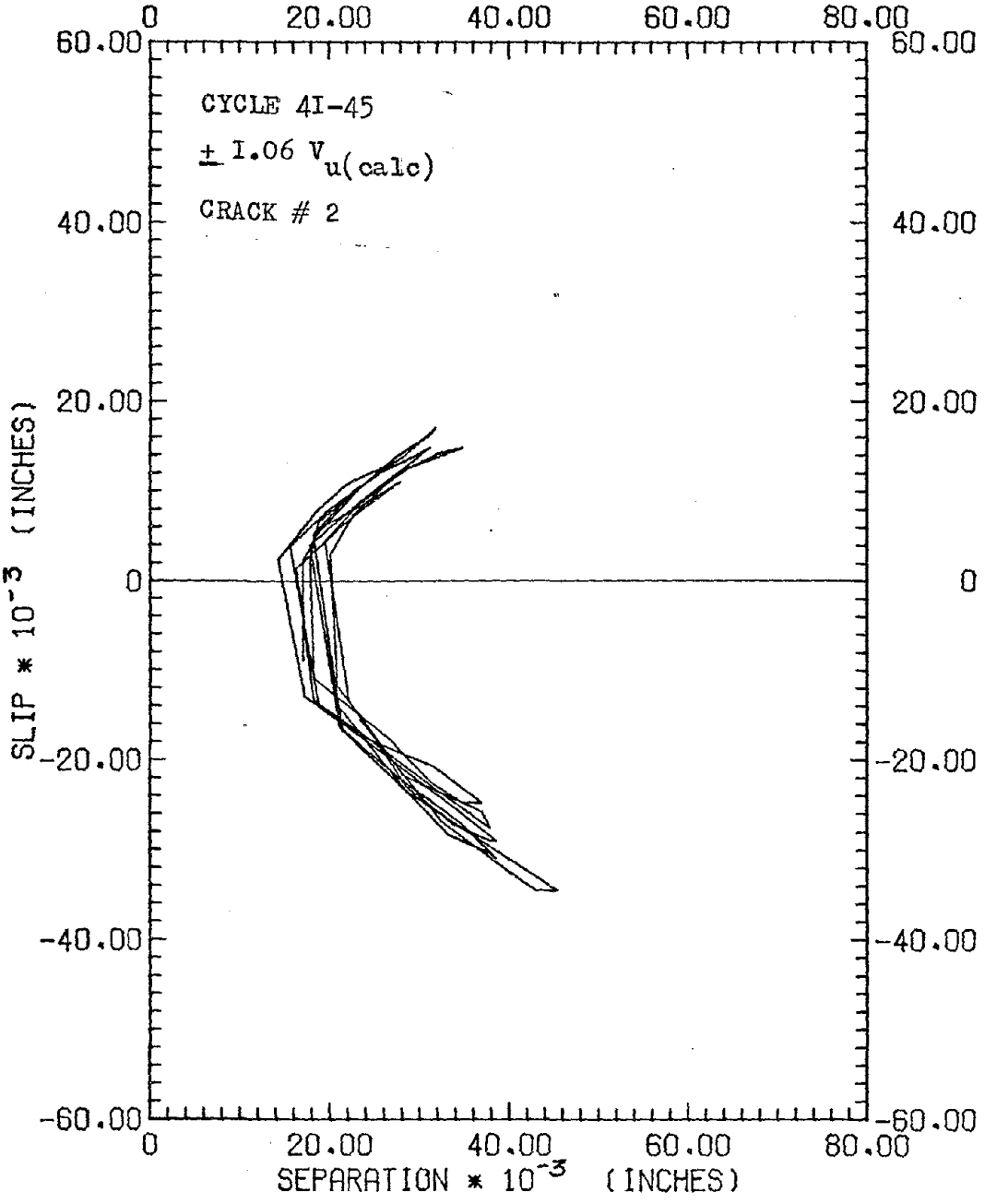

FIG.-C34, SLIP-SEPARATION CURVES, C10A

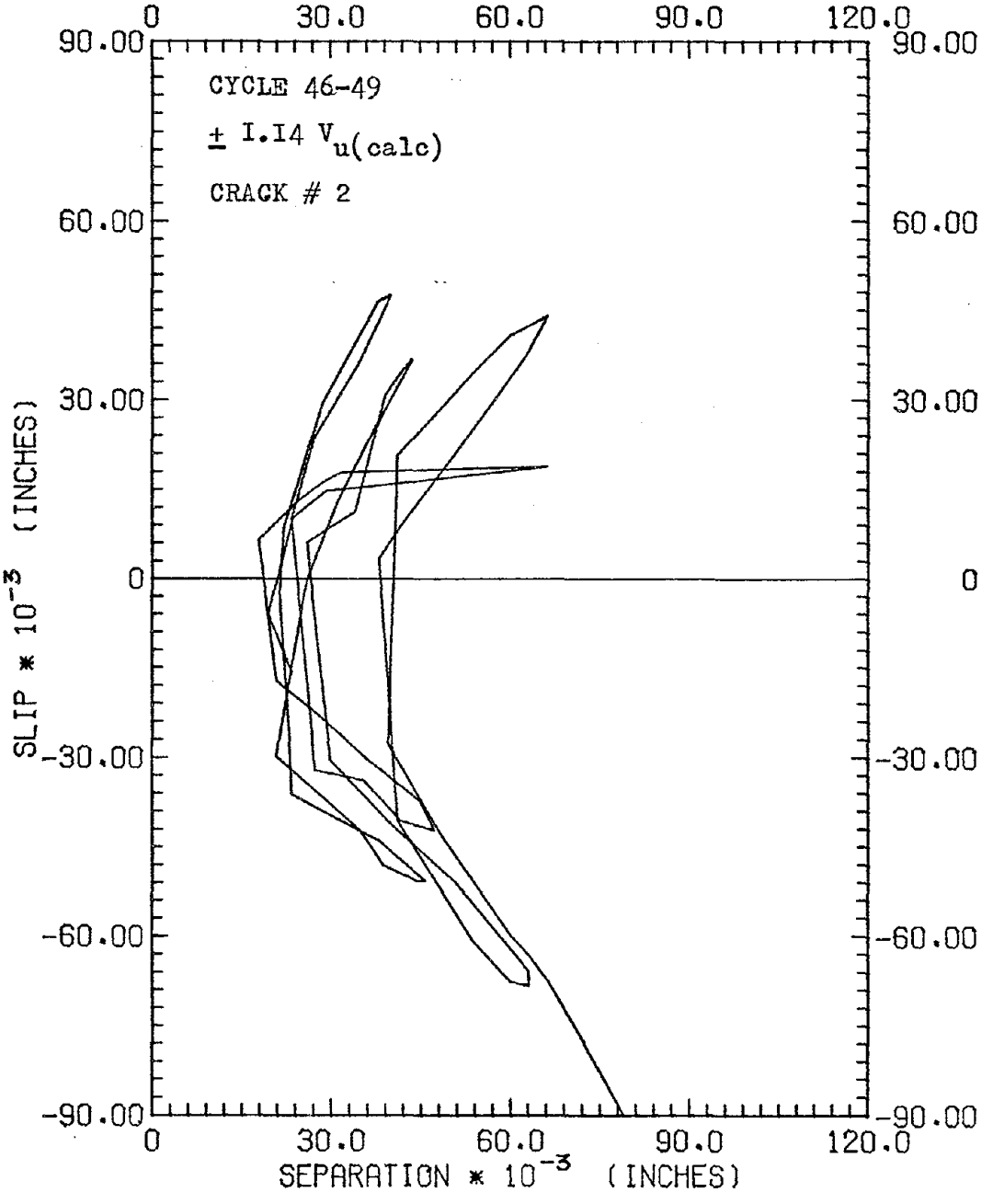

FIG.-C35, SLIP-SEPARATION CURVES, C10A

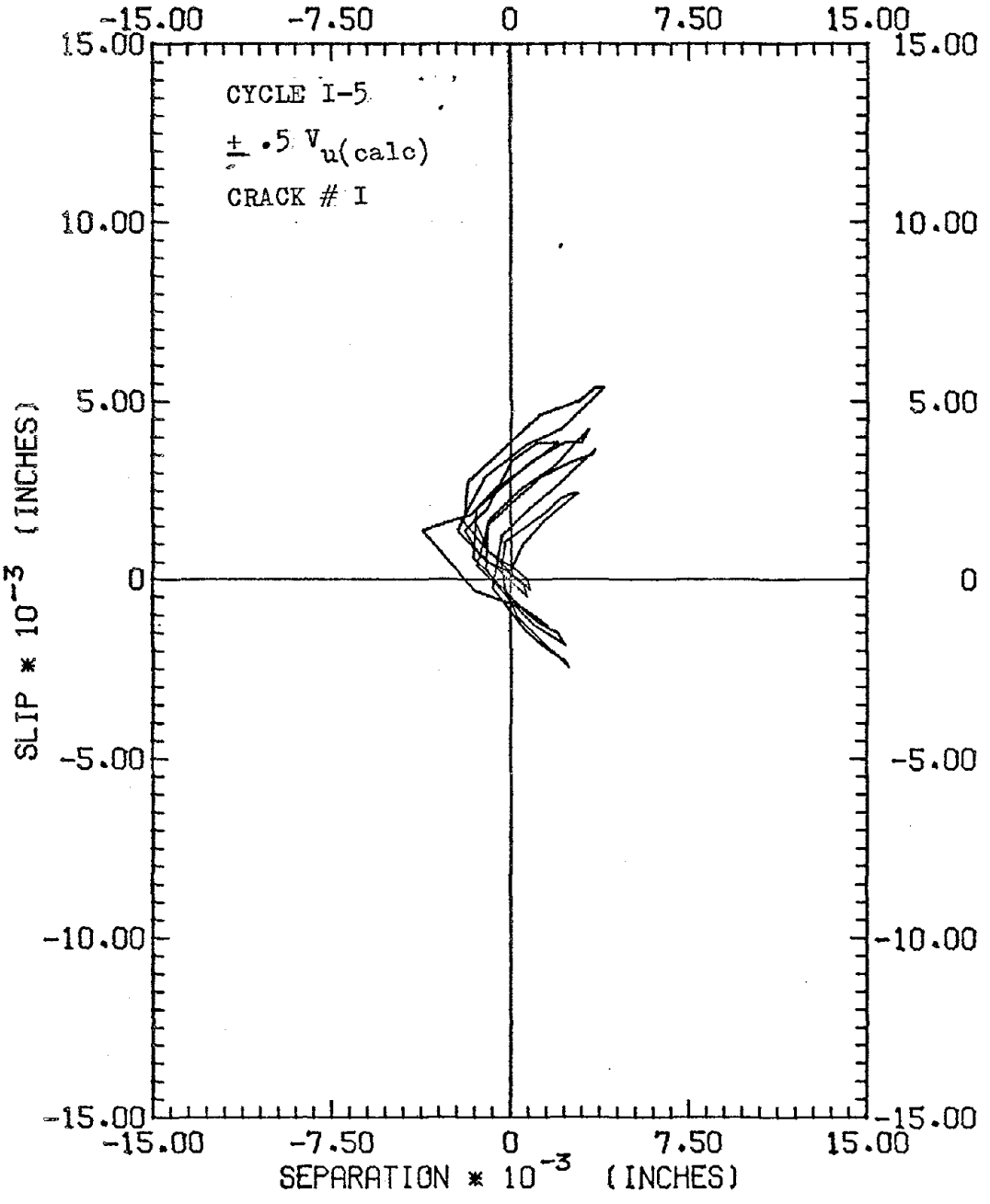

FIG.-C36, SLIP-SEPARATION CURVES, C14A

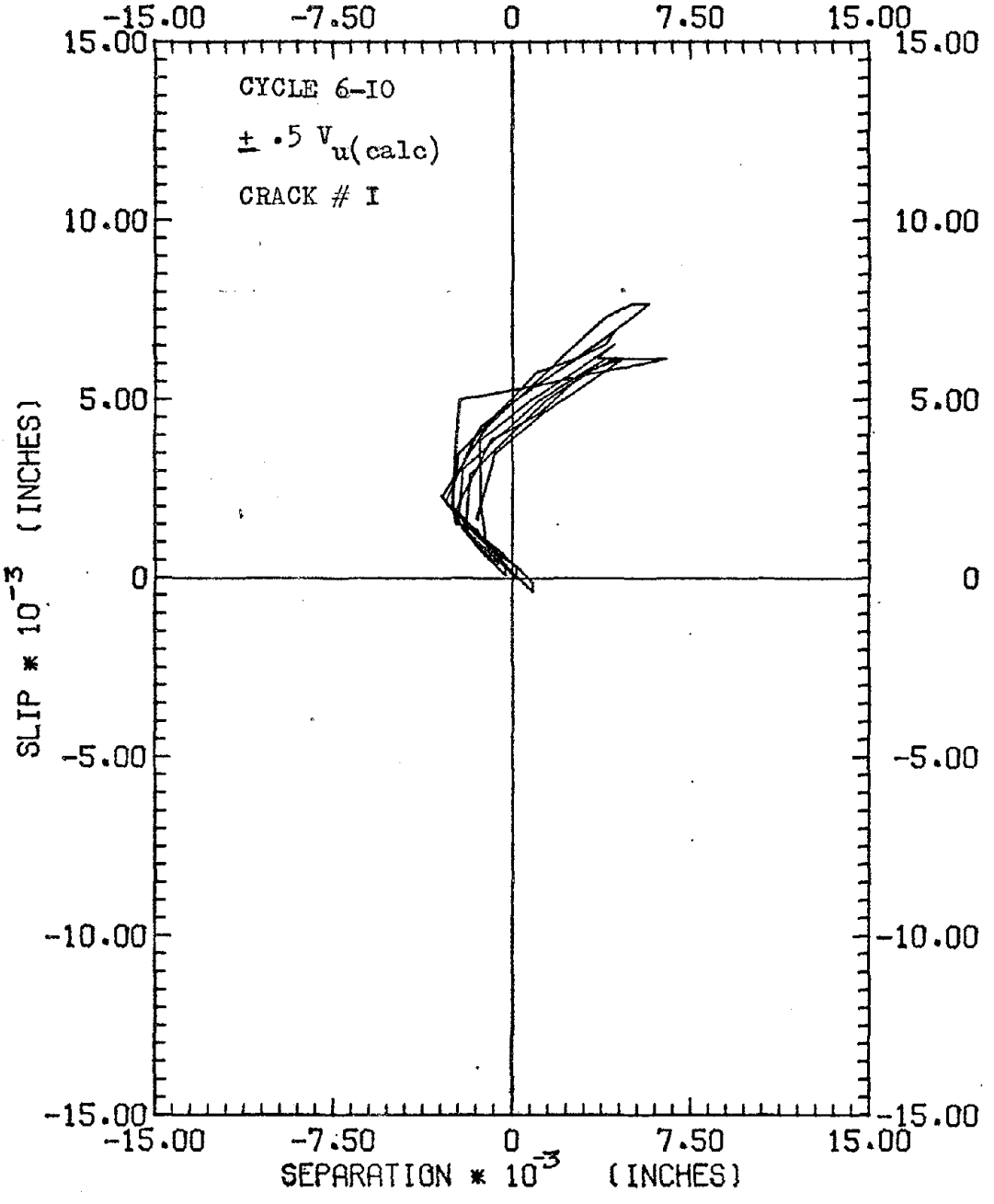

FIG.-C37, SLIP-SEPARATION CURVES, C14A

C40

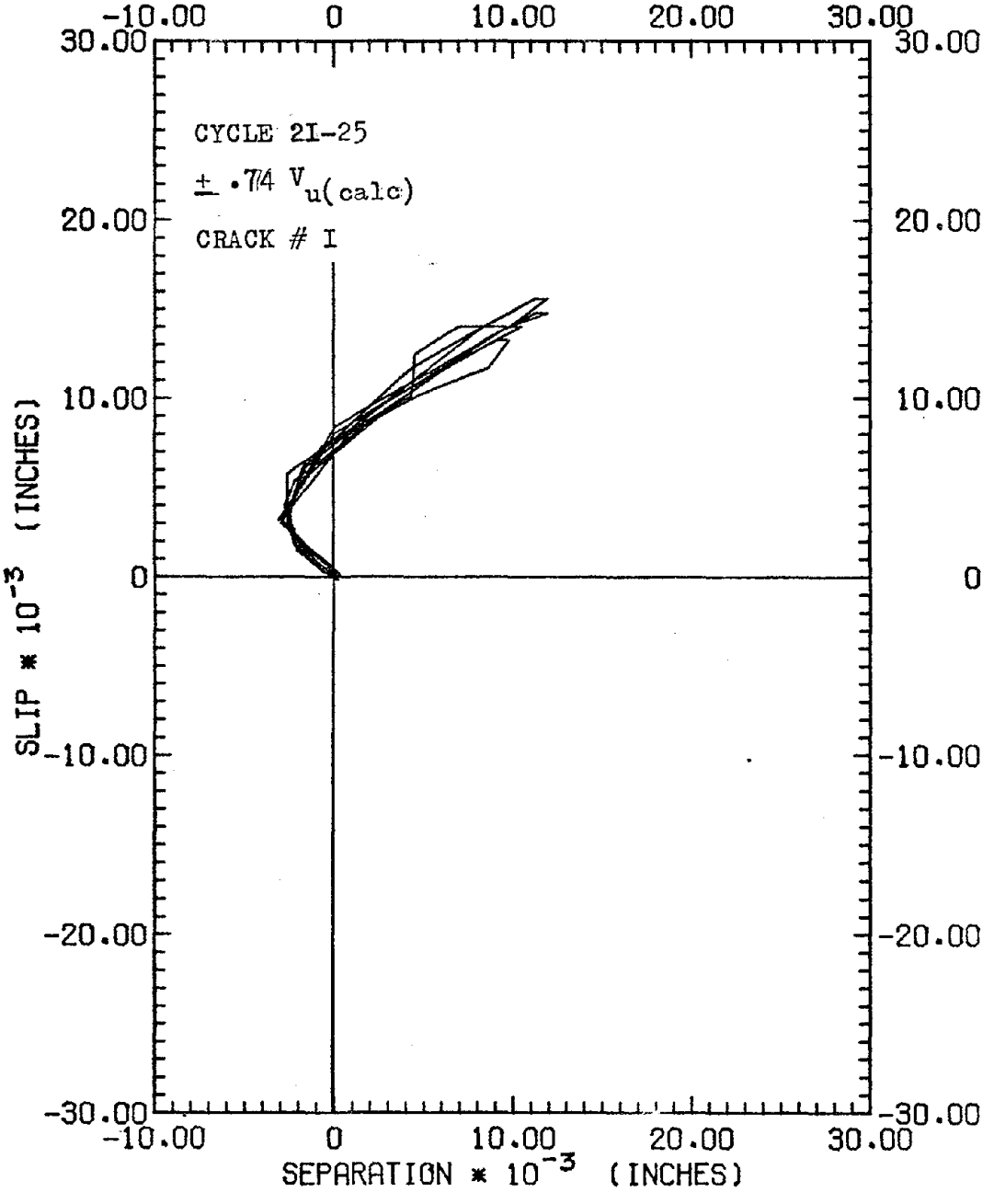

FIG.-C38, SLIP-SEPARATION CURVES, C14A

C41

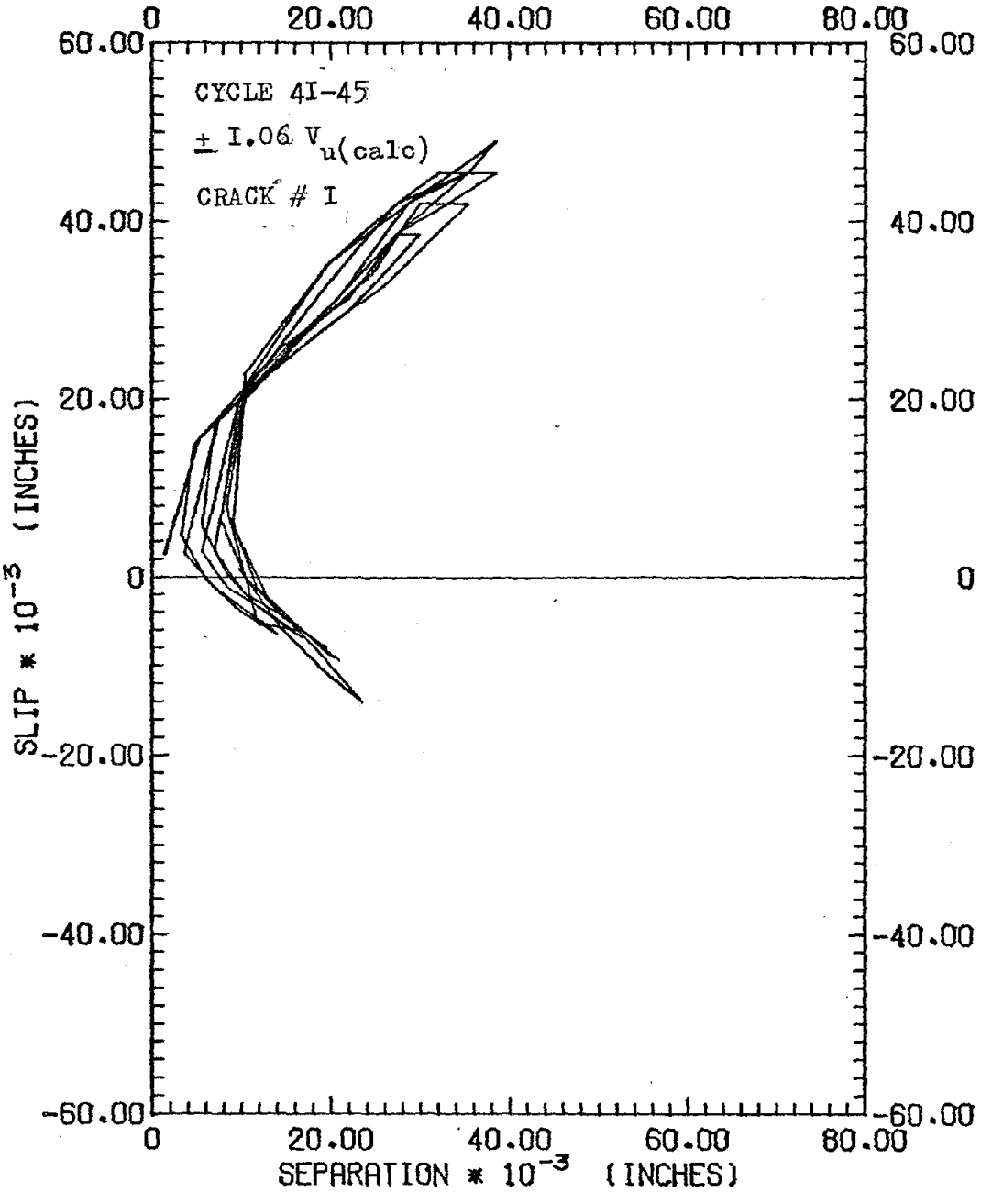

FIG.-C39, SLIP-SEPARATION CURVES, C14A

C 42

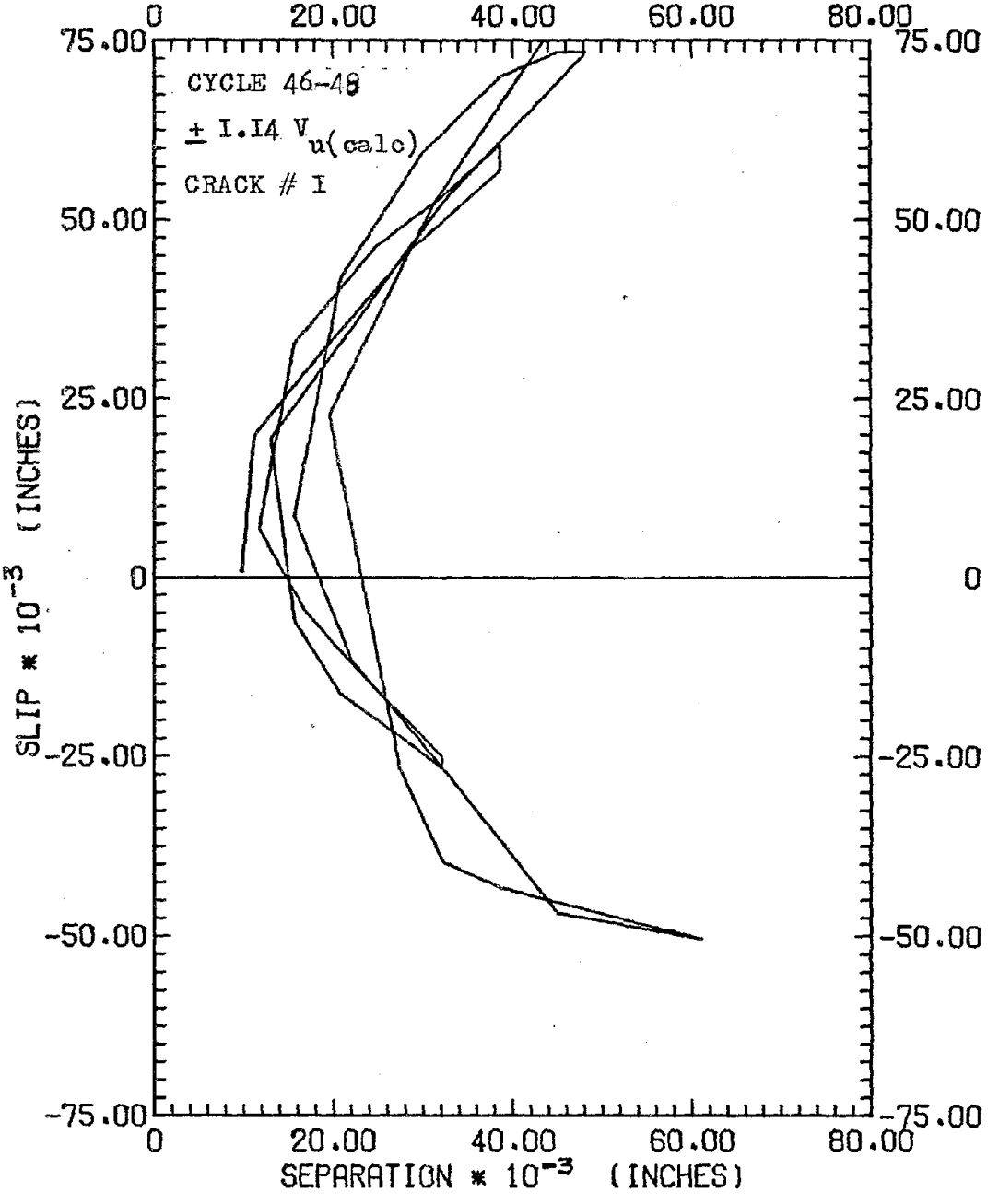

FIG.-C40, SLIP-SEPARATION CURVES, C14A

C43

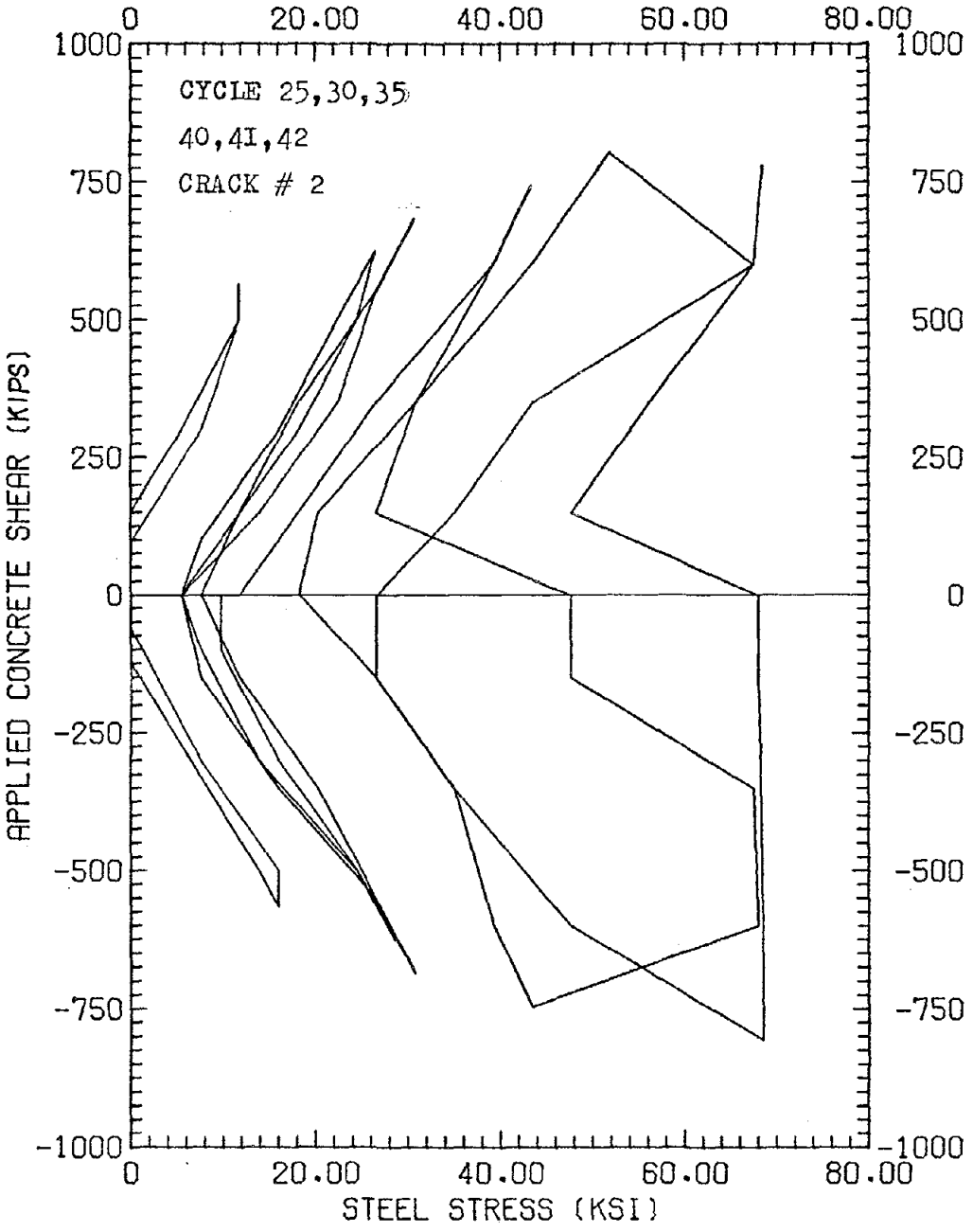

FIG.-C41, SHEAR-STEEL STRESS CURVES, C4A

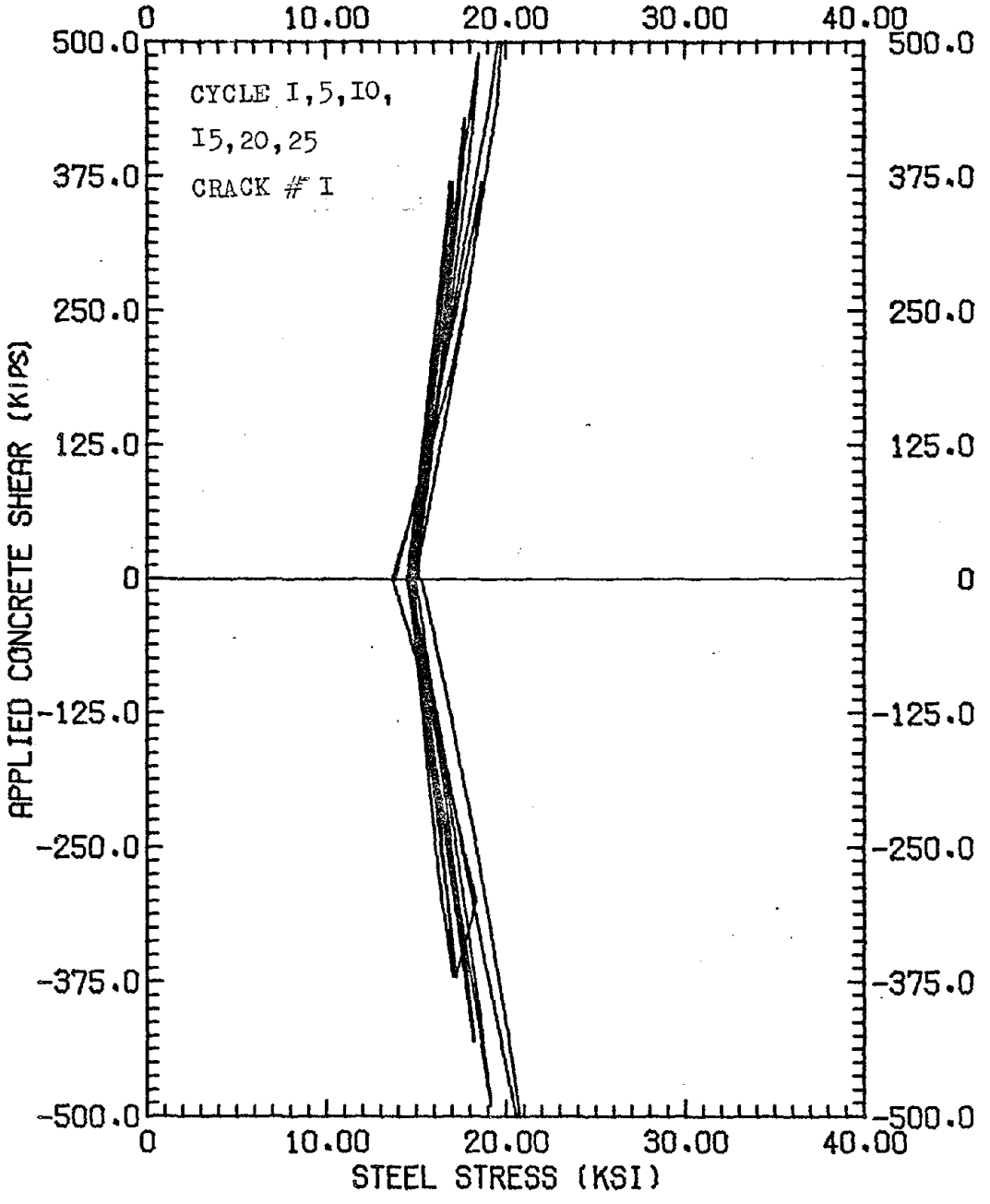

FIG.-C42 SHEAR-STEEL STRESS CURVES, C8A

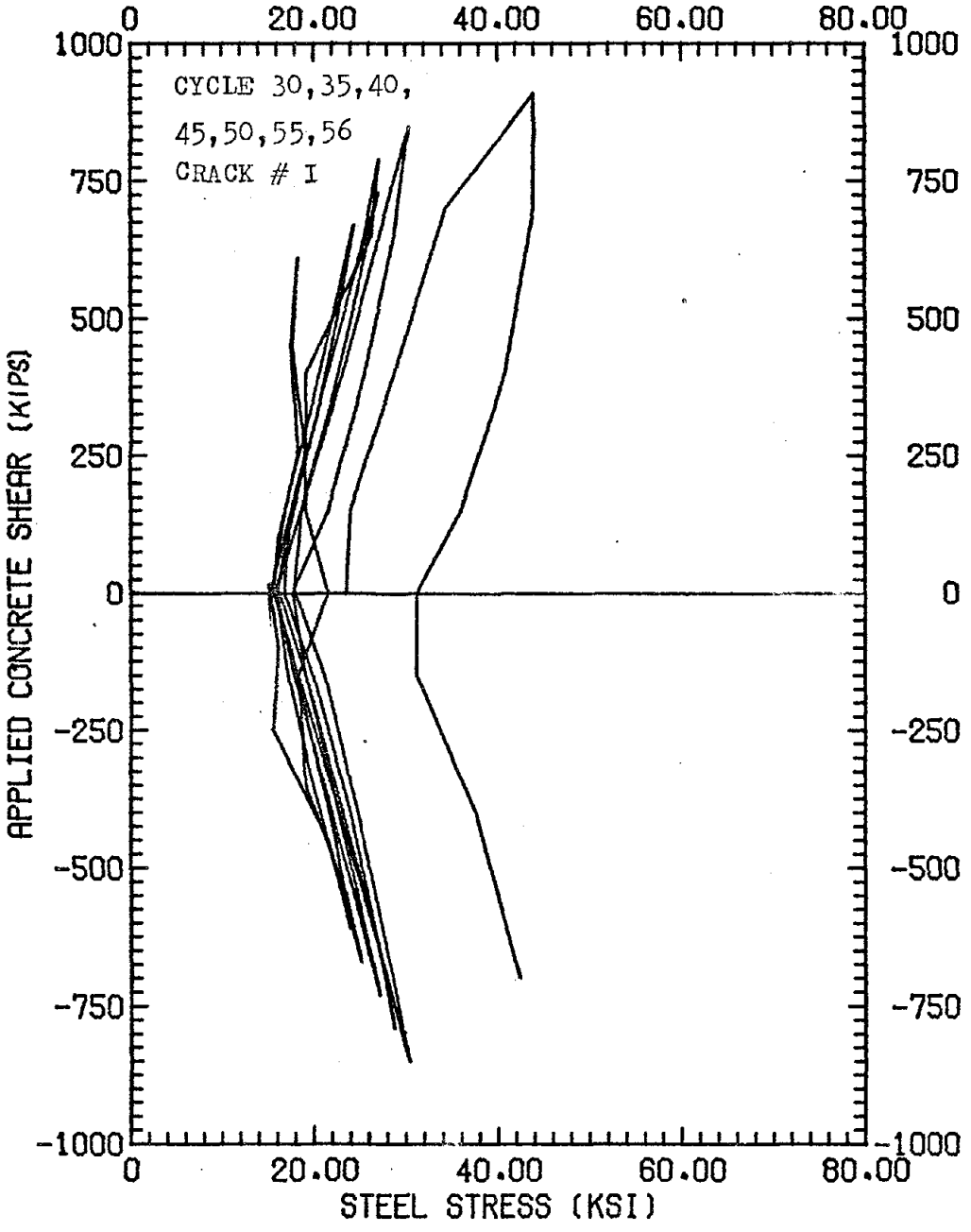

FIG.-C43, SHEAR-STEEL STRESS CURVES, C8A

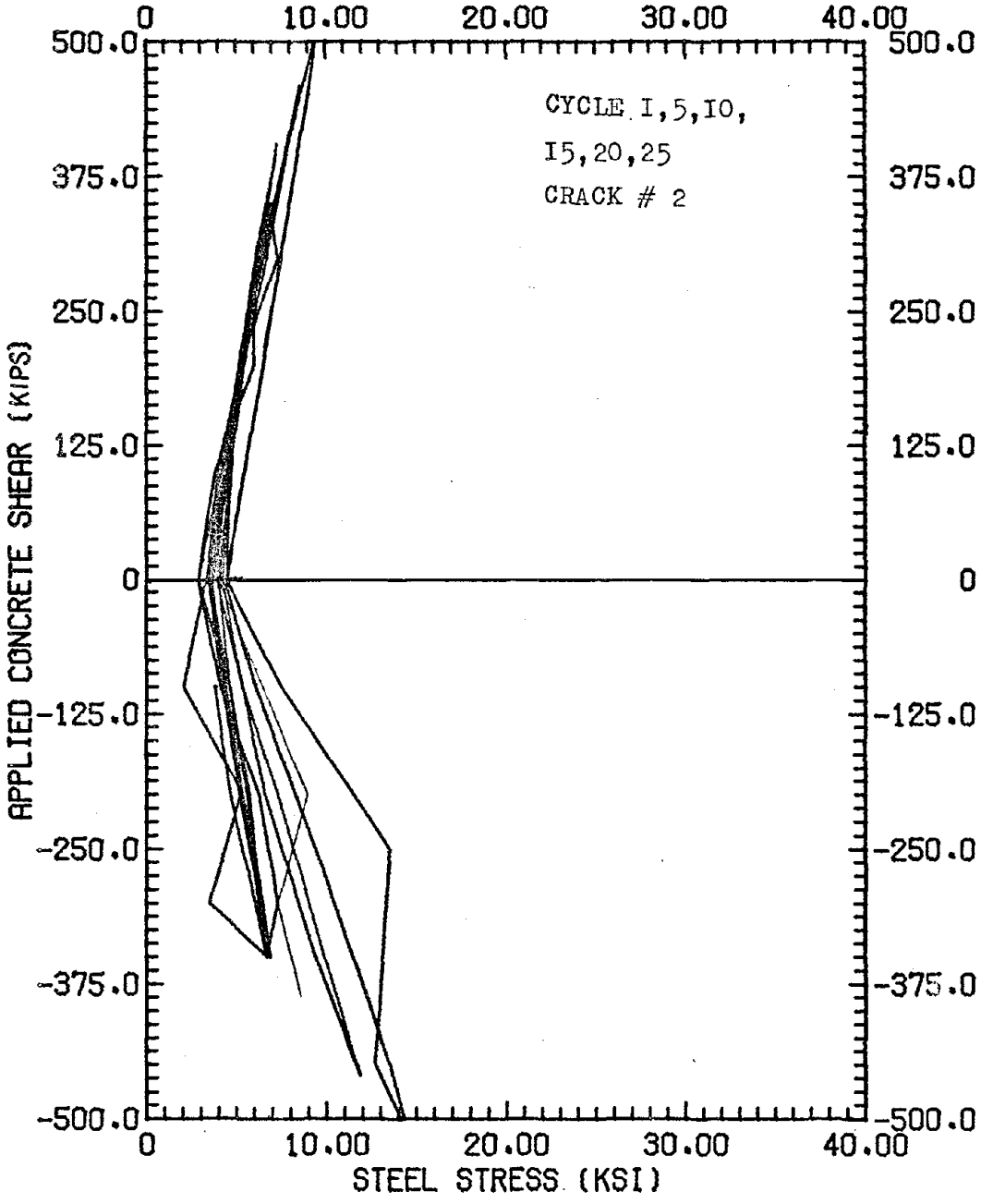

FIG.-C44, SHEAR-STEEL STRESS CURVES, C10A

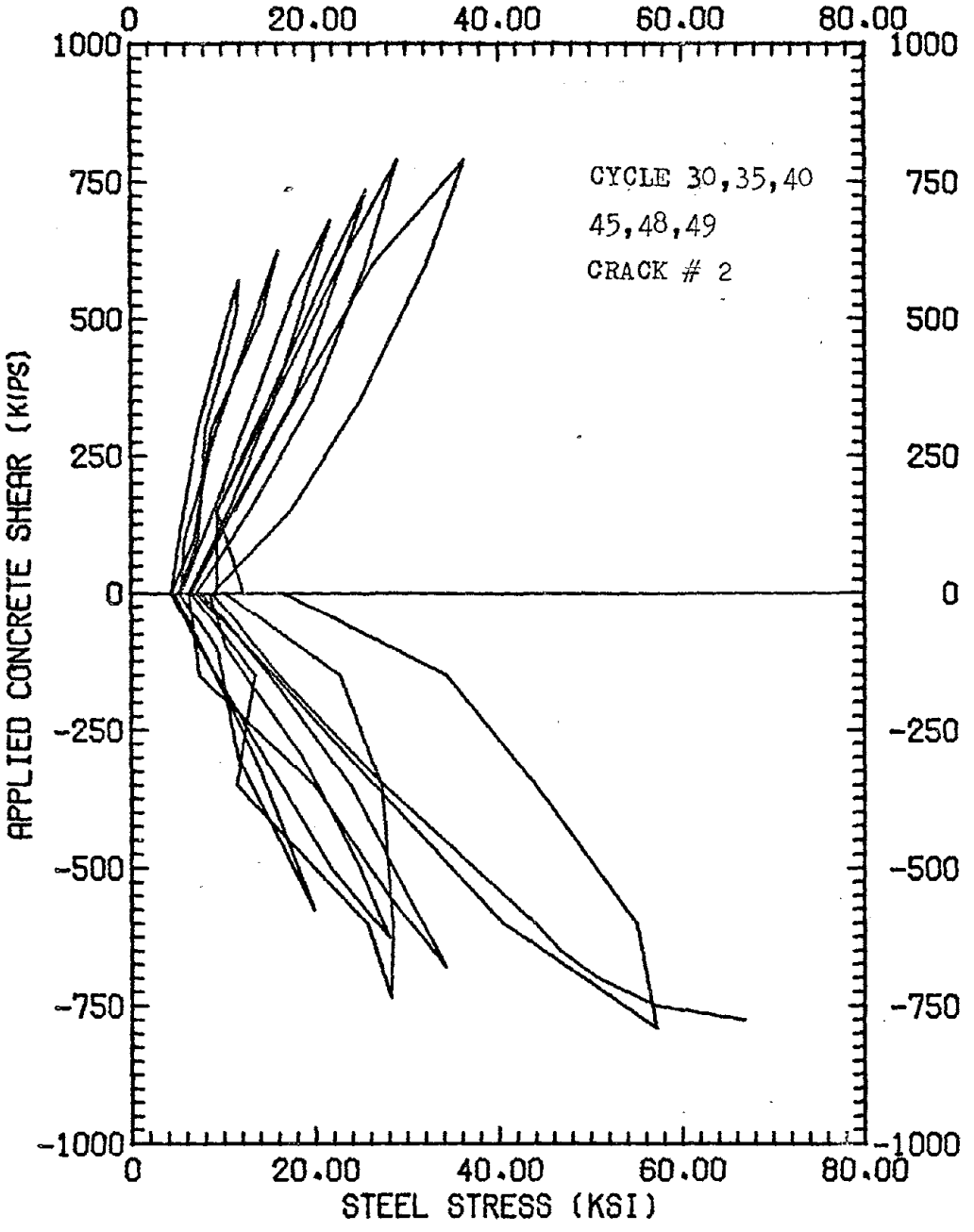

FIG.-C45, SHEAR-STEEL STRESS CURVES, C10A

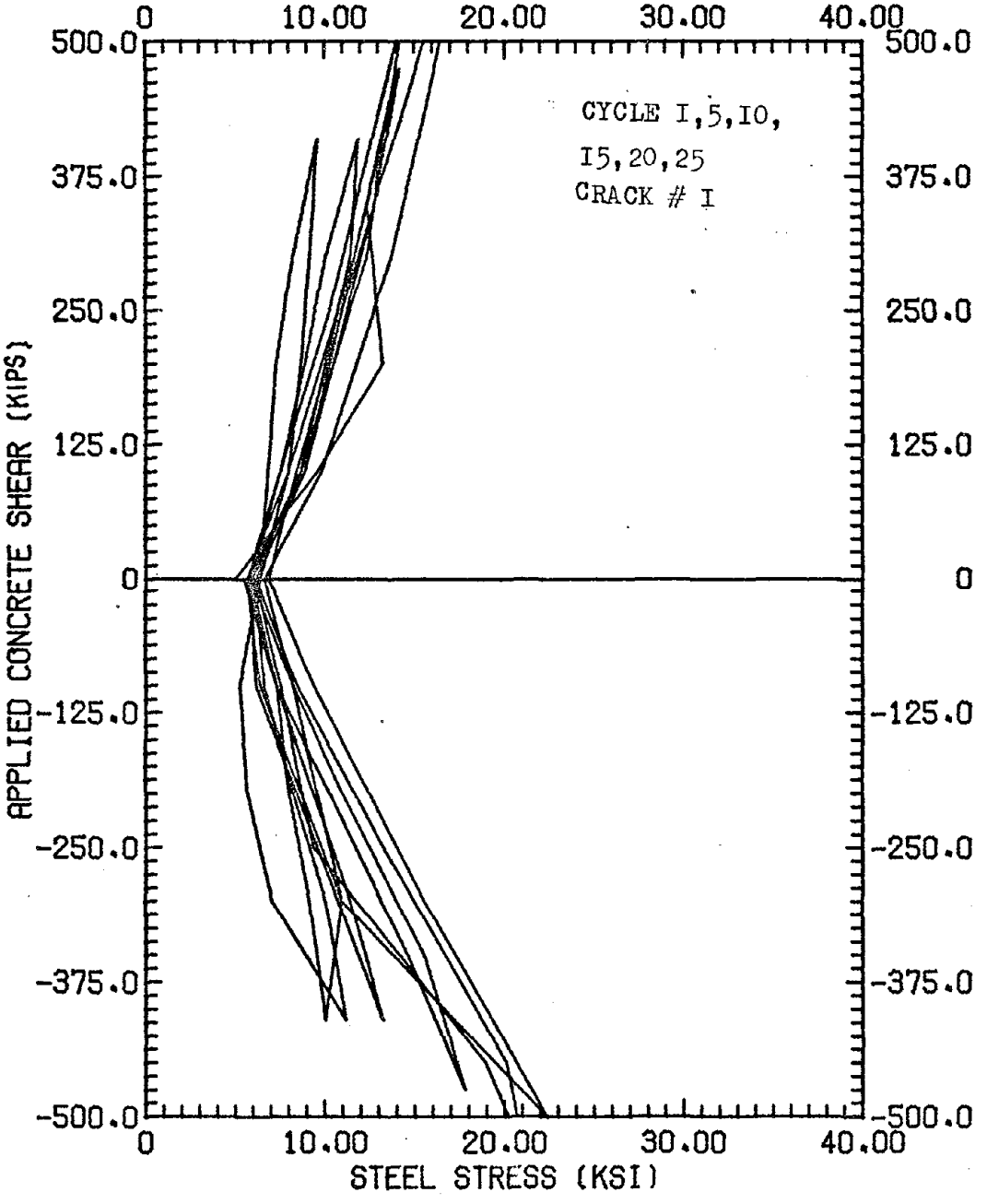

FIG.-C46, SHEAR-STEEL STRESS CURVES, C14A

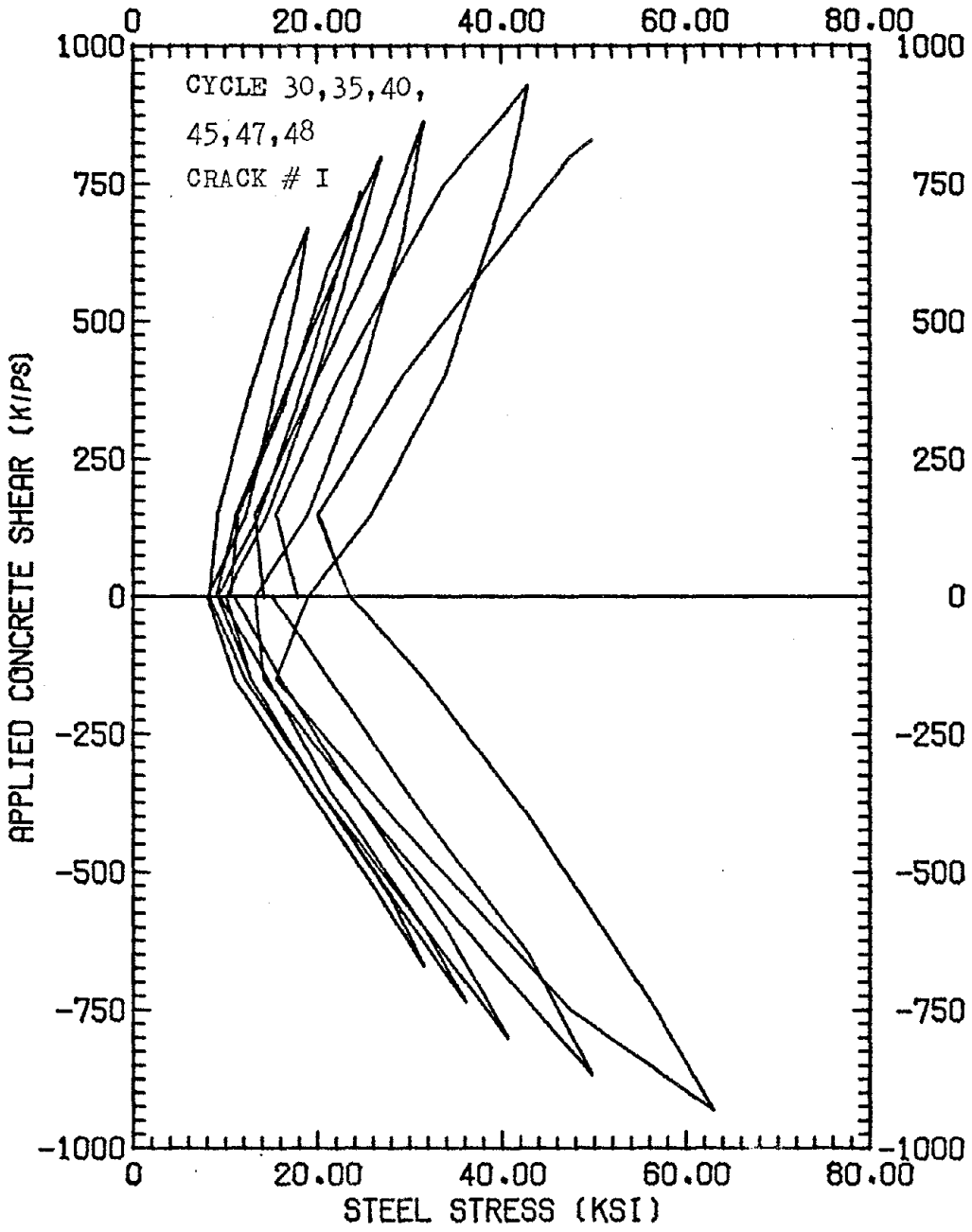

FIG.-C47, SHEAR-STEEL STRESS CURVES, C14A

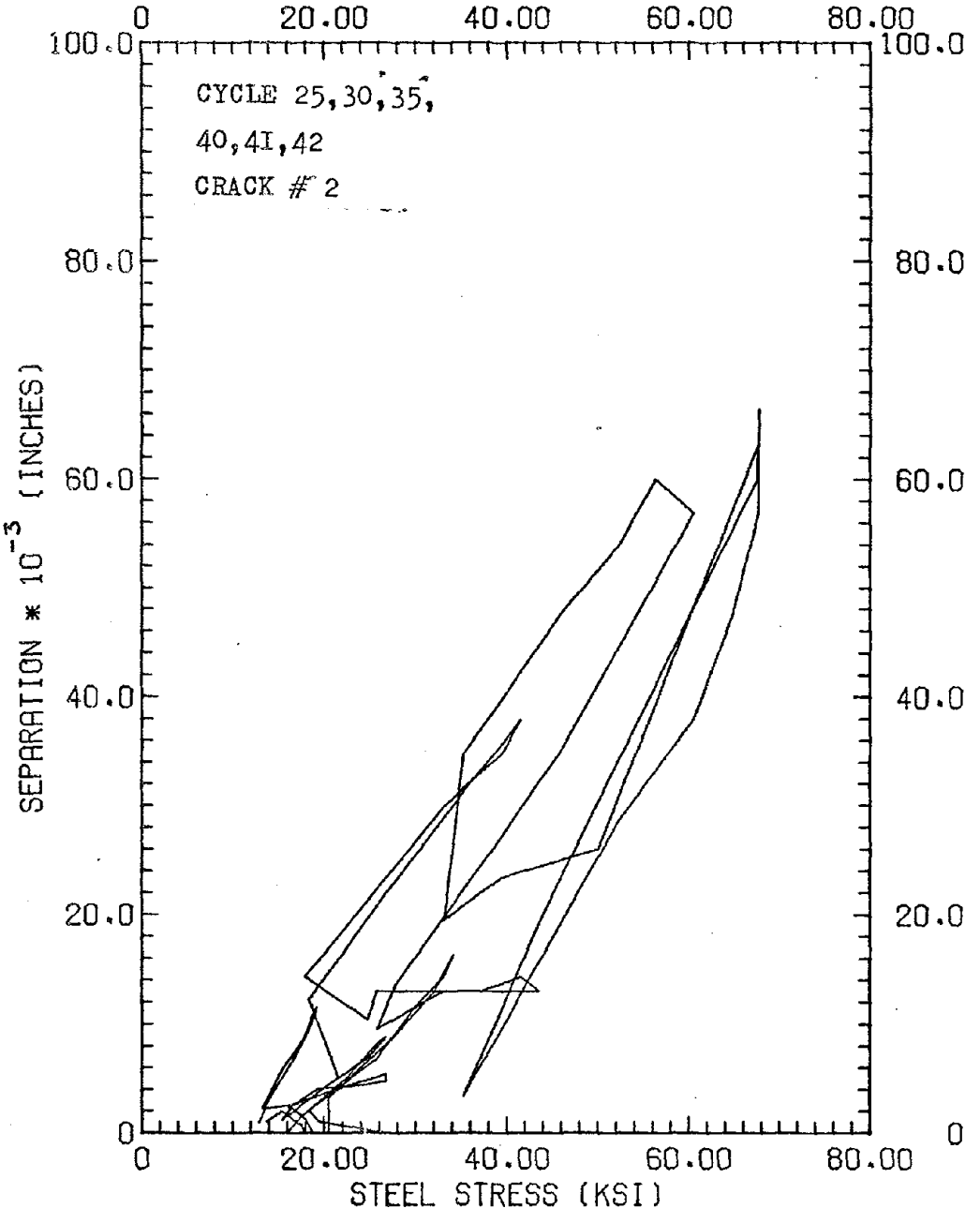

FIG.-C48, SEP.-STEEL STRESS CURVES, C4A

C51

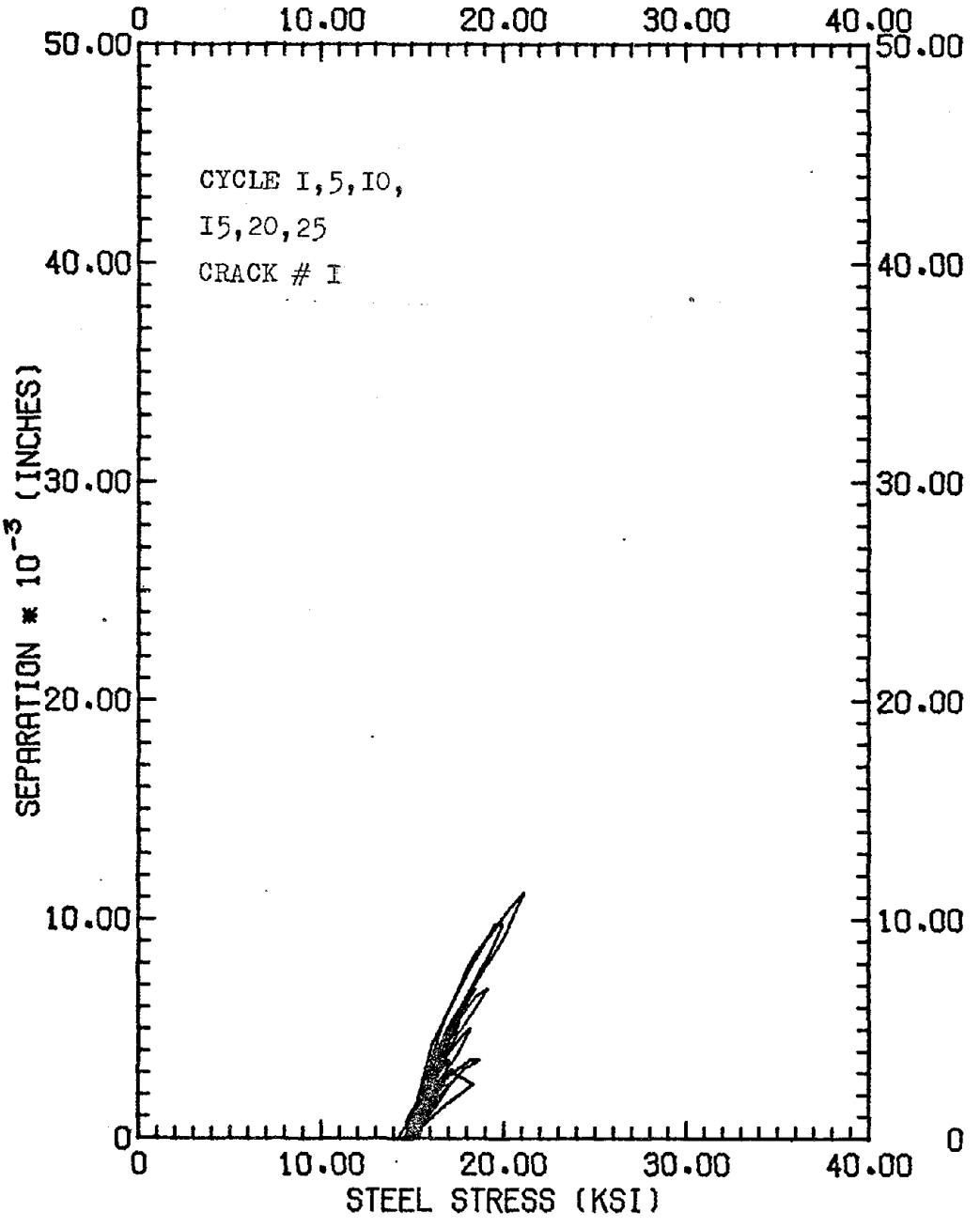

FIG.-C49, SEP.-STEEL STRESS CURVES, C8A

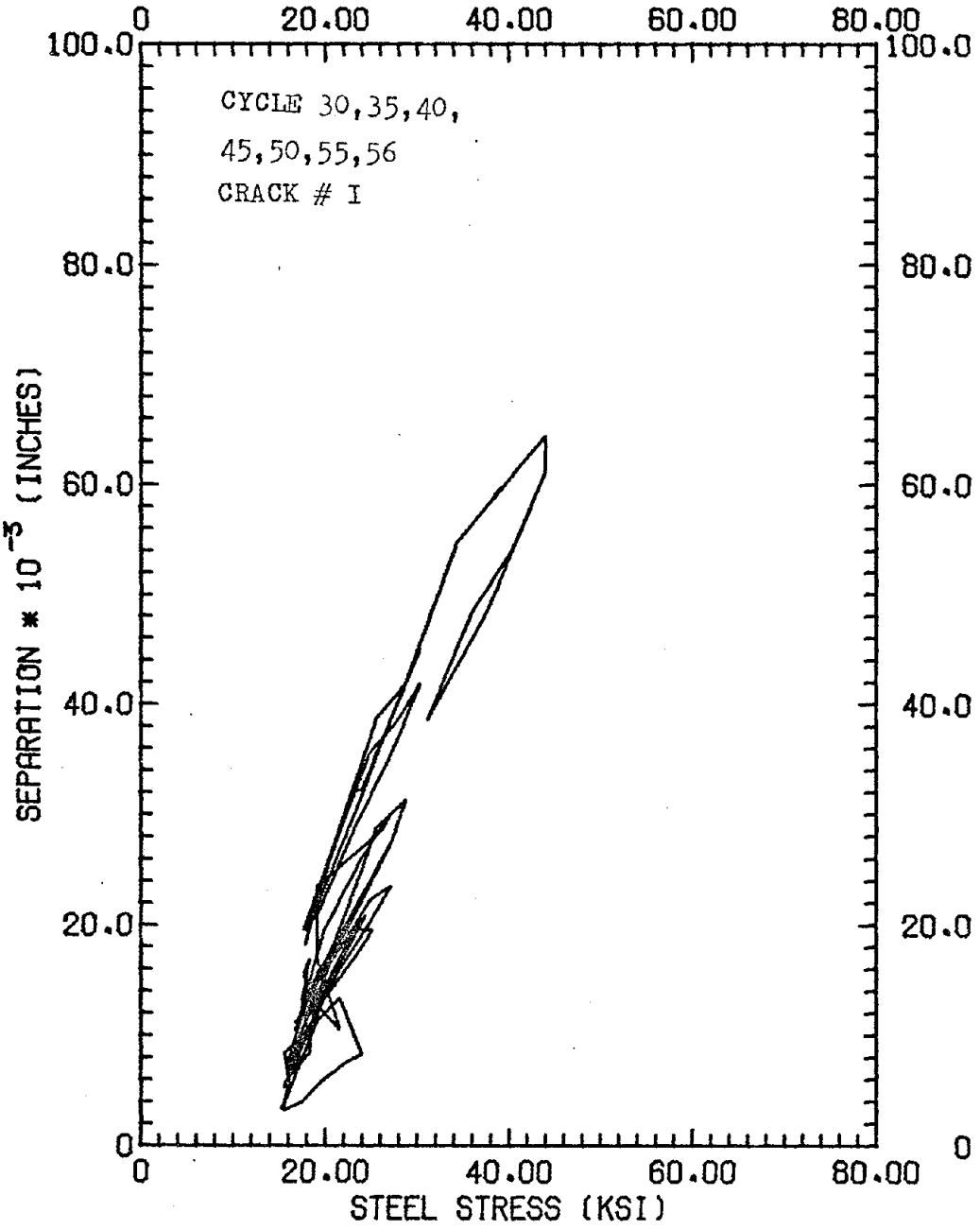

FIG.-C50,SEP.-STEEL STRESS CURVES,C8A

C53

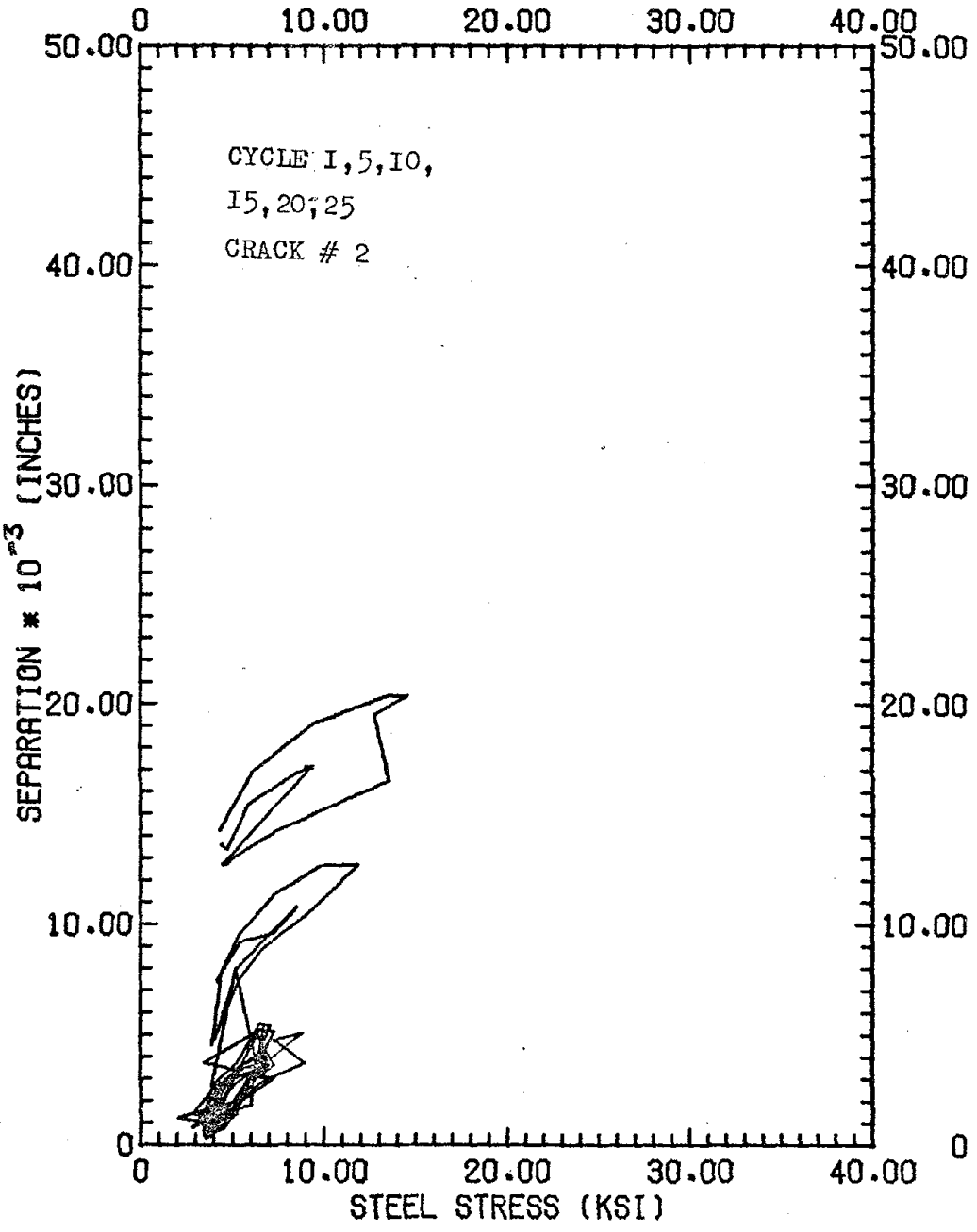

FIG.-C51, SEP.-STEEL STRESS CURVES, C10A

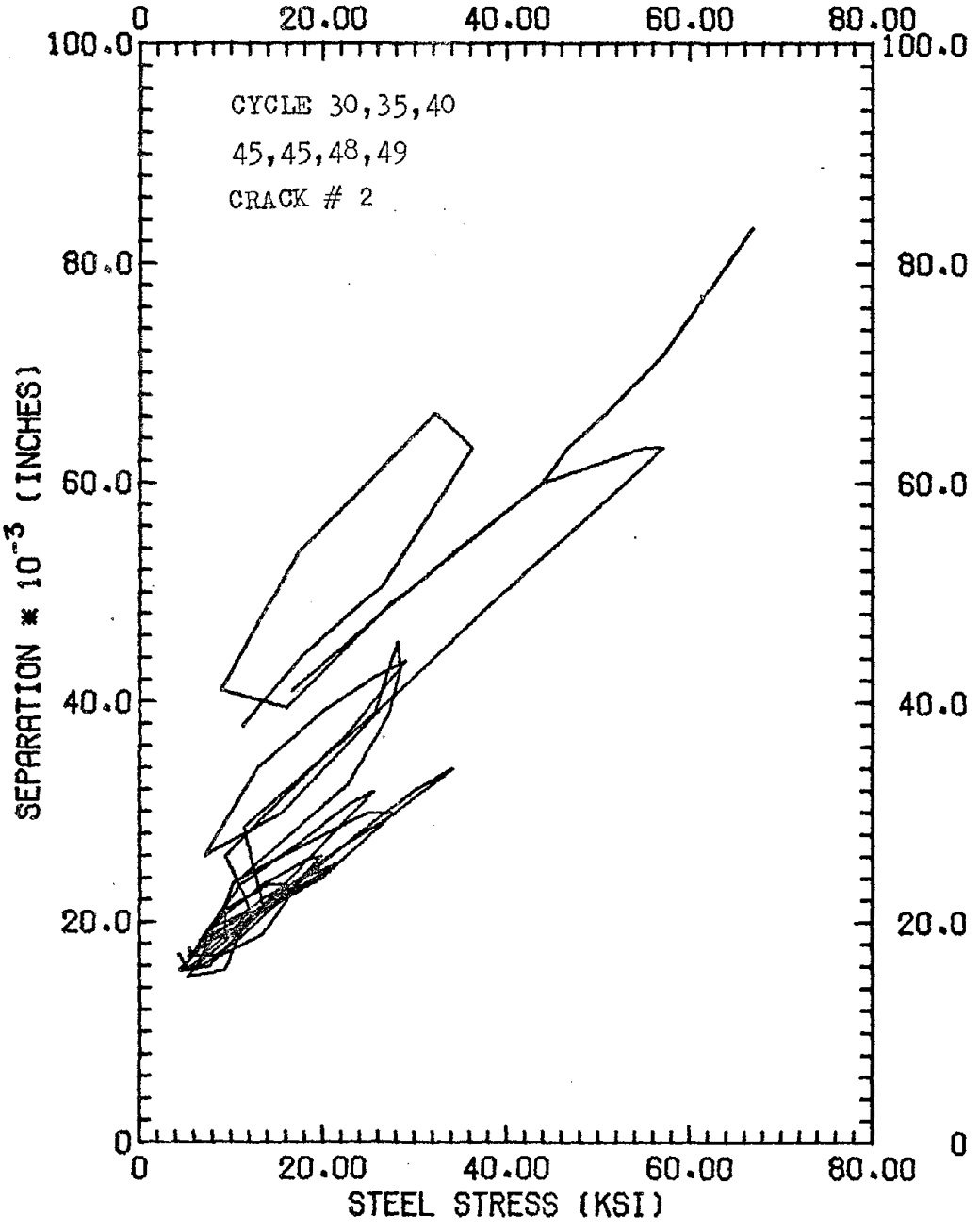

FIG.-C52, SEP.-STEEL STRESS CURVES, C10A

C55

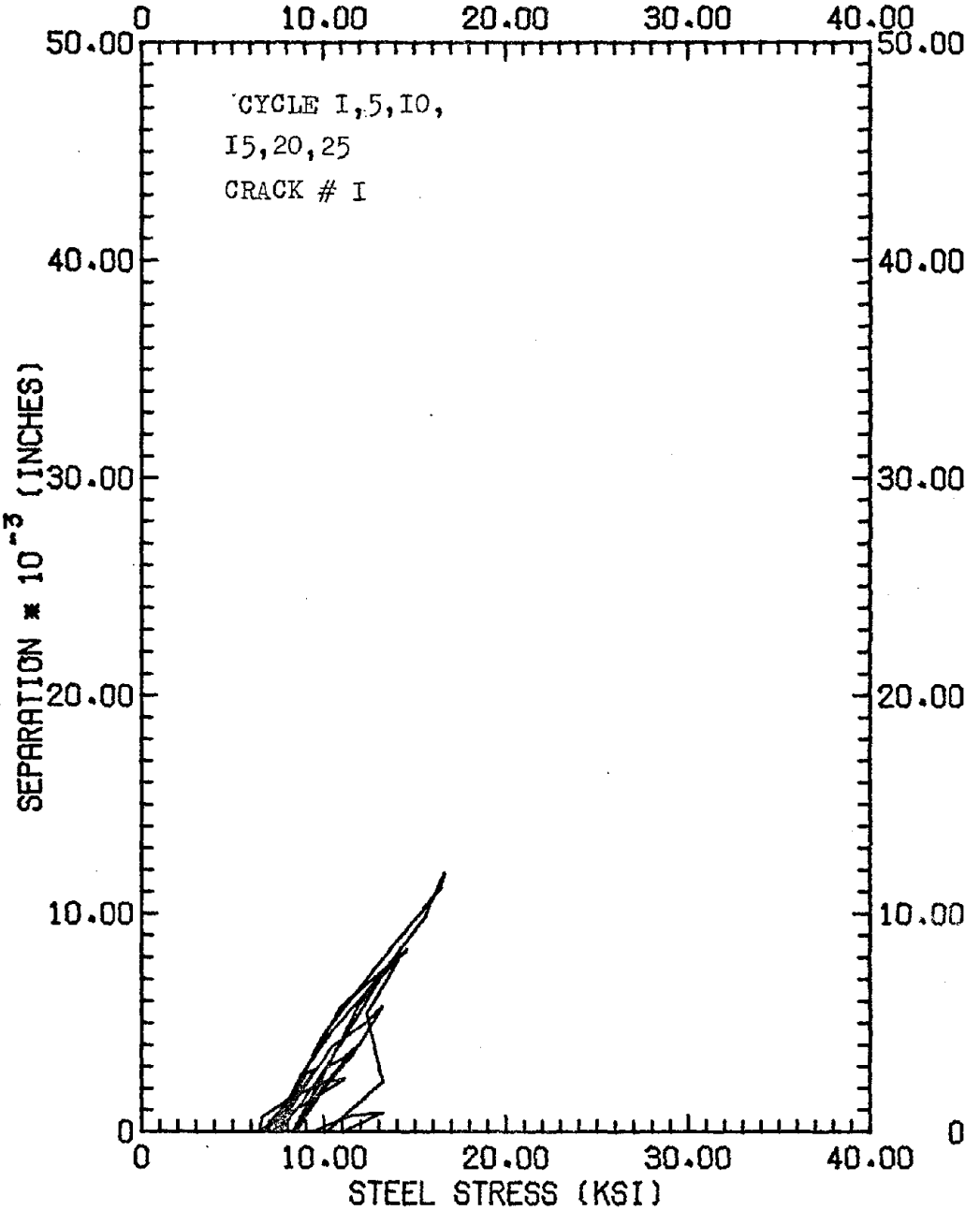

FIG.-C53, SEP.-STEEL STRESS CURVES, C14A

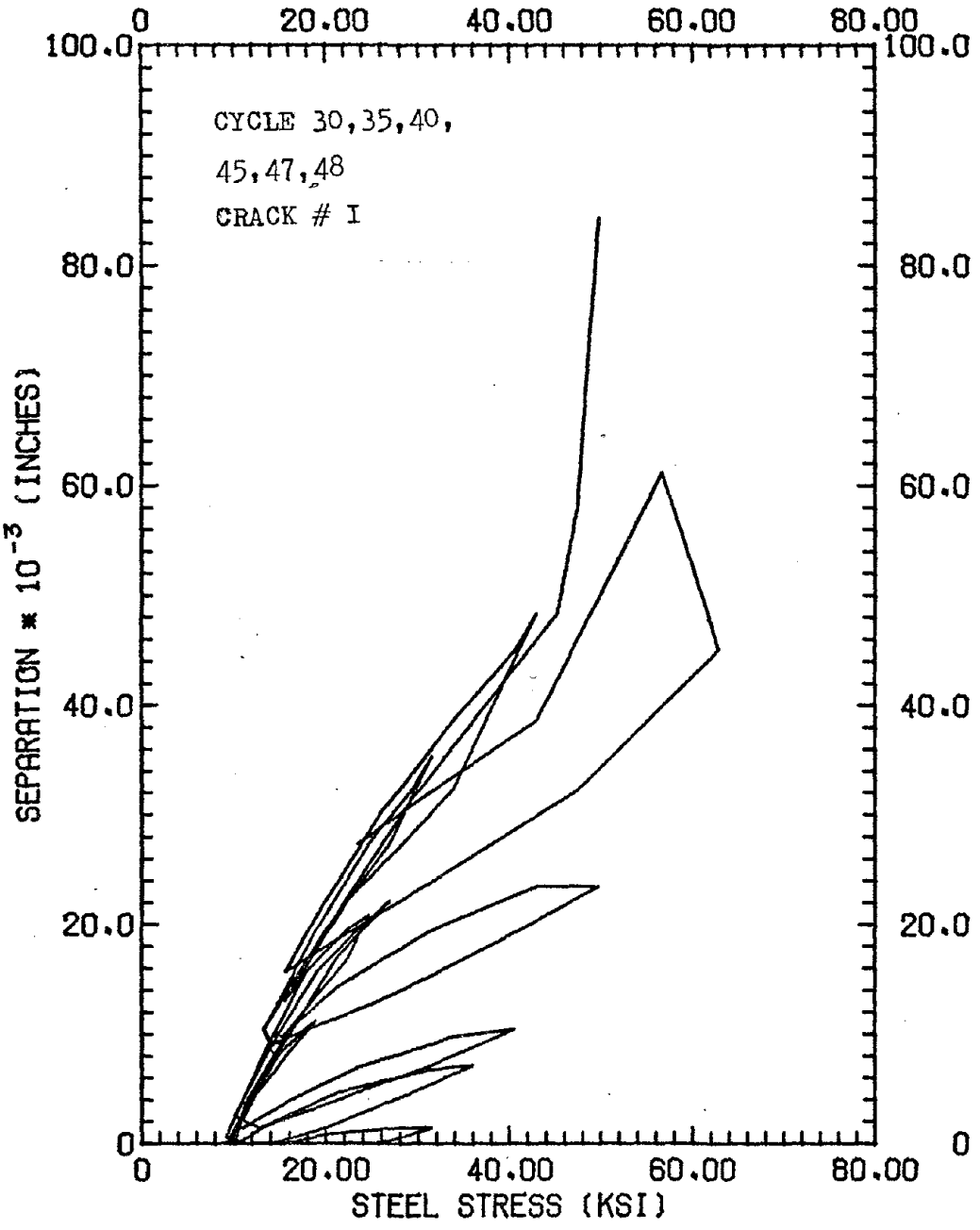

FIG.-C54, SEP.-STEEL STRESS CURVES, C14A